Archaean fluid-assisted crustal cannibalism recorded by low $\delta^{18}O$ and negative $\varepsilon Hf(T)$ isotopic signatures of West Greenland granite zircon

Joe Hiess[a,b]*, Vickie C. Bennett[a], Allen P. Nutman[a,c] and Ian S. Williams[a]

[a]Research School of Earth Sciences, Australian National University, Canberra, ACT 0200, Australia

[b]Division of Earth and Environmental Sciences, Korea Basic Science Institute, 804-1 Yangcheong-ri, Ochang, Cheongwon-gun, Chungbuk 363-883, South Korea

[c]School of Earth and Environmental Sciences, University of Wollongong, Wollongong, NSW 2522, Australia

*Corresponding author contact details: NERC Isotope Geosciences Laboratory
British Geological Survey
Keyworth, Nottingham
NG12 5GG, United Kingdom
+44 (0)115 936 3037 (office)
+44 (0)115 936 3302 (fax)
jies@bgs.ac.uk (email)

Word count: 445 (abstract)
8,072 (main text)
3,096 (references)
407 (captions)

Number of Tables: 1
Number of Figures: 7 (Figure 5 with free online color)
Number of Online Resources: 3

Abstract

The role of fluids during Archaean intra-crustal magmatism has been investigated via integrated SHRIMP U-Pb, δ^{18}O and LA-MC-ICPMS ^{176}Hf isotopic zircon analysis. Six rock samples studied are all from the Nuuk region (southern West Greenland) including two ~3.69 Ga granitic and trondhjemitic gneisses, a 3.64 Ga granitic augen gniess, a 2.82 Ga granodioritic Ikkattoq gneiss, a migmatite with late Neoarchaean neosome and a homogeneous granite of the 2.56 Ga Qôrqut Granite Complex (QGC). All zircon grains were thoroughly imaged to facilitate analysis of magmatic growth domains. Within the zircon analysed or their overall populations, there is no evidence for metamictization.

Initial ε_{Hf} zircon values (n=63) are largely sub-chondritic, indicating the granitic host magmas were generated by the remelting of older, un-radiogenic crustal components. Zircon from some granite samples displays more than one ^{207}Pb/^{206}Pb age, and correlated with ^{176}Hf/^{177}Hf compositions can trace multiple phases of remelting or recrystallisation during the Archaean. Model ages calculated using Lu/Hf arrays for each sample indicate that the crustal parental rocks to the granites, granodiorites and trondhjemites segregated from a chondrite-like reservoir at an earlier time during the Archaean, corresponding to known formation periods of more primitive tonalite-trondhjemite-granodiorite (TTG) gneisses. Zircon from the ~3.69 Ga granite, the migmatite and QGC granite contains Eoarchaean cores with chondritic ^{176}Hf/^{177}Hf and mantle-like δ^{18}O compositions. The age and geochemical signatures from these inherited components are identical to those of surrounding tonalitic gneisses, further suggesting genesis of these granites by remelting of broadly tonalitic protoliths.

Zircon oxygen isotopic compositions (n=62) over nine age populations (six igneous and three inherited) have weighted mean or mean δ^{18}O values ranging from 5.8±0.6‰ to 3.7±0.5‰. The 3.64 Ga granitic augen gneiss sample displays the highest δ^{18}O with a mildly supra-mantle composition of 5.8±0.6‰. Inherited Eoarchaean TTG-derived zircon shows mantle-like values. Igneous zircon from all other samples, spanning more than a billion years of Archaean time, record low δ^{18}O sub-mantle compositions. These are the first low δ^{18}O signatures reported from Archaean zircon and represent low δ^{18}O magmas formed by the remelting and metamorphism of

older crustal rocks following high-temperature hydrothermal alteration by meteoric water. Meteoric fluid ingress coupled with crustal extension, associated high heat flow and intra-crustal melting are a viable mechanism for the production of the low $\delta^{18}O$ granites, granodiorites and trondhjemites reported here.

Both high and low $\delta^{18}O$ magmas may have been generated in extensional environments and are distinct in composition from Phanerozoic I-type granitic plutonic systems, which are typified by increasing $\delta^{18}O$ during intra-crustal reworking. This suggests that Archaean magmatic processes studied here were subtly different from those operating on the modern Earth, and involved extensional tectonic regimes and the predominance of remelting of hydrothermally-altered crystalline basement.

Keywords: zircon, oxygen, hafnium, Archaean, crust, granite, Greenland

1. Introduction

Attempts to understand the origin of Archaean gneiss complexes in the Nuuk region, southern West Greenland have used a range of approaches including solely field geology (McGregor 1973; Chadwick and Nutman, 1979), regional tectonics (Friend et al. 1987, 1988; Nutman et al. 1989; Crowley 2002; Friend and Nutman 2005a; Nutman and Friend 2007), use of U-Th-Pb geochronology (Baadsgaard 1973, 1976; Nutman et al. 1993, 1996, 1999, 2000, 2007a, 2007b) or Rb-Sr and Sm-Nd radiogenic isotopes (Black et al. 1971; Moorbath et al. 1972; O'Nions and Pankhurst 1978; Bennett et al. 1993, 2007). These studies recognized that the tonalite-trondhjemite-granodiorite (TTG) components of the gneisses largely represent juvenile crust formation, whereas granites were produced from these older sources in a time frame ranging from a few million years to over a billion years later (Moorbath 1975; Taylor et al. 1980; Moorbath et al. 1981; Nutman and Bridgwater 1986; Friend and Nutman 2005b). The influence of juvenile versus recycling/remelting processes has implications for the budgets of continental growth, and the redistribution of radiogenic elements within the lithosphere. Determining the source of recycled crustal materials and the role and nature of crustal fluids participating in crustal reworking, will permit identification of mechanisms producing voluminous granitoids during Earth's early history.

The approach used here differs from that of previous studies noted above, in that the focus is on the use of integrated isotopic information contained within well documented individual igneous zircons to reveal the petrogenetic history of their host granitoids. For example, hafnium isotopes in igneous zircon can be used to identify the involvement of evolved crustal components during magmatism, and to constrain the timing of the segregation of those older components from the mantle (e.g. Amelin et al. 1999). Zircon oxygen isotopic compositions can be used to track incorporation of weathered supracrustal materials in igneous protoliths (Peck et al. 2001; Cavosie et al. 2005), or the cannibalization of country rock altered by hydrothermal meteoric fluids (Gilliam and Valley 1997; Bindeman and Valley 2000, 2001; Monani and Valley 2001; Wei et al. 2002).

Zircon is the ideal mineral to capture and retain this petrogenetic information, because it robustly records the isotopic composition of primary magmas from which it crystallized (Valley 2003; Kinny and Mass 2003). A common accessory phase in igneous rocks, zircon is a precise U-Pb chronometer (Parrish and Noble 2003; Ireland and Williams 2003). It is also relatively un-reactive through most geological processes, apart from highest-grade metamorphism and magmatic systems, when a single zircon is capable of undergoing multiple phases of growth. Due to the exceptionally low diffusivity of zircon (Watson and Cherniak 1997; Cherniak et al. 1997a, 1997b; Cherniak and Watson 2000, 2003, 2007; Page et al. 2007) such zoned grains can also reveal isotopically distinct sources and open-system processes operating during multiple phases of magmatism and metamorphism (Corfu et al. 2003).

Hiess et al. (2009) interpreted the oldest (3.7 to 3.85 Ga) Eoarchaean juvenile tonalitic magmas from the Itsaq Gneiss Complex (IGC; Nutman et al. 1996) in the Nuuk region as partial melts of hydrated oceanic crust via $\delta^{18}O$ and $^{176}Hf/^{177}Hf$ isotopic compositions preserved within precisely dated zircon. Here we apply these integrated techniques to younger, more evolved Archaean granites and granodiorites intruding the primitive tonalitic suites. This information is used to highlight the role of crustal reworking, the important contribution of fluids to magmatism and the influence of extensional tectonics. Also the styles of granitoid formation operating during the Archaean are contrasted with that of Phanerozoic magmas derived from metaluminous, I-type igneous systems (Kemp et al. 2007; Bolhar et al. 2008).

2. Samples and their geological setting

All samples are from the Nuuk area, southern West Greenland (Fig. 1). The region is dominated by polyphase TTG orthogneisses of the Archaean North Atlantic craton (McGregor et al. 1991). Exposed crust is predominantly tonalites with lesser trondhjemites, quartz-diorites, diorites, granodiorites, granites, metagabbros, ultramafic rocks and supracrustal associations (McGregor et al. 1991). All have been metamorphosed to amphibolite, and locally granulite facies (e.g. Wells 1976; Griffin et al. 1980) accompanied by intensive and heterogeneous ductile deformation (Nutman et al. 2000). Estimated pressures range from 0.5 to 1.0 GPa (Wells 1976) indicating these lithologies represent the deep levels of ancient orogens. Orthogneiss units can be divided into several tectonostratigraphic terranes with unique ages, structural geometries, and early metamorphic histories. Each terrane is separated by folded and recrystallised, amphibolite facies mylonites (Friend et al. 1987, 1988). Following continental collision and tectonic juxtaposition, all terranes experienced a common phase of Neoarchaean deformation and granite intrusion (Nutman et al. 1989; McGregor et al. 1991; Friend et al. 1996; Friend and Nutman 2005b; Nutman and Friend 2007).

2.1. ~3.69 Ga granitic gneiss 248251 and trondhjemitic gneiss 248212

The Isukasia area in the northern part of the Nuuk region (Fig. 1) consists of the 3.8 and 3.7 Ga Isua supracrustal belt that separates the "central gneisses" to the north dominated by ~3.7 Ga tonalites, from the "southern gneisses" dominated by ~3.8 Ga tonalites (Nutman et al. 1996, 1997; Nutman and Friend 2009). The southern fringe of the central gneisses is the source of samples 248251 and 248212 discussed here. Minimal regional strain in the central gneisses allows the typically heterogeneous and banded Eoarchaean gneisses of the IGC (McGregor 1973; Nutman et al. 1996) to be resolved into their major components of predominantly grey tonalitic gneisses, intruded by paler granitic and less commonly granodioritic and trondhjemitic components (Nutman et al. 1983; Nutman and Bridgwater 1986). The central ~3.7 Ga grey gneisses (Baadsgaard et al. 1986a) are dominated by juvenile tonalitic compositions, formed by the partial melting of hydrated mafic rocks (Nutman et al. 1999; Hiess et al. 2009).

There are swarms of anastomising granite-granodiorite and pegmatite sheets that intrude the tonalites of the central gneisses ('white gneisses' of Nutman and Bridgwater 1986; Fig. 4d of Nutman et al. 2000). U-Pb zircon geochronology has indicated that most of these granitic phases are 3.65-3.60 Ga old (Baadsgaard et al. 1986a; Nutman et al. 1996, 2000, 2002; Crowley et al. 2002). Recently, the ~3.7 Ga tonalitic phases have been divided into two suites on the basis of field relationships and U-Pb zircon geochronology (Nutman and Friend 2009), with a volumetrically subordinate suite of 3.72-3.71 Ga more melanocratic tonalite and quartz diorite now recognized. This suite is most common along the southern and western fringes of the central gneisses, and locally intrudes coeval metavolcanic rocks of the Isua supracrustal belt (Nutman and Friend, 2009). A second more volumetrically important suite of paler tonalites and low-K granodiorites has U-Pb zircon ages of 3.70-3.69 Ga (Nutman et al. 1996, 2000, 2002; Crowley et al. 2002). Rocks of this suite intruded the older 3.72-3.71 Ga suite prevalent along the southern and western fringes of the central gneisses, and both suites in turn were intruded by the granitic (sensu-stricto) white gneisses with U-Pb zircon ages of 3.65-3.64 Ga (Nutman et al. 1996, 2000; Crowley et al. 2002). The samples used here were collected by H. Baadsgaard in 1978, and are pale gneiss sheets intruding darker tonalites from the southern fringe of the central gneisses (Fig. 1).

Samples 248251 (Fig. 1; 65°07.72'N 49°57.89'W) and 248212 (Fig. 1; 65°06.15'N 50°01.50'W), were initially reported by Baadsgaard (1983) with bulk zircon, apatite and titanite U-Pb isotope data. U-Pb zircon analyses indicated an upper intercept age on a Concordia diagram of ~3650 Ma. Unpublished whole rock major element geochemical data for samples 248251 and 248212 was acquired in 1980 with XRF on fused glass discs, at Grønlands Geologiske Undersøgelse. 248251 with SiO_2 of 72.41 and K_2O of 4.82 wt.% is a granite. 248212 has a more trondhjemitic composition with SiO_2 of 71.07 and K_2O of only 0.84 wt.%. Samples 248251 and 248212 were originally regarded as part of the 3.65-3.64 Ga white gneiss suite (e.g. Baadsgaard et al. 1986a). However on the basis of more recent data, including SHRIMP U-Pb dating presented below, they are actually ~3.69 Ga sheets intruded into primitive ~3.72-3.71 Ga tonalites, and should not be correlated with the 3.65-3.64 Ga regional white gneiss sheet swarms.

2.2. ~3.64 Ga granitic augen gneiss G97/111

South of the fjord Ameralik, 3.85 to 3.69 Ga IGC TTG gneisses are intruded by the ~3.64 Ga augen gneiss or iron-rich suite (McGregor 1973; Baadsgard 1973; Nutman et al. 1984, 1996, 2000). Augen gneiss suite lithologies form part of an association of K-feldspar megacrystic, mafic granitic - granodioritic - quartz-monzonitic gneisses, with lesser ferrodiorites and gabbros. The suite is geochemically distinct from the regional banded gneisses (e.g. with Fe, Ti and REE enrichment, low SiO_2 and Al_2O_3 contents; Nutman et al. 1984) and characterized as a 'within plate granite suite' based on general characteristics such as elevated Nb-Y concentrations (Nutman et al. 1996). The augen gneiss suite has been interpreted as the product of deep crustal melting (under granulite facies?) with the melting triggered by the emplacement of an underplate of mantle-derived gabbroic magma (Nutman et al. 1984). Fractionation of the gabbroic magma and its intermingling with crustally-derived melts produced a broad range of generally high Fe, Ti rocks. Early isotopic evidence to support this interpretation came from data of Vervoort et al. (1996), where the bulk zircon analysis of a ferrogabbro sample had a more elevated initial ε_{Hf} value than a sample of granitic augen gneiss.

Within the augen gneisses, sample G97-111 (Fig. 1; Honda et al. 2003), is an A-type meta-granite with vestiges of igneous K-feldspar preserved as phenocrysts. It is located at 64°01.96'N 51°36.60'W, from a low strain domain on the west of Narssaq peninsula, at the southern mouth of Ameralik. The sample is relatively mafic with abundant K-feldspar augen and probably represents a crustal melt with mantle contamination (Nutman et al. 1984, 1996). Zircons are prismatic, typically 150 - 300 μm long, have numerous ilmenite inclusions, oscillatory zonation parallel to grain boundaries, and are devoid of inherited cores in CL. Some exteriors are corroded while others have thin (<15 μm) overgrowths. The best oscillatory zoned domains yielded a weighted mean $^{207}Pb/^{206}Pb$ age of 3642 ± 3 Ma (2SD, MSWD = 1.0) and record the crystallization age of the protolith (Honda et al. 2003).

2.3. ~2.82 Ga granodioritic Ikkattoq gneiss VM97/01

The Mesoarchaean amphibolite facies Ikkattoq orthogneisses of the Tre Brødre Terrane (Friend et al. 1987; Nutman et al. 1989; McGregor et al. 1991; Nutman and Friend 2007; Friend et al. 2009) are found in tectonic contact with the IGC throughout the southern Nuuk region. Most are granodioritic in composition, and contain abundant gabbro-anorthosite inclusions and widely spaced, concordant pegmatite banding. Eleven SHRIMP U-Pb zircon dated samples of single phase gneisses record magmatic ages within a narrow range from 2817±9 to 2829±11 Ma (Nutman and Friend 2007) consistent with ID-TIMS analysis of zircon from one sample yielding an age of 2824±2 Ma (Crowley 2002). Based on Sr, Nd and Pb isotopic data, the Ikkattoq gneisses contain a significant contribution of mixed older crustal materials (Friend et al. 2009). In respect to their generally granodioritic composition and their clear evidence of major contamination by older crust based on Sr, Nd and Pb whole rock isotopic data, they are an exception amongst the Eo- Neoarchaean TTG suites of the Nuuk region, where contamination by older crust is either absent or considerably muted (Moorbath et al. 1986; Bennett et al. 1993; Garde et al. 2000; Friend et al. 2009). Sample VM97/01, collected from the top of Hjortetakken, south of Nuuk (Fig. 1; 1225m; approximately 64°07.30'N 51°34.70'W), is a representative sample from the unit and was previously SHRIMP dated at 2821±8 Ma by Nutman and Friend (2007). Zircons are typically prismatic, ~200 µm in length, with fine scaled oscillatory zonation and Th/U > 0.3.

2.4. Neoarchaean migmatite 195392 and granite 195376 of the Qôrqut granite complex (QGC)

The QGC (McGregor 1973; Brown et al. 1981; Friend et al. 1985) is a NE-SW elongated body of late Neoarchaean leucocratic, biotite composite granites, intruded as multiple granitic sheets into Eoarchaean, Mesoarchaean and Neoarchaean banded gneisses. The main part of the complex was not subject to major regional deformation following emplacement (Brown et al. 1981), and was emplaced at shallow to intermediate crustal levels into already evolved 'continental' crust. Age determinations by Baadsgaard (1976) and Moorbath et al. (1981) indicated formation at ~2.55 Ga while compositions indicate the granites approximate minimum melts formed by the partial melting of older surrounding crustal rocks (Brown et al. 1981; Moorbath et al. 1981). At deep structural levels in the main outcrop area of the QGC and at its northern fringes there are migmatites, which appear to contain neosome coeval with, or marginally older than the QGC (e.g. Friend et al., 1985; Nutman and Friend, 2007). Additionally, major ductile shear zones along strike with the QGC were active when the granite was emplaced (Nutman et al., 1989, In review). Sample 195392 (Fig. 1; 64°16.33'N 51°04.00'W; Friend et al. 1985) is a migmatite sourced from a diatexite between regional biotite gneiss and a homogeneous leucocratic granite. Sample 195376 (Fig. 1; 64°16.50'N 51°00.00'W) is a sample of homogeneous Qôrqut granite previously dated by Nutman et al. (2007c) at 2564±12 Ma with Mesoarchaean and Eoarchaean inheritance.

3. Methods and results

Zircons were extracted using standard heavy liquid and magnetic separation techniques. The grains were cast into epoxy “megamounts” (Ickert et al. 2008) along with zircon reference materials. New generation SHRIMP megamounts have been found to greatly improve reproducibility of oxygen isotope analyses using SHRIMP II and details regarding their geometric design and performance can be found in Ickert et al. (2008). Following imaging using transmitted and reflected light and catholuminescence, U-Pb zircon ages were determined using SHRIMP RG at the Australian National University (ANU). The zircon mounts were then lightly re-polished and oxygen isotopic compositions were measured from spots placed on top of the original U-Pb sampling area for each zircon with SHRIMP II at ANU. Lutetium - hafnium isotopic compositions were determined by laser ablation MC-ICPMS (ANU Neptune). Although a larger spot size was used, care was taken to sample in the same growth domains of the zircon as for the U-Pb and O analyses. The details of the analytical methods used here and the statistical treatment of data (rejection of outliers and calculation of mean or weighted mean values) are the same as in Hiess et al. (2009) and are described fully in Online Resource 1. Mean (1σ) or weighted mean (95% confidence limit, c.l.) $^{207}Pb/^{206}Pb$ ages from this study typically have larger uncertainties, owing to fewer pooled analyses, but agree within uncertainties with previous U-Pb zircon age determinations on these samples, obtained using larger datasets where available. An integrated summary of the 90 U-Pb, 62 $\delta^{18}O$ and 63 $\varepsilon_{Hf(T)}$ determinations is presented in Table 1. Complete reference material and sample data for oxygen and Lu-Hf analyses is given in Online Resource 2. A descriptive summary of the zircon characteristics and main geochemical results for each sample is presented in Online Resource 3. Representative cathodoluminesence zircon images with analysis locations and associated results for ~3.69 Ga granitic gneiss 248251 and trondhjemitic gneiss 248212 are given in Fig. 2a, ~3.64 Ga granitic augen gneiss G97/111 in Fig. 2b, ~2.82 Ga granodioritic Ikkattoq gneiss VM97/01 in Fig. 2c, and Neoarchaean migmatite sample 195392 and QGC granite 195376 in Fig. 2d. Tera-Wasserburg $^{238}U/^{206}Pb–^{207}Pb/^{206}Pb$ diagrams, summary plots of $\delta^{18}O$ and $\varepsilon_{Hf(T)}$ values against corresponding $^{207}Pb/^{206}Pb$ crystallisation age for each zircon analysis, and sample weighted means or means are illustrated in Fig. 3. The field for mantle zircon ($\delta^{18}O$ = 5.3±0.3‰) is the composition of zircon derived from the mantle (Valley et al. 1998). The field for Archaean and Hadean “supracrustal zircon” ($\delta^{18}O$ = 6.5 to 7.5‰) reflects the composition of zircon from igneous protoliths whose source materials were altered by low temperature interaction with liquid water near Earth’s surface (i.e. weathered before incorporation back into an igneous system; Cavosie et al. 2005). The Lu-Hf chondritic uniform reservoir (CHUR) composition and uncertainty estimates are from Bouvier et al. (2008). Plots of $\delta^{18}O$ against U, Th, Th/U, % common ^{206}Pb, and % discordance for samples analysed for $^{18}O/^{16}O$ are presented in Fig. 4.

4. Discussion

4.1. The origin of Archaean granites - insights from initial $^{176}Hf/^{177}Hf$ isotopic compositions

Hiess et al (2009) previously determined zircon weighted mean initial ε_{Hf} values of +0.5±0.6 to -0.1±0.7 for five Eoarchaean tonalite and felsic volcanic units from the IGC, implying derivation of these juvenile magmas from a largely unfractionated, chondritic source reservoir. In contrast, samples described here record largely sub-chondritic weighted mean or mean $\varepsilon_{Hf(T)}$ compositions of -0.7±1.6 (2821±8 Ma), -0.8±0.8 (3686±22 Ma), -1.1±1.0 (3690±8 Ma), -1.1±0.8 (3635±14 Ma), -2.0±1.7 (3627±38 Ma), -14.6±4.0 (3032±46 Ma), -14.7±1.7 (2571±10 Ma), -19.4±1.0 (2726±5 Ma) and -22.6±1.8 (2570±4 Ma). These values consistently lie at the lower limit of, or clearly beneath the error envelope for the chondritic reference line of $\varepsilon_{Hf(T)}$ = 0.0±0.4 (Bouvier et al 2008; Figs. 3c, 3f, 3i, 3l, 3o and 3r), and imply that the magmas from which this zircon crystallized was derived, at least in part, from the remelting of more mature, crustal sources with lower Lu/Hf than CHUR.

The evolved source or sources for each sample cannot be precisely identified from these data. However, the timing of the source's segregation from its ultimate mantle reservoir, here taken to be represented by a chondritic composition (Bouvier et al. 2008) and assumed to be equivalent to Bulk Silicate Earth (BSE), can be resolved by projecting the $^{176}Lu/^{177}Hf$ ratio defined by the zircon array to the intersection with the chondritic reference line. This is a form of model age, with the distinction that instead of assuming an average crustal $^{176}Lu/^{177}Hf$ for Hf isotopic evolution of the crustal source, prior to zircon crystallization as is commonly done for model age calculations of detrital zircons, the $^{176}Lu/^{177}Hf$ ratio as defined by the zircon populations within the given rock is used. Model ages are here calculated with reference to CHUR rather than a depleted mantle reference line on the basis of the initial Hf isotopic compositions determined from the oldest, most primitive Eoarchaean tonalites (Hiess et al. 2009), which show no evidence for long term, high Lu-Hf mantle sources.

Data from granitic gneiss sample 248251 ($\varepsilon_{Hf(T)}$ = -0.8±0.8, 3686±22 Ma, ^{176}Lu/^{177}Hf = 0.001) indicate segregation of its source from BSE composition at ~3724 Ma (Fig. 3c), consistent with remelting of 3.72 Ga components of the northern Isua composite ca. 3.7 Ga package (Nutman and Friend, 2009). Therefore, these data supports the earlier interpretation of IGC granite petrogenesis by episodic partial melting of broadly tonalitic grey gneiss sources (Baadsgaard et al. 1986a).

The CHUR model age of A-type granitic augen gneiss G97/111 ($\varepsilon_{Hf(T)}$ = -1.1±0.8, 3635±14 Ma, ^{176}Lu/^{177}Hf = 0.002) is ~3681 Ma (Fig. 3i). This age is consistent with that of components of the surrounding TTG orthogneisses from the IGC gneisses south of the Ameralik Fjord (Nutman et al. 1996, 2000). While a precise source for the augen gneisses from the iron rich suite has not been previously identified, they have been interpreted by Nutman et al. (1984) as products of incomplete mixing between lower crustal melts adjacent to fractionated, mantle-derived basic intrusions.

The range of initial ε_{Hf} values from granodioritic Ikkattoq gneiss sample VM97/01 (-0.5±1.2 to -3.1±4.8) indicates that the zircons were probably derived from the melting of mixed crustal components, with a range of ages sourced from both near-chondritic and low $\varepsilon_{Hf(T)}$ reservoirs. This is in accord with the whole rock ε_{Nd} (2825 Ma) values for this suite, which range from -1.8 to -7.1 (Friend et al., 2009).

The crustal source of migmatite sample 195392 with a youngest 2570±4 Ma component, marginally older than, or coincident with the main QGC intrusion ($\varepsilon_{Hf(T)}$ = -22.6±1.8, ^{176}Lu/^{177}Hf = 0.004) initially segregated from BSE at ~3735 Ma (Fig. 3o). This age is broadly consistent with the timing of formation of surrounding Eoarchaean IGC orthogneisses. The Eoarchaean protolith is directly represented in the sample by inherited zircon cores (e.g. 195392-1.1, 3689±7 Ma, $\varepsilon_{Hf(T)}$ = 0.6±1.2, Fig. 2d). Similar chondritic initial ε_{Hf} compositions are commonly observed within zircon from Eoarchaean meta-tonalite samples in the Nuuk region (Hiess et al. 2009) but are not observed within any younger zircon domains from this sample. The migmatite sample 195392 also contains a significant population of zircon domains of Mesoarchaean age (3032±46 Ma; Fig. 3o), that either reflects a rock component in the migmatite of that age (coeval with the orthogneisses of the Kapisillik or Akia Terranes (Friend and Nutman 2005a; Nutman and Friend 2007; Fig. 1), or alternatively, U-Pb isotopic resetting during recrystallisation of Eoarchaean components in a tectonothermal event at that time. The sub-chondritic $\varepsilon_{Hf(T)}$ values measured in those zircon domains (weighted mean = -14.6±4.0) however indicate that if any Mesoarchaean rocks were involved, these were formed by the remelting of Eoarchaean rocks, and not as new juvenile additions to the crust. A Neoarchaean zircon population at 2726±5 Ma (weighted mean $\varepsilon_{Hf(T)}$ = -19.4±1.0; Fig 3o) possibly relates to zircon recrystallisation and growth during a regional phase of crustal thickening and associated high-grade metamorphism at that time (Friend et al. 1996; Nutman and Friend 2007). While a Neoarchaean population at 2570±4 Ma (weighted mean $\varepsilon_{Hf(T)}$ = -22.6±1.8), representing the age and composition of the granite sheet, largely falls on the same ^{176}Lu/^{177}Hf trajectory intersecting Eoarchaean and Mesoarchaean components (Fig. 3o). The observation that the different zircon populations fall on a single ^{176}Lu/^{177}Hf array implies the QGC largely formed by a relatively “closed” system cannibalistic remelting of the older, surrounding rocks. Two outlier analyses $\varepsilon_{Hf(T)}$ = -14.0±1.4 (2546±31 Ma) and -18.0±0.6 (2572±2 Ma) might represent a minor infiltrating component of young, higher $\varepsilon_{Hf(T)}$ melt during genesis of the QGC.

Homogeneous granite sample 195376 of the QGC with $\varepsilon_{Hf(T)}$ = -14.7±1.7 was probably formed by remelting of juvenile Mesoarchaean and Eoarchaean rocks as represented by zircon inheritance with primitive Mesoarchaean compositions, distinct from un-radiogenic Mesoarchaean components of sample 195392. This demonstrates that the migmatite sample 195392 might not be genetically related to the main body of the QGC. This observation from sample 195376 that the QGC was largely derived by the remelting of regional Eoarchaean (IGC) and Mesoarchaean (possibly Kapisillik or Akia Terrane) banded gneisses is entirely consistent with the earlier Rb-Sr and Pb/Pb whole rock isochrons and interpretation of Moorbath et al. (1981).

The slope of zircon $\varepsilon_{Hf(T)}$ – ^{207}Pb/^{206}Pb arrays for samples of Eoarchaean granite 248251, Eoarchaean augen gneiss granite G97/111 and Neoarchaean migmatite 195392 define ^{176}Lu/^{177}Hf ratios of 0.001, 0.002 and 0.004 respectively, and are lower than that of Eoarchaean tonalites ranging from 0.007 to 0.012 (Hiess et al 2009). This is consistent with the expectation that the granitic crustal reservoirs from which these zircons crystallized would become progressively more fractionated to lower Lu/Hf, following partial melting of a broadly tonalitic source.

Granite 248251 records a ^{176}Lu/^{177}Hf array of 0.001 (Fig. 3c), identical to the ^{176}Lu/^{177}Hf (~0.001) measured within the individual zircon for that sample (Table 1). This indicates for 248251 that ^{207}Pb/^{206}Pb ages younger than the magmatic age of 3686±22 Ma simply represent resetting of the zircon U-Pb systematics (Pb loss) during recrystallisation, without resetting of the Lu-Hf isotopic composition. Augen gneiss granite G97/111 and migmatite 195392 have ^{176}Lu/^{177}Hf arrays of 0.002 and 0.004 (Figs. 3i, 3o) that are slightly higher than the ^{176}Lu/^{177}Hf ratios ~0.0005 measured in zircon (Table 1). This indicates that zircon ^{207}Pb/^{206}Pb ages younger than the magmatic ages could represent metamorphic resetting of zircon U-Pb systematics combined with the growth of new magmatic zircon from remelting the surrounding low Lu/Hf crust. Whole-rock data from 3.81 to 3.70 Ga gneisses from the region record low ^{176}Lu/^{177}Hf compositions of ~0.001 to ~0.002 (Vervoort and Blichert-Toft 1999). The low ^{176}Lu/^{177}Hf ratios in these evolved rocks and zircons represent strong Lu/Hf fractionation in the garnet source region of the initial TTG magmas, further enhanced by progressive remelting of Hf-enriched granitic crust.

Significantly, no samples within this study record distinctly, positive values for initial ε_{Hf}. As their parental melts formed by the remelting of older crustal components, these zircon compositions do not reflect that of the Archaean mantle at the time of their formation. However, they also provide no evidence that those older crustal protolith sources were derived from a radiogenic, high Lu/Hf mantle reservoir with respect to chondrites. Although there is no evidence for super-chondritic Hf isotopic compositions in the samples from southwest Greenland, it is unclear at present how representative the Archaean terranes of Greenland are of wider processes of crustal growth during the Archaean. Consequently, while these data cannot exclude other models, it would support those for slow (Hurley and Rand 1969) or progressive (Bennett 2003) continental crust growth that may have been balanced by rapid subduction recycling.

4.2. The role of fluids in Archaean granitoid complex evolution - Insights from $\delta^{18}O$ compositions of igneous zircons

Zircon from juvenile Eoarchaean tonalite and felsic volcanic samples recorded weighted mean $\delta^{18}O$ values of 5.1±0.4‰ to 4.9±0.7‰ and largely imply derivation from a mantle or gabbroic source, with little influence from weathered crustal material with its elevated $\delta^{18}O$ compositions (Hiess et al. 2009). In contrast, (with exception of augen gneiss granite G97/111 – see below) the younger, more evolved samples in this study typically record mean or weighted mean $\delta^{18}O$ values that are distinctly below the field for mantle zircon with values of 4.2±1.0‰ (3686±22 Ma, Fig. 3b), 4.6±0.6‰ (3690±8 Ma, Fig. 3e), 4.0±0.8‰ (2821±8 Ma, Fig. 3k), 3.7±0.5‰ (3032±46 Ma, Fig. 3n), 4.0±0.5‰ (2726±5 Ma, Fig. 3n), 4.7±0.4‰ (2570±4 Ma, Fig. 3n) and 4.2±0.7‰ (2571±10 Ma, Fig. 3q). These compositions suggest that the parental magmas from which these samples crystallized included rocks that had been hydrothermally altered at high temperatures. In contrast, augen gneiss sample G97/111 is an exception with a $\delta^{18}O$ of 5.8±0.6‰ (3635±14 Ma, Fig. 3h) and lying above the field for mantle zircon but beneath the field for Archaean – Hadean "supracrustal zircon". This suggests the involvement of mildly evolved crustal components during the formation of G97/111, but does not strictly require protoliths that were altered near the Earth's surface by liquid water at low temperatures. The rare, older Eoarchaean inherited zircon components of Eoarchaean granitic gneiss 248251, trondhjemite 248212, and the 3627±38 Ma population from migmatite sample 195392 at 5.0±0.4‰ (Fig. 3n) all preserve values that lie within the range of mantle zircon. Similar mantle-like $\delta^{18}O$ compositions are commonly observed within zircon from Eoarchaean meta-tonalite samples (Hiess et al. 2009) but are not observed within any younger zircon domains from these samples.

4.3. Do these zircons preserve their magmatic $\delta^{18}O$?

It is important to investigate whether the variable zircon $\delta^{18}O$ values measured represent the primary composition of the magmas from which the zircon crystallized, are analytical artifacts, or are products of secondary hydrothermal alteration and isotopic exchange (e.g. Cavosie et al. 2005). In consideration of potential instrumental effects, we note that sample HfO_2 concentrations for the zircons measured here are comparable with those of the standardizing reference materials, suggesting that variable matrix effects within the zircon lattice are not significant (see Online Resource 1). Additionally, zircons recording the entire $\delta^{18}O$ compositional range were measured sequentially during single analytical sessions, arguing against a unidirectional analytical fractionation, related to mount geometry or instrument tuning during a single analytical session. For example, samples G97/111 (6.1±0.3‰, n=8, Online Resource 2b), FC1 (5.3±0.3‰, n=10, Online Resource 2a) and 248212 (4.6±1.1‰, n=4, Online Resource 2b) were all part of analytical session 3. Also, several samples analysed in multiple analytical sessions record the same range of values, indicating the experiments are reproducible (e.g. 248212 in sessions 3 and 4, G97/111 in sessions 1 and 3, 195392 in sessions 6 and 7; Online Resource 2b).

The possibility of post magmatic grain alteration must also be considered. We note that the analysed zircons generally display euhedral habits, well preserved oscillatory growth zonation (e.g. Cavosie et al. 2005) and a high level of U-Pb concordance that is expressed in their coherent initial ε_{Hf} behaviour. Calculated $\varepsilon_{Hf(T)}$ values are highly sensitive to inaccuracy or disturbance in U-Pb systematics, which result in erratic compositions and highly scattered $^{176}Lu/^{177}Hf$ arrays. The presence of such features would also likely indicate disturbance of oxygen isotopic compositions. However for the zircons analysed here, even the inherited Eoarchaean zircon cores typically retain distinct, original, mantle-like compositions e.g. 248251-10.1 (Fig. 2a), 195392-1.1, 195392B-8.2 and 195392B-8.4 (Fig. 2c) characteristic of their assumed tonalitic source rocks (Hiess et al. 2009). This suggests the grains were not subject to pervasive secondary alteration and demonstrates the robustness of the oxygen isotopic values. Inherited Eoarchaean components with lower U and Th concentrations (10 - 100 ppm) are less likely to experience secondary alteration as compared to Mesoarchaean and Neoarchaean overgrowths. However, no correlation exists between $\delta^{18}O$ and U, Th, Th/U, % common ^{206}Pb, and % discordance for any sample (Fig. 4) suggesting that the range in $\delta^{18}O$ cannot be directly associated with differences in radiation dose or U-Th-Pb systematics. Consequently, we contend that the range of compositions measured within the sample zircons accurately reflects that of their primary magmas.

4.4. Comparison between zircon and quartz $\delta^{18}O$

Neoarchaean migmatite sample 195392, which includes components coeval with the QGC, records distinct measured $\delta^{18}O_{Zr}$ values for different zircon age populations (Fig. 3n). The weighted mean composition of the oldest population at 5.0±0.4‰ (3627±38 Ma) lies within the lower limit of the field for mantle zircon. This probably reflects the original composition of an inherited Eoarchaean tonalitic gneiss component within the 195392 migmatite unit. The compositions of Mesoarchaean and Neoarchaean zircon populations at 3.7±0.5‰, 4.0±0.5‰ and 4.7±0.4‰ are systematically lower than those of the inherited Eoarchaean component and imply a different petrogenetic process operating during their crystallization. This is interpreted to be the melting of hydrothermally altered, broadly tonalitic rocks. We assume that the youngest (2570±4 Ma) zircon population at 4.7±0.4‰ was in equilibrium with the rest of the 195392 migmatite during the emplacement, minus unmelted inherited components e.g. zircon cores. Using the empirical zircon – quartz fractionation calibration of Trail et al. (2009) the 2.57 Ga population would correspond to a calculated $\delta^{18}O_{Qtz}$ composition of 7.0±0.4‰. Measured duplicate $\delta^{18}O_{Qtz}$ values of 8.7±0.1‰ and 9.2±0.1‰ indicate a discrepancy of ~1.7 to ~2.2‰ between measured and calculated $\delta^{18}O_{Qtz}$ that is likely to reflect the recystallization of quartz during regional metamorphism (e.g. Valley and Graham 1996; King et al. 1997). Homogeneous Qôrqut granite sample 195376, with a mean $\delta^{18}O_{Zr}$ composition of 4.2±1.2‰ would correspond to a calculated $\delta^{18}O_{Qtz}$ value of 6.5±1.2‰. Duplicate measured $\delta^{18}O_{Qtz}$ at 8.2±0.1‰ and 8.9±0.1‰ again indicates disequilibrium on the order of ~1.7 to ~2.4‰ that is also attributed to quartz recrystallisation. Overall, it may be the case that even the “freshest” Archaean samples reflect the effects of recrystallisation during metamorphism. Under these conditions, highly robust zircon is capable of retaining its primary igneous composition (Page et al. 2007) while other phases such as feldspar and quartz recrystallise during metamorphism, are more prone to diffusive exchange, and will re-equilibrate with the surrounding rock (Wei et al. 2002).

4.5. The generation of low $\delta^{18}O$ magmas

The intrusion of new granitoid magmas can fracture the surrounding country rock and drive groundwater through lateral temperature gradients (Taylor 1977). Low $\delta^{18}O$ meteoric fluids become heated and can undergo isotopic exchange with wall rocks at heterogeneous scales that are dictated by fracture permeability. Convection cells eventually collapse following the crystallization and cooling of the intrusion. In addition, multiple episodes of magmatism can lead to the melting of earlier altered products and the acquisition of averaged compositions from fossilized hydrothermal systems (Bacon et al. 1989; Bindeman et al. 2001, 2008). The significant amount of isotopic and age heterogeneity within some samples from the Greenland suite probably relate to the operation of such open fluid system processes (e.g. assimilation, magma mixing) during zircon crystallization. Previous work on the IGC leucogranites has also provided strong evidence that crystallization took place within a water-rich environment (Nutman and Bridgwater 1986). In such settings and possible analogous ones for the Ikkattoq gneiss, Neoarchaean migmatite and QGC samples, there is a likely potential for large isotopic fractionations and shifts towards low $\delta^{18}O$ magmatic compositions. Low $\delta^{18}O$ magmas can also form by the melting of ^{18}O-depleted oceanic slabs (Eiler 2001). However, whole rock and isotopic compositions from these granitic samples are inconsistent with direct melting of a basaltic source and require an intermediate compositional step matched by the regional tonalites (Brown et al. 1981; Moorbath et al. 1981; Nutman and Bridgwater 1986).

Major Archaean – Proterozoic faults and regional mylonites cut the orthogneiss complexes of the Nuuk Region (Fig. 1). Local hydrothermal alteration is often associated with those major shear zones, as well as other intrusive contacts (Glassley et al. 1984; Nutman 1982). Measured whole rock $\delta^{18}O$ values typically demonstrate significant fractionations within close proximity to these features. For example, emplacement of mid to late Archaean Tarssartôq dikes in the Isua area (possibly equivalent to the Ameralik dike swarms in Godthåbsfjord; Nutman and Bridgwater 1986), results in their host TTG gneisses showing lower $\delta^{18}O$ in proximity to the dikes (Read 1976, Baadsgaard et al. 1986b). Also, an altered mylonite from within the Ataneq fault zone near Isua records a whole rock composition of -1.3‰ (Baadsgaard et al. 1986b). This alteration is attributed to low $\delta^{18}O$ fluids such as meteoric water emanating from such structures (Longstaffe 1979; Baadsgaard et al. 1986b). These relationships provide a clear mechanism by which low $\delta^{18}O$ fluids have been able to access and locally alter the TTG gneisses during the Archaean.

It is also noted that hydrothermal alteration is generally restricted to geothermal systems at relatively shallow crustal levels, above the brittle-ductile transition. Therefore, it could be difficult to reconcile the occurrence of low $\delta^{18}O$ zircon with these processes in mid-crustal levels granitoids. However, these samples are collected from terranes that have been assembled into their current configuration along Neoarchaean mylonites, probably reactivated during several tectonic switching events through the Archaean (Friend et al. 1987, 1988; Nutman et al. 1989; Crowley 2002; Friend and Nutman 2005a; Nutman and Friend 2007). Consequently, it is feasible that the broadly tonalitic protolith sources that these melts were derived from could have been at medium to high crustal levels at some early stage during their history. At lower pressures these rocks may have been exposed to hydrothermal alteration by fluids percolating down from the surface or near surface. The most efficient conduits for this would be major faults with extensional components. Following alteration they could be transported back to mid-crustal levels, prior to the partial melting that formed low $\delta^{18}O$ granitic magmas, which in turn crystallized low $\delta^{18}O$ zircon.

4.6. Worldwide occurrences of low $\delta^{18}O$ magma and zircon, and their petrogenetic significance

Occurrences of low $\delta^{18}O$ (<5‰) zircons are common in the Phanerozoic, but Archaean and Proterozoic zircon with low $\delta^{18}O$ is a significantly minor component of the global zircon $\delta^{18}O$ compilation of Valley et al. (2005), with only a scattering of analyses falling within this compositional range (Fig. 5). Here a new field is established for Archaean "low $\delta^{18}O$ zircon" that falls within a compositional range from $\delta^{18}O$ = 2.0 to 4.0‰. The upper limit is conservatively set to resolve values from that of mantle zircon, given the limited analytical precision of ion probe measurements which are on the order of ±0.5‰ or better. The lower limit to this low $\delta^{18}O$ field may be much lower than 2‰, however Archaean zircon compositions <2‰ have not been reported to date. The prevalence of low $\delta^{18}O$ Greenland zircon values and the absence of mantle-like compositions for the granitic-granodioritic samples <3.7 Ga is striking, particularly in comparison with the Eoarchaean tonalitic dataset of Hiess et al. (2009), in which all zircon falls within error of the mantle field. This suggests a different style of crustal petrogenesis, which facilitated the incorporation of meteoric water and the formation of hydrothermally altered materials, was active during the later parts of the Archaean that is not seen in the earlier dataset. The high $\delta^{18}O$ value of sample G97/111 and others in the global compilation however, indicate that processes involving low $\delta^{18}O$ fluids and magmas were not ubiquitous, and crustal components with $\delta^{18}O$ above the mantle were clearly also involved in Archaean magmatism. The dataset for this study however reinforces the earlier observation in Hiess et al. (2009), that supracrustal materials that had been involved in low temperature weathering cycles near the Earth's surface leading to the production of $\delta^{18}O$ compositions >7.5‰, were not involved to any significant degree in the Archaean magmatism that formed the Greenland suite samples.

Low $\delta^{18}O$ zircons are commonly observed in samples <150 Ma and have generally been targeted for analysis due to the previous identification of their low $\delta^{18}O$ parent magmas (e.g. Gilliam and Valley 1997; Bindeman and Valley 2000, 2001; Monani and Valley 2001). The apparent rarity of low $\delta^{18}O$ magmas and zircon before about 150 Ma may plausibly relate to a preservation or sampling bias (Valley et al. 2005) or alternatively may accurately reflect the rarity of such melt compositions (Balsley and Gregory 1998). In previously studied low $\delta^{18}O$ samples, fractionated oxygen isotopic zircon compositions are typically interpreted to reflect the remelting or assimilation of hydrothermally altered wall-rocks in shallow, sub-volcanic, felsic magma chambers e.g. The British Tertiary Igneous Province (Gilliam and Valley 1997; Monani and Valley 2001), Yellowstone (Bindeman and Valley 2000, 2001) and Mesozoic granitoids of eastern China (Wei et al. 2002).

Modern basalts from Iceland show anomalous $\delta^{18}O$ values that are systematically lower than basalts of other oceanic islands or oceanic ridges, and cannot be explained by processes of secondary alteration (Muehlenbachs et al. 1974). Mechanisms offered to produce these magmas include exchanges with hydrothermally altered rocks or meteoric water, or as the result of a distinct mantle source beneath Iceland (Muehlenbachs et al. 1974). Glaciated Pleistocene silicic volcanic provinces such as Kamchatka and the Aleutians also recorded low $\delta^{18}O$ magmas and phenocrysts (Bindeman et al. 2001, 2004). Here at high-latitudes, shallow hydrothermal systems are interpreted to be charged with highly fractionated, glacially derived, melt waters ($\delta^{18}O$ <-25‰). These extreme values require significantly less fluid-rock interaction to lever the bulk composition of altered wall-rock.

Neoproterozoic igneous zircon, with extremely low $\delta^{18}O$ has also been measured within coesite-bearing Triassic rocks of the Dabie-Sulu terrane, China (Rumble et al. 2002; Zheng et al. 2003, 2004, 2007; Zhao et al. 2008). Despite experiencing ultrahigh pressure metamorphic conditions, the oxygen isotopic value of these zircons has been interpreted to reflect the composition of their primary magmas. In these samples the zircon protolith is believed to have experienced high temperature interaction with glacially derived melt-water formed during Neoproterozoic Snowball Earth events (Rumble et al. 2002). The records of ancient hydrothermal systems preserved in the zircons can thus be used as palaeoclimate proxies.

It is interesting to speculate on the source of low $\delta^{18}O$ Archaean hydrothermal fluids that interacted with Greenland tonalitic protoliths to produce the low $\delta^{18}O$ granitoids. Glacial melt water has been previously argued as an effective agent to charge low $\delta^{18}O$ magmatic systems, and provide a regional fingerprint on rocks, magmas, zircons and other phases (Bindeman et al. 2001, Rumble et al. 2002; Bindeman et al. 2004). In these studies, arguments for glaciated conditions have been substantiated by various other independent lines of evidence. For example, in Kamchatka, several phases of voluminous glaciation during the Pleistocene (Grosswald 1988) are demonstrated to have covered volcanic edifices across the peninsular (Savoskul 1999) and reached the coastline (Prueher and Rea 2001). The hypothesis of a global glaciation during the Cryogenian period has been based on a worldwide association of glacial deposits and limestones on Neoproterozoic platforms, with associated isotopic evidence (Hoffman et al. 1998).

The Earth's surface conditions during the Archaean have been extensively debated (e.g. Knauth and Lowe 2003; Perry and Lefticariu 2003; Kasting and Ono 2006). One argument has suggested the existence of a cold, glaciated climate, forced by a faint young sun (Ringwood 1961; Sagan and Mullen 1972; Zahnle et al. 2007). Other competing environmental factors include a CO_2 and CH_4 rich atmosphere that was outgassed during vigorous phases of volcanic activity (Walker 1977; Kasting 1987, 1993; Kasting et al. 2006) and is suggested to have driven an Archaean temperate or greenhouse Earth. Although it is interesting to speculate on the role of early climate conditions in generating the pervasive and long-lived low $\delta^{18}O$ signatures of Archaean granitoids presented here, the paleolatitude of these Greenland rocks during the Archaean cannot be established, nor can the degree of fluid interaction or δD, to confidently constrain fluid compositions or sources. Therefore we conservatively interpret these signatures as originating in, shallow hydrothermal systems fed by meteoric fluids at moderate temperatures.

4.7. Magmatism during extensional tectonics

Eoarchaean tonalitic magmas from the IGC have been associated with the formation of continental crust at convergent plate boundaries (e.g. Nutman et al. 2007a; Hiess et al. 2009). For example well preserved 3.7 Ga tonalites north of Isua (Nutman and Bridgwater, 1986) are separated from 3.8 Ga tonalites to the south (Nutman et al. 1999) by early Archaean mylonites along the Isua supracrustal belt (Nutman 1984; Nutman et al. 1997). Such crust would be highly unstable following a relaxation of the shortening tectonic regime, leading to orogenic collapse (e.g. Hermann et al. 2001). These processes may be repeated during multiple cycles over the duration of a large collisional event, with such extensional settings known to have high heat flow and granite production by intracrustal melting (e.g. Rubatto et al. 1998; Beltrando et al. 2007).

Within the Isua area, the timing of formation for the ~3.7 Ga grey and ~3.65 Ga white gneisses can be clearly resolved by U-Pb dating (Baadsgaard et al., 1986a). Phases of extensional tectonics and continental breakup can produce abundant mafic magmas that can intrude the crust as dike swarms (McKenzie and Bickle 1988). It has been previously argued that the Inaluk dikes of the Isua region are such evidence for a high heat flow and regional extension during the formation of the granitic white gneisses 3660-3640 Ma (Nutman and Bridgwater 1986; Friend and Nutman 2005b). Extensional tectonics would be highly favorable for the generation of low $\delta^{18}O$ magmas (Taylor 1977) as major faults can act as conduits for meteoric fluids to enter the crust. Crustal thinning can lead to asthenospheric upwelling and the compression of local geotherms that promote melting and metamorphism of the lower crust (Wickham and Oxburgh 1985; Sandiford and Powell 1986). A schematic model depicting the generation of evolved granitoid magmas in the Nuuk region is presented in Figure 6.

An extension related environment has been envisaged for formation of the ~3.64 Ga iron-rich suite (Nutman et al. 1984). Compositionally the suite resembles Proterozoic rapakivi granite-ferrodiorite-norite (anorthosite) associations, which characteristically form in rifted, recently thickened, sialic crust following collisional tectonics (Emslie 1978). This tectonic regime would again provide sufficient heat from the mantle to melt the lower continental crust. Anatectic melts mixed and mingled with residual basic magmas that largely stayed in the ductile zone in the deep crust. The restriction of this suite to the ductile zone may explain why meteoric water had not penetrated to depress $\delta^{18}O$ values. Underplating by a cushion of mafic magma is envisaged and melting of deep crust that may have included some sedimentary rocks.

Other cycles of juvenile crust formation and subsequent differentiation with tectonic switching may be represented later in the Archaean. Dated deformational fabrics in the Kapisillit and Færingehavn areas suggest that during the formation of the QGC, the crust was partitioned by active ductile shear zones with a component of extensional displacement (Nutman and Friend 2007c; Nutman et al. In review). This suggests that ductile deformation and amphibolite facies metamorphism continued until the end of the Neoarchaean and was synchronous with, or outlasted, the intrusion of the QGC.

4.8. Comparison of Archaean and Phanerozoic magmatic styles

Recent studies have reported the combined O and Hf isotopic composition of zircon from classic Phanerozoic I-type plutonic systems in Eastern Australia and New Zealand (Kemp et al. 2007; Bolhar et al. 2008). Granitoids from the Lachlan Fold Belt in southeastern Australia record correlated shifts in $\varepsilon_{Hf(T)}$ and $\delta^{18}O$ within individual suites. Mafic dioritic, basaltic and gabbroic lithologies anchor the arrays at mantle-like $\delta^{18}O$, and chondritic or super-chondritic $^{176}Hf/^{177}Hf$ zircon isotopic compositions. Each suite then progressively trends towards higher $\delta^{18}O$ (>7‰), and sub-chondritic or lower initial ε_{Hf} in their tonalitic and granitic samples. These arrays were interpreted to reflect the assimilation of surrounding ^{18}O-enriched metasedimentary country rocks by the primitive mantle derived melts. It was argued that this provides direct evidence that I-type magmatism drives the coupled growth and differentiation of the continental crust.

The Paleozoic Australian suites demonstrate some overall similar evolutionary behaviour to that seen within the Archaean Greenland samples (Fig. 7). Compositions from both studies become progressively less radiogenic in $\varepsilon_{Hf(T)}$ as the bulk compositions become more evolved, reflecting the incorporation of older, low Lu/Hf crustal materials and they diverge away from mantle $\delta^{18}O$ through time. However, they differ significantly in that the reworked crustal materials from the

Lachlan Fold Belt were sedimentary rocks, none of which were hydrothermally altered prior to magmatism, such that their O isotopic fractionations are in a reversed sense compared to that of most of the Greenland rocks. That is, they trend towards higher $\delta^{18}O$, above mantle values (similar to that of granitic augen gneiss G97/111), rather than the lower $\delta^{18}O$ seen in the granitic, trondhjemitic, granodioritic and migmatitic gneisses of the other Greenland granitic suites (Fig. 7). All arrays are anchored to the mantle-like oxygen and near-chondritic hafnium isotopic composition of the Eoarchaean inherited components reflective of the juvenile tonalitic protolith to the evolved granites. It is emphasized that the Greenland trends of decreasing $\delta^{18}O$ and more negative initial ε_{Hf} are repeated in multiple rock suites spanning over a billion year time span.

Granitoids from the Cretaceous Separation Point Suite of New Zealand record heterogeneous zircon $\varepsilon_{Hf(T)}$ compositions ranging from +12 to -4 units indicating the sources for these magmas were less radiogenic than the depleted mantle at ~120 Ma ($\varepsilon_{Hf(T)}$ = ~+16). Variable $\delta^{18}O$ values range from 8 to 0‰ indicating their magmas incorporated both ^{18}O-enriched supracrustal material, and ^{18}O-depleted country rocks, hydrothermally altered by meteoric water. In this latter respect the New Zealand rocks show clear similarities to the samples from the Greenland suite. The heterogeneity of isotopic compositions within individual samples from the Separation Point Suite has also been associated with open system processes such as assimilation during magma evolution and zircon crystallization.

Although the details of reservoirs contributing to each magmatic system differ from case to case, the data for southwest Greenland samples presented in Hiess et al. (2009) and this study suggest that the styles of crustal petrogenesis operating during the Archaean were different than those on the modern Earth. The rates and styles of crustal recycling and subduction may have been different, with a greater role for extensional tectonic regimes in crustal reworking during the Archaean. This resulted in the more common development of hydrothermal systems associated with felsic magma genesis, and perhaps enhanced by low temperature climatic conditions, lead to the widespread formation of low $\delta^{18}O$ magmas. Early crustal formation and evolution, however, need not be attributed to massive super-event cycles or unusual processes, but rather to progressive episodic behaviour of continental growth and reworking through time.

5. Conclusions

- Initial $\varepsilon_{Hf(T)}$ values for zircons from 3.69 to 2.56 Ga granitic rocks range from chondritic to highly negative values and indicate granitoid formation by the remelting of surrounding TTG rocks and documenting intensive processes of crustal reworking throughout the Archaean.
- Inherited Eoarchaean zircon cores record chondritic initial ε_{Hf} values and mantle-like $\delta^{18}O$ isotopic values, reflecting derivation from surrounding older tonalites. In contrast, younger zircons, recording their host magma composition, diverge from these primitive values.
- Five of six analysed evolved granitoids, spanning a large (>1 billion year) temporal and geographic range, have low $\delta^{18}O$ compared to mantle compositions, indicating the incorporation of an ^{18}O-depleted source component. These are the first reported low $\delta^{18}O$ values from Archaean zircons. The signatures are interpreted to reflect the influence of crustal protoliths that were hydrothermally altered by meteoric fluids.
- Extensional regimes, promoting the formation of hydrothermal cells, are suitable tectonic environments for the generation of the evolved granitic magmas and are a geologically plausible scenario for the origin of the analysed samples.
- Archaean plutonic systems have distinct geochemical differences from those from the Phanerozoic reflecting subtle changes in crust formation and evolution processes through time, with a likely more pronounced role for extensional tectonics in early crustal reworking.

Acknowledgements

We thank two anonymous reviews for helpful comments that improved the clarity of the paper. Apart from VM97/01, the samples were collected during field work funded by ANU or the

Geological Survey of Denmark and Greenland who we thank for permission to publish data on these samples. The late Vic McGregor is acknowledged for collecting sample VM97/01. Clark Friend is acknowledged for providing samples 159352 and 159376. We thank Bud Baadsgaard for supplying zircon separates of 248251 and 248212. All analytical work was supported by the Australian Research Council grants DP0342798 and DP0342794 and was undertaken while Hiess was a PhD student at ANU supported by APA and Jaeger scholarships. We thank Shane Paxton and Jon Mya for zircon separations; Ryan Ickert and Peter Holden for contributions to SHRIMP oxygen analysis development; Malcolm McCulloch for access to the Neptune; Les Kinsley for assistance with running LA-MC-ICPMS; Steve Eggins for providing a template for Hf data reduction; Chuck McGee for technical assistance with LA-ICPMS analysis; Antti Kallio for providing LABRAT software; Yuri Amelin, Bob Rapp, Joerg Herman and Trevor Ireland for helpful discussions. We thank John Eiler, Carsten Munker and Pete Kinny for helpful reviews of an earlier version of this manuscript as a chapter in Hiess' PhD thesis.

References

Amelin Y, Lee D-C, Halliday AN, Pidgeon RT (1999) Nature of the Earth's earliest crust from hafnium isotopes in single detrital zircons. Nature 399:252-255

Baadsgaard H (1973) U-Th-Pb dates on zircons from the early Precambrian Amitsoq Gneisses, Godthaab District, West Greenland. Earth Planet Sci Lett 19:22-28

Baadsgaard H (1976) Further U-Pb dates on zircons from the early Precambrian rocks of the Godthaabsfjord area, West Greenland. Earth Planet Sci Lett 33:261-267

Baadsgaard H (1983) U-Pb isotope systematics on minerals from the gneiss complex at Isukasia, West Greenland. Rapport Grønlands Geologiske Undersøgelse 112:35-42

Baadsgaard H, Nutman AP, Bridgwater D (1986a) Geochronology and isotopic variation of the early Archaean Amitsoq gneisses of the Isukasia area, southern West Greenland. Geochim Cosmochim Acta 50:2173-2183

Baadsgaard H, Nutman AP, Rosing MT, Bridgwater D, Longstaffe FJ (1986b) Alteration and metamorphism of Amitsoq gneisses from the Isukasia area, West Greenland: Recommendations for isotope studies of the early crust. Geochim Cosmochim Acta 50:2165-2172

Bacon CR, Adami LH, Lanphere MA (1989) Direct evidence for the origin of $\delta^{18}O$ silicic magmas: quenched samples of a magma chamber's partially-fused granitoid walls, Crater Lake, Oregon. Earth Planet Sci Lett 96:199-208

Balsley SD, Gregory RT (1998) Low-^{18}O silicic magmas: why are they so rare? Earth Planet Sci Lett 162:123-136

Beltrando M, Hermann J, Lister G, Compagnoni R (2007) On the evolution of orogens: Pressure cycles and deformation mode switches. Earth Planet Sci Lett 256:372-388

Bennett V (2003) Compositional evolution of the mantle. Treatise on Geochem 2:493-519

Bennett VC, Nutman AP, McCulloch MT (1993) Nd isotopic evidence for transient, highly depleted mantle reservoirs in the early history of the Earth. Earth Planet Sci Lett 119:299-317

Bennett VC, Brandon AD, Nutman AP (2007) Coupled ^{142}Nd-^{143}Nd isotopic evidence for Hadean mantle dynamics. Science 318:1907-1910

Bindeman IN, Valley JW (2000) Formation of low-$\delta^{18}O$ rhyolites after caldera collapse at Yellowstone, Wyoming, USA. Geology 28:719-722

Bindeman IN, Valley JW (2001) Low-$\delta^{18}O$ rhyolites from Yellowstone: Magmatic evolution based on analyses of zircon and individual phenocrysts. J Pet 42:1491-1517

Bindeman IN, Fournelle JH, Valley JW (2001) Low-$\delta^{18}O$ tephra from a compositionally zoned magma body: Fisher Caldera, Unimak Island, Aleutians. J Volc Geotherm Res 111:35-53

Bindeman IN, Ponomareva VV, Bailey JC, Valley JW (2004) Volcanic arc of Kamchatka: a province with high-$\delta^{18}O$ magma sources and large-scale $^{18}O/^{16}O$ depletion of the upper crust. Geochim Cosmochim Acta 68:841-865

Black LP, Gale NH, Moorbath S, Pankhurst RJ, V.R. M (1971) Isotopic dating of very early Precambrian amphbolite facies gneisses from the Godthaab district, West Greenland. Earth Planet Sci Lett 12:245-259

Bolhar R, Weaver SD, Whitehouse MJ, Palin JM, Woodhead JD, Cole JW (2008) Sources and evolution of arc magmas inferred from coupled O and Hf isotope systematics of plutonic zircons from the Cretaceous Separation Point Suite (New Zealand). Earth Planet Sci Lett 268:312-324

Bouvier A, Vervoort JD, Patchett J (2008) The Lu-Hf and Sm-Nd isotopic composition of CHUR: Constraints from unequilibrated chondrites and implications for the bulk composition of the terrestrial planets. Earth Planet Sci Lett 273:48-57

Brown M, Friend CRL, McGregor VR, Perkins WT (1981) The late Archaean Qôrqut Granite Complex of southern West Greenland. J Geophys Res 86:10617-10632

Cavosie AJ, Valley JW, Wilde SA, E.I.M.F. (2005) Magmatic $\delta^{18}O$ in 4400-3900 Ma detrital zircons: A record of the alteration and recycling of crust in the Early Archean. Earth Planet Sci Lett 235:663-681

Chadwick B, Nutman AP (1979) Archaean structural evolution in the northwest of the Buksefjorden region, southern West Greenland. Precambrian Res 9:199-226

Cherniak DJ, Watson EB (2000) Pb diffusion in zircon. Chem Geol 172:5-24

Cherniak DJ, Watson EB (2003) Diffusion in zircon. In: Hanchar JM, Hoskin PWO (eds) Zircon. Reviews in Mineralogy and Geochemistry, vol 53. pp 113-143

Cherniak DJ, Watson EB (2007) Ti Diffusion in zircon. Chem Geol 242:470-483

Cherniak DJ, Hanchar JM, Watson EB (1997a) Diffusion of tetravalent cations in zircon. Contrib Mineral and Petrol 127:383-390

Cherniak DJ, Hanchar JM, Watson EB (1997b) Rare-earth diffusion in zircon. Chem Geol 134:289-301

Corfu F, Hanchar JM, Hoskin PWO, Kinny PD (2003) Atlas of zircon textures. In: Hanchar JM, Hoskin PWO (eds) Zircon. Reviews in Mineralogy and Geochemistry, vol 53. pp 468-500

Crowley JL (2002) Testing the model of late Archean terrane accretion in southern West Greenland: a comparison of the timing of geological events across the Qarliit Nunaat Fault, Buksefjorden region. Precamb Res 116:57-79

Crowley JL, Myers JS, Dunning GR (2002) Timing and nature of multiple 3700–3600 Ma tectonic events in intrusive rocks north of the Isua greenstone belt, southern West Greenland. GSA Bull 114:1311-1325

Eiler JM (2001) Oxygen isotope variations of basaltic lavas and upper mantle rocks. In: Valley JW, Cole DR (eds) Stable Isotope Geochemistry. Reviews in Mineralogy and Geochemistry, vol 43. pp 319-364

Emslie RT (1978) Anorthosite massifs, rapakivi granites, and late Proterozoic rifting of North America. Precamb Res 7:61-98

Friend CRL, Nutman AP (2005a) New pieces to the Archaean terrane jigsaw puzzle in the Nuuk region, southern West Greenland: steps in transforming a simple insight into a complex regional tectonothermal model. J Geol Soc London 162:147-162

Friend CRL, Nutman AP (2005b) Complex 3670-3500 Ma orogenic episodes superimposed on juvenile crust accreted between 3850 and 3690 Ma, Itsaq Gneiss Complex, southern West Greenland. J Geol 113:375-397

Friend CRL, Brown M, Perkins WT, Burwell ADM (1985) The geology of the Qorqut granite complex north of Qorqut, Godthabsfjord, southern West Greenland. Bulletin Grønlands Geologiske Undersøgelse 151, pp 43

Friend CRL, Nutman AP, McGregor VR (1987) Late-Archaean tectonics in the Faeringehavn-Tre Brodre area, south of Buksefjorden, southern West Greenland. J Geol Soc London 144:369-376

Friend CRL, Nutman AP, McGregor VR (1988) Late Archaean terrane accertion in the Godthåb region, southern West Greenland. Nature 355:535-538

Friend CRL, Nutman AP, Baadsgaard H, Kinny PD, McGregor VR (1996) Timing of late Archaean terrane assembly, crustal thickening and granite emplacement in the Nuuk region, southern West Greenland. Earth Planet Sci Lett 142:353-365

Friend CRL, Nutman AP, Baadsgaard H, Duke MJ (2009) The whole rock Sm–Nd 'age' for the 2825 Ma Ikkattoq gneisses (Greenland) is 800 Ma too young: Insights into Archaean TTG petrogenesis. Chem Geol 261:61-75

Garde AA, Friend CRL, Marker M, Nutman AP (2000) Rapid maturation and stabilisation of Middle Archaean continental crust: the Akia terrane, southern West Greenland. Bull Geol Soc Denmark 47:1-27

Gilliam CE, Valley JW (1997) Low $\delta^{18}O$ magma, Isle of Skye, Scotland: Evidence from zircons. Geochim Cosmochim Acta 61:4975-4981

Glassley WE, Bridgwater D, Konnerup-Madsen J (1984) Nitrogen in fluids effecting retrogression of granulite facies gneisses: a debatable mantle connection. Earth Planet Sci Lett 70:417-425

Griffin WL, McGregor VR, Nutman A, Taylor PN, Bridgwater D (1980) Early Archaean granulite-facies metamorphism south of Ameralik, West Greenland. Earth Planet Sci Lett 50:59-74

Grosswald MG (1998) Late-Weichselian ice sheets in Arctic and Pacific Siberia. Quat Int 45/46:3-18

Hermann J, Rubatto D, Korsakov A, Shatsky VS (2001) Multiple zircon growth during fast exhumation of diamondiferous, deeply subducted continental crust (Kokchetav Massif, Kazakhstan). Contrib Mineral Petrol 141:66-82

Hiess J, Bennett VC, Nutman AP, Williams IS (2009) In situ U–Pb, O and Hf isotopic compositions of zircon and olivine from Eoarchaean rocks, West Greenland: New insights to making old crust. Geochim Cosmochim Acta 73:4489-4516

Hoffman PF, Kaufman AJ, Halverson GP, Schrag DP (1998) A Neoproterozoic Snowball Earth. Science 281:1342-1346

Honda M, Nutman AP, Bennett VC (2003) Xenon compositions of magmatic zircons in 3.64 and 3.81 Ga meta-granitoids from Greenland; a search for extinct ^{244}Pu in ancient terrestrial rocks. Earth Planet Sci Lett 207:69-82

Hurley PM, Rand JR (1969) Pre-drift continental nuclei. Science 164:1229-1242

Ireland TR, Williams IS (2003) Considerations in Zircon Geochronology by SIMS. In: Hanchar JM, Hoskin PWO (eds) Zircon. Reviews in Mineralogy and Geochemistry, vol 53. pp 215-241

Kasting JF (1987) Theoretical constraints on oxgen and carbon dioxide concentrations in the Precambrian atmosphere. Precamb Res 34:205-229

Kasting JF (1993) Earth's Early Atmosphere. Science 259:920-926

Kasting JF, Ono S (2006) Palaeoclimates: the first two billion years. Phil Trans Royal Soc London B 361:917-929

Kasting JF, Howard MT, Wallmann K, Veizer J, Shields G, Jaffrés J (2006) Paleoclimates, ocean depth, and the oxygen isotopic composition of seawater. Earth Planet Sci Lett 252:82-93

Kemp AIS, Hawkesworth CJ, Foster GL, Paterson BA, Woodhead JD, Hergt JM, Gray CM, Whitehouse MJ (2007) History of Granitic Rocks from Hf-O Isotopes in Zircon. Science 315:980-983

King EM, Barrie CT, Valley JW (1997) Hydrothermal alteration of oxygen isotope ratios in quartz phenocrysts, Kidd Creek mine, Ontario: Magmatic values are preserved in zircon. Geology 25:1079-1082

Kinny PD, Maas R (2003) Lu-Hf and Sm-Nd isotope systems in zircon. In: Hanchar JM, Hoskin PWO (eds) Zircon. Reviews in Mineralogy and Geochemistry, vol 53. pp 327-341

Knauth LP, Lowe DR (2003) High Archean climatic temperature inferred from oxygen isotope geochemistry of cherts in the 3.5 Ga Swaziland Supergroup, South Africa. Geol Soc Am Bull 115:566-580

Longstaffe FJ (1979) The oxygen isotope geochemistry of Archaean granitoids. In: Barker F (ed) Trondhjemites and Related Rocks, vol. Elsevier, Amsterdam, pp 363-399

McGregor VR (1973) The early Precambrian gneisses of the Godthaab district, West Greenland. Phil Trans Royal Soc London A 273:343-358

McGregor VR, Friend CRL, Nutman AP (1991) The late Archaean mobile belt through Godthabsfjord, southern West Greenland: a continent–continent collision zone? Geol Soc Denmark Bull 39

McKenzie D, Bickle MJ (1988) The volume and composition of melt generated by extension of the lithosphere. J Pet 29:625-679

Monani S, Valley JW (2001) Oxygen isotope ratios of zircon: magma genesis of low $\delta^{18}O$ granites from the British Tertiary Igneous Province, western Scotland. Earth Planet Sci Lett 184:377-392

Moorbath S (1975) Evolution of Precambrian crust from srtontium isotope evidence. Nature 254:395-398

Moorbath S, O'Nions RK, Pankhurst RJ, Gale NH, McGregor VR (1972) Further rubidium-strontium age determinations on the very early Precambrian rocks of Godthåb district: West Greenland. Nature, Phys Sci 240:78-82

Moorbath S, Taylor PN, Goodwin R (1981) Origin of granitic magma by crustal remobilisation: Rb-Sr and Pb/Pb geochronology and isotope geochemistry of the late Archaean Qôrqut Granite Complex of southern West Greenland. Geochim Cosmochim Acta 45:1051-1060

Moorbath S, Taylor PN, Jones NW (1986) Dating the oldest terrestrial rocks — fact and fiction. Chem Geol 57:63-86

Muehlenbachs K, Anderson ATJ, Sigvaldason GE (1974) Low-O^{18} basalts from Iceland. Geochim Cosmochim Acta 38:577-588

Nutman AP (1982) Further work on the early Archaean rocks of the Isukasia area, southern West Greenland. Rapport Grønlands Geologiske Undersøgelse 110:49-54

Nutman AP (1984) Early Archaean crustal evolution of the Isukasia area, southern West Greenland. In: Kroner GR (ed) Precambrian tectonics illustrated, vol. E. Scheizerbart'sche Verlagsbuchhandlung, Stuttgart, pp 79-94

Nutman AP, Bridgwater D (1986) Early Archaean Amitsoq tonalites and granites of the Isukasia area, southern West Greenland; development of the oldest-known sial. Contrib Mineral Petrol 94:137-148

Nutman AP, Friend CRL (2007) Adjacent terranes with ca. 2715 and 2650 Ma high-pressure metamorphic assemblages in the Nuuk region of the North Atlantic Craton, southern West Greenland: Complexities of Neoarchaean collisional orogeny. Precamb Res 155:159-203

Nutman AP, Friend CRL (2009) New 1:20,000 scale geological maps, synthesis and history of investigation of the Isua supracrustal belt and adjacent orthogneisses, southernWest Greenland: A glimpse of Eoarchaean crust formation and orogeny. Precamb Res 172: 189-211

Nutman AP, Bridgwater D, Dimroth E, Gill RCO, Rosing M (1983) Early (3700 Ma) Archaean rocks of the Isua supracrustal belt and adjacent gneisses. Rapport Grønlands Geologiske Undersøgelse 112:5-22

Nutman AP, Bridgwater D, Fryer Brian J (1984) The iron-rich suite from the Amitsoq gneisses of southern West Greenland; early Archaean plutonic rocks of mixed crustal and mantle origin. Contrib Mineral and Petrol 87:24-34

Nutman AP, Friend CRL, Baadsgaard H, McGregor VR (1989) Evolution and assembly of Archean gneiss terranes in the Godthåbsfjord region, southern west Greenland: structural, metamorphic and isotopic evidence. Tectonics 8:573-589

Nutman AP, Friend CRL, Kinny PD, McGregor VR (1993) Anatomy of an Early Archean gneiss complex: 3900 to 3600 Ma crustal evolution in southern West Greenland. Geology 21:415-418

Nutman AP, McGregor VR, Friend CRL, Bennett VC, Kinny PD (1996) The Itsaq Gneiss Complex of southern West Greenland; the world's most extensive record of early crustal evolution (3900-3600 Ma). Precamb Res 78:1-39

Nutman AP, Bennett VC, Friend CRL, Rosing MT (1997) ~ 3710 and ≥ 3790 Ma volcanic sequences in the Isua (Greenland) supracrustal belt; structural and Nd isotope implications. Chem Geol 141:271-287

Nutman AP, Bennett VC, Friend CRL, Norman MD (1999) Meta-igneous (non-gneissic) tonalites and quartzdiorites from an extensive ca. 3800 Ma terrain south of the Isua supracrustal belt, southern West Greenland; constraints on early crust formation. Contrib Mineral Petrol 137:364-388

Nutman AP, Bennett VC, Friend CRL, McGregor VR (2000) The early Archaean Itsaq Gneiss Complex of southern West Greenland; the importance of field observations in interpreting age and isotopic constraints for early terrestrial evolution. Geochim Cosmochim Acta 64:3035-3060

Nutman AP, Friend CRL, Bennett VC (2002) Evidence for 3650–3600 Ma assembly of the northern end of the Itsaq Gneiss Complex, Greenland: Implication for early Archaean tectonics. Tectonics no.1, 10.1029/2000TC001203

Nutman AP, Friend CRL, Horie K, Hidaka H (2007a) The Itsaq Gneiss Complex of southern West Greenland and the construction of Eoarchaean crust at convergent plate boundaries. In: van Kranendonk MJ, Smithies RH, Bennett VC (eds) Earth's Oldest Rocks, vol. Elsevier, Amsterdam, pp 187-218

Nutman AP, Bennett VC, Friend CRL, Horie K, Hidaka H (2007b) ~3,850 Ma tonalites in the

Nuuk region, Greenland: geochemistry and their reworking within an Eoarchaean gneiss complex. Contrib Mineral Petrol 154:385-408

Nutman AP, Christiansen O, Friend CRL (2007c) 2635 Ma amphibolite facies mineralisation near a terrane boundary (suture?) on Storø, Nuuk region, southern West Greenland. Precambrian Research 159:19-32

Nutman AP, Friend CRL, Hiess J (In review) Archaean gneiss complex in West Greenland: Intra-continental tectonic partitioning with granite intrusion following crust formation by amalgamation of arc complexes. American Journal of Science (accepted February 2010 pending revision)

O'Nions RK, Pankhurst RJ (1978) Early Archaean rocks and geochemical evolution of the Earth's crust. Earth Planet Sci Lett 38:211-236

Page FZ, Ushikubo T, Kita NT, Riciputi LR, Valley JW (2007) High-precision oxygen isotope analysis of picogram samples reveals 2 µm gradients and slow diffusion in zircon. Am Mineral 92:1772-1775

Parrish RR, Noble SR (2003) Zircon U-Th-Pb geochronology by isotope dilution - thermal ionization mass spectrometry (ID-TIMS). In: Hanchar JM, Hoskin PWO (eds) Zircon. Reviews in Mineralogy and Geochemistry, vol 53. pp 183-213

Peck WH, Valley JW, Wilde SA, Graham CM (2001) Oxygen isotope ratios and rare earth elements in 3.3 to 4.4 Ga zircons: Ion microprobe evidence for high $\delta^{18}O$ continental crust and oceans in the Early Archean. Geochim Cosmochim Acta 65:4215-4229

Perry ECJ, Lefticariu L (2003) Formation and geochemistry of Precambrian cherts. Treatise on Geochemistry 7:99-113

Prueher LM, Rea DK (2001) Volcanic triggering of late Pliocene glaciation: evidence from the flux of volcanic glass and ice rafted debris to the North Pacific Ocean. Paleogeography, Paleoclimatology, Paleoecology 173:215-230

Read DL (1976) Oxygen isotope composition of the 3800 m.y. old Isua gneiss of Southwest Greenland. In, vol M.Sc. Nothern Illinois University, DeKalb, p 47

Ringwood AE (1961) Changes in solar luminosity and some possible terrestrial consequences. Geochim Cosmochim Acta 21:295-296

Rubatto D, Gebauer D, Fanning M (1998) Jurassic formation and Eocene subduction of the Zermatt-Saas-Fee ophiolites: implications for the geodynamic evolution of the Central and Western Alps. Contrib Mineral Petrol 132:269-287

Rumble D, Giorgis D, Ireland T, Zhang Z, Xy H, Yuo TF, Yang J, Xu Z, Liou JG (2002) Low $\delta^{18}O$ zircons, U-Pb dating, and the age of the Qinglongshan oxygen and hydrogen isotope anomaly near Donghai in Jiangsu Province, China. Geochim Cosmochim Acta 66:2299-2306

Sagan C, Mullen G (1972) Earth and Mars: Evolution of Atmospheres and Surface Temperatures. Science 177:52-56

Sandiford M, Powell R (1986) Deep crustal metamorphism during continental extension: modern and ancient axamples. Earth Planet Sci Lett 79:151-158

Savoskul OS (1999) Holocene Glacier Advances in the Headwaters of Sredniaya Avacha, Kamchatka, Russia. Quat Res 52:14-26

Taylor HPJ (1977) Water/rock interactions and the origin of H2O in granitic batholiths: Thirtieth William Smith lecture. J Geol Soc London 133:509-558

Taylor PN, Moorbath S, Goodwin R, Petrykowski AC (1980) Crustal contamination as an indicator of the extent of early Archaean continental crust: Pb isotopic evidence from the late Archaean gneisses of West Greenland. Geochim Cosmochim Acta 44: 1437-1453

Trail D, Bindeman IN, Watson EB, Schmitt AK (2009) Experimental calibration of oxygen isotope fractionation between quartz and zircon. Geochim Cosmochim Acta 73: 7110-7126

Valley JW (2003) Oxygen isotopes in zircon. In: Hanchar JM, Hoskin PWO (eds) Zircon. Reviews in Mineralogy and Geochemistry, vol 53. pp 343-385

Valley JW, Graham CM (1996) Ion microprobe analysis of oxygen isotope ratios in quartz from Skye granite: healed micro-cracks, fluid flow, and hydrothermal exchange. Contrib Mineral Petrol 124:225-234

Valley JW, Kinny PD, Schulze DJ, Spicuzza MJ (1998) Zircon Megacrysts from Kimberlite: Oxygen Isotope Variability Among Mantle Melts. Contrib Mineral Petrol 133:1-11

Valley J, Lackey J, Cavosie A, Clechenko C, Spicuzza M, Basei M, Bindeman I, Ferreira V, Sial A, King E, Peck W, Sinha A, Wei C (2005) 4.4 billion years of crustal maturation: oxygen isotope ratios of magmatic zircon. Contrib Mineral Petrol 150:561-580

Vervoort JD, Bilchert-Toft J (1999) Evolution of the depleted mantle: Hf isotope evidence from juvenile rocks through time. Geochim Cosmochim Acta 63: 533–556

Vervoort JD, Patchett PJ, Geherels GE, Nutman AP (1996) Constraints on early differentiation from hafnium and neodymium isotopes. Nature 379: 624-627

Walker JCG (1977) Evolution of the atmosphere, vol. Macmillan, New York

Watson EB, Cherniak DJ (1997) Oxygen diffusion in zircon. Earth Planet Sci Lett 148:527-544

Wei C-S, Zheng Y-F, Zhao Z-F, Valley JW (2002) Oxygen and neodymium isotope evidence for recycling of juvenile crust in northeast China. Geology 30:375-378

Wells PRA (1976) Late Archean Metamorphism in the Buksefjorden Region, Southwest Greenland. Contrib Mineral Petrol 56:229-242

Wickham SM, Oxburgh ER (1985) Continental rifts as a setting for regional metamorphism. Nature 318:330-333

Zahnle K, Arndt N, Cockell C, Halliday A, Nisbet E, Selsis F, Sleep NH (2007) Emergence of a Habital Planet. Space Sci Rev 129:35-78

Zhao Z-F, Zheng Y-F, Wei C-S, Chen F-K, Liu X, Wu F-Y (2008) Zircon U–Pb ages, Hf and O isotopes constrain the crustal architecture of the ultrahigh-pressure Dabie orogen in China. Chem Geol 253:222-242

Zheng Y-F, Gong B, Zhao Z-F, Li Y-L (2003) Two types of gneisses associated with eclogite at Shuanghe in the Dabie terrane: carbon isotope, zircon U–Pb dating and oxygen isotope. Lithos 70:321-343

Zheng Y-F, Wu Y-B, Chen F-K, Gong B, Li Y-L, Zhao Z-F (2004) Zircon U-Pb and oxygen isotope evidence for a large-scale ^{18}O depletion event in igneous rocks during the Neoproterozoic. Geochim Cosmochim Acta 68:4145-4165

Zheng Y-F, Zhang S-B, Zhao Z-F, Wu Y-B, Li Y-L, Li Z, Wu F-Y (2007) Contrasting zircon Hf and O isotopes in the two episodes of Neoproterozoic granitoids in South China: Implications for growth and reworking of continental crust. Lithos 96:127-150

Table Caption

Table 1 Summary of zircon and quartz U-Pb, $\delta^{18}O$ and $\varepsilon_{Hf(T)}$ results with sample weighted mean and mean ages and compositions

Figure Captions

Fig. 1 Sketch geological map of Nuuk region, southern West Greenland with major lithological units and samples localities indicated. Adapted after Nutman et al. (2007b)

Fig. 2 Representative CL images recording analysis locations, $^{207}Pb/^{206}Pb$ crystallization ages, % discordance, Th/U ratios, $\delta^{18}O$, $\varepsilon_{Hf(T)}$ for: a) White gneisses 248251 and 248212, b) Augen granite G97/111, c) Ikkattoq gneiss VM97/01 and d) Qôrqut Granite Complex samples 195392 and 195376. Scale bars are 100µm

Fig. 3 Tera-Wasserburg diagrams and plots of $\delta^{18}O$ and $\varepsilon_{Hf(T)}$ against corresponding $^{207}Pb/^{206}Pb$ crystallisation ages for zircon analysis. Tera-Wasserburg data-point error crosses are at the 2σ level. $\delta^{18}O$ and $\varepsilon_{Hf(T)}$ uncertainties are 1σ and 2σ respectively while $^{207}Pb/^{206}Pb$ ages are at 1σ level. Fields for mantle zircon, Archaean - Hadean "supracrustal zircon" and CHUR from Valley et al. (1998), Cavosie et al. (2005) and Bouvier et al. (2008). $^{176}Lu/^{177}Hf$ ratios for samples were determined by linear regression with R^2 values indicating correlation coefficients

Fig. 4 Plots of $\delta^{18}O$ against U-Th-Pb systematics for all samples. The lack of correlations is evidence that the $\delta^{18}O$ values are primary features and not the result of alteration

Fig. 5 $\delta^{18}O$ values of dated zircon from Archaean Greenland in this study, Hiess et al. (2009) and the global compilation of Valley et al. (2005). Field for mantle zircon from Valley et al. (1998) and Archaean - Hadean "supracrustal zircon" from Cavosie et al. (2005). A new field is defined for Archaean "low $\delta^{18}O$ zircon"

Fig. 6 Schematic diagram depicting key components and processes involved in the generation of evolved granitoids in the Nuuk region

Fig. 7 Correlated shifts in $\delta^{18}O$ and $\varepsilon_{Hf(T)}$ for Greenland zircon. Fields for mantle zircon from Valley et al. (1998) and CHUR from Bouvier et al. (2008). Greenland sample trends anchored at compositions from Eoarchaean tonalites of Hiess et al. (2009). Comparative isotopic arrays for zircons from Phanerozoic granitoid suites from Kemp et al. (2007) in grey

Online Resource Captions

Online Resource 1 Analytical methods and the statistical treatment of data

Online Resource 2a Zircon reference materials $\delta^{18}O$

Online Resource 2b Zircon unknowns $\delta^{18}O$

Online Resource 2c Zircon reference materials $\delta^{18}O$ and ε_{Hf}

Online Resource 2d Zircon reference materials ε_{Hf}

Online Resource 2e Zircon unknowns materials ε_{Hf}

Online Resource 2f Zircon reference materials ε_{Hf}

Online Resource 3 Zircon characteristics and main geochemical results

Table 1 Summary of zircon and quartz U-Pb, $\delta^{18}O$ and $\varepsilon_{Hf(T)}$ results with sample weighted mean and mean ages and compositions

Sample Spot	Grain	U (ppm)	Th (ppm)	Th/U	Comm. ^{206}Pb%	$^{238}U/^{206}Pb$	1σ err	$^{207}Pb/^{206}Pb$	1σ err	$^{207}Pb/^{206}Pb$ Age (Ma)	1σ err	Disc. (%)	$\delta^{18}O_{VSMOW}$ (‰)[a]	1σ err	$^{176}Lu/^{177}Hf$	2σ err[b]	$^{176}Hf/^{177}Hf$ Meas.	2σ err[b]	ε_{Hf} Init.[c]	2σ err	Abs. err
248251 Granitic gneiss (65°07.72'N 49°57.89'W)																					
1.1	p m os	2556	850	0.34	0.01	1.346	0.014	0.3234	0.0013	3586	6	0									
3.1[d]	p m os	630	56	0.09	0.10	1.432	0.017	0.3419	0.0007	3671	3	8	3.1	0.3	0.000950	25	0.280417	32	-1.8	1.1	2.4
4.1[d]	p m os	132	48	0.37	0.06	1.444	0.016	0.3477	0.0011	3697	5	9	4.2	0.3	0.001008	45	0.280428	39	-1.0	1.4	2.5
8.2[d]	p f os	211	33	0.16	0.08	1.401	0.016	0.3450	0.0009	3685	4	6			0.000537	14	0.280412	40	-0.7	1.4	2.5
10.1[d]	p c os	231	104	0.46	0.06	1.299	0.014	0.3517	0.0010	3715	4	1	5.4	0.3	0.001151	17	0.280469	37	0.5	1.3	2.5
10.2[d]	p m os	722	93	0.13	0.02	1.300	0.014	0.3504	0.0005	3709	2	1	4.3	0.3	0.001160	94	0.280454	32	-0.2	1.2	2.4
11.1	p c h	199	22	0.10	0.15	1.553	0.018	0.2977	0.0009	3458	5	8	3.6	0.3							
12.1	p e os	632	119	0.19	0.06	1.572	0.017	0.2699	0.0006	3305	4	4	2.3	0.3	0.001350	26	0.280427	31	-10.9	1.1	2.4
13.1[d]	p m os	218	64	0.30	0.05	1.370	0.015	0.3492	0.0009	3704	4	5			0.000792	27	0.280417	33	-0.7	1.2	2.4
13.2[d]	p c os	847	257	0.31	0.07	1.300	0.023	0.3390	0.0016	3658	7	-1									
14.1[d]	p m os	357	160	0.46	0.12	1.425	0.015	0.3499	0.0007	3707	3	8			0.000850	31	0.280430	49	-0.3	1.7	2.7
18.1[d]	an m h	824	2	0.00	0.11	1.323	0.015	0.3386	0.0007	3656	3	1			0.000827	8	0.280414	25	-2.0	0.9	2.3
20.1	an c t	3960	944	0.25	0.04	1.438	0.016	0.2864	0.0008	3398	4	0			0.000884	50	0.280445	41	-7.0	1.5	2.6
22.1[d]	p e os	763	47	0.06	0.02	1.307	0.014	0.3457	0.0005	3688	2	1			0.001217	31	0.280471	43	-0.2	1.5	2.6
23.1[d]	an m os	144	30	0.21	0.15	1.455	0.017	0.3384	0.0011	3655	5	8			0.001471	137	0.280479	41	-1.3	1.5	2.6
Weighted Mean[e] ± 95% confidence limits or Mean[f] ± 1σ										3686[f]	22		4.2[f]	1.0					-0.8[e]		0.8
n										11 of 15			4 of 6						10 of 12		
MSWD																			0.4		
248212 Trondhjemitic gneiss (65°06.15'N 50°01.50'W)																					
1.1[d]	p c os	215	104	0.50	0.01	1.329	0.016	0.3465	0.0008	3692	3	2	5.0	0.3	0.001108	30	0.280408	34	-2.1	1.2	2.4
2.1[d]	p c os	771	261	0.35	0.01	1.280	0.015	0.3435	0.0008	3678	3	-1	5.2	0.3	0.001014	16	0.280449	35	-0.7	1.3	2.4
3.1[d]	p m os	350	28	0.08	0.01	1.419	0.017	0.3455	0.0006	3687	3	7	3.6	0.3	0.000659	3	0.280366	31	-2.5	1.1	2.4
4.1	p m os	2032	272	0.14	0.00	1.424	0.016	0.3277	0.0010	3607	5	5	4.8	0.3	0.001022	97	0.280354	34	-5.8	1.2	2.4
5.1[d]	p m os	232	85	0.38	0.01	1.328	0.016	0.3488	0.0007	3702	3	2	4.3	0.4	0.001040	20	0.280431	31	-0.9	1.1	2.4
6.1[d]	an f os	128	71	0.57	0.03	1.313	0.017	0.3458	0.0009	3688	4	1	5.1	0.4	0.000609	17	0.280434	33	0.0	1.2	2.4
7.1	an m os	172	78	0.47	0.04	1.362	0.018	0.3305	0.0027	3619	12	2	5.0	0.4	0.001171	58	0.280469	36	-1.8	1.3	2.5
9.1[d]	an m os	225	92	0.42	0.02	1.234	0.021	0.3473	0.0009	3695	4	-3	4.8	0.4	0.001018	28	0.280452	31	-0.2	1.1	2.4

Sample Spot	Grain	U (ppm)	Th (ppm)	Th/U	Comm. ^{206}Pb%	$^{238}U/^{206}Pb$	1σ err	$^{207}Pb/^{206}Pb$	1σ err	$^{207}Pb/^{206}Pb$ Age (Ma)	1σ err	Disc. (%)	$\delta^{18}O_{VSMOW}$ (‰)[a]	1σ err	$^{176}Lu/^{177}Hf$	2σ err[b]	$^{176}Hf/^{177}Hf$ Meas.	2σ err[b]	ε_{Hf} Init.[c]	2σ err	Abs. err
Weighted Mean[e] ± 95% confidence limits or Mean[f] ± 1σ										3690[f]	8		4.6[f]	0.6					-1.1 [e]		1.0
n										6 of 8			6 of 8						6 of 8		
MSWD																			0.7		
G97/111 Granitic augen gneiss (64°01.96'N 51°36.60'W)																					
1.1[d]	an m os	24	18	0.77	0.00	1.341	0.029	0.3313	0.0021	3623	10	1	6.6	0.3	0.000602	5	0.280474	27	0.0	1.0	2.3
1.3[d]	an m os	323	158	0.51	0.01	1.317	0.015	0.3284	0.0007	3610	3	-1									
2.1[d]	an m os	225	104	0.48	0.03	1.445	0.017	0.3319	0.0011	3626	5	7	4.7	0.3	0.000663	28	0.280456	27	-0.8	0.9	2.3
3.1[d]	an m os	323	166	0.53	0.06	1.387	0.016	0.3353	0.0008	3641	4	4	6.0	0.3	0.000494	11	0.280430	22	-0.9	0.8	2.2
4.1[d]	p m os	178	112	0.65	0.01	1.308	0.016	0.3343	0.0009	3637	4	-1			0.000642	4	0.280445	25	-0.9	0.9	2.3
B-1.1[d]	an f m os	225	112	0.51	0.02	1.326	0.011	0.3369	0.0008	3649	4	1	6.5	0.3	0.000712	24	0.280419	33	-1.7	1.2	2.4
B-2.1[d]	an m os	89	40	0.46	0.05	1.390	0.014	0.3339	0.0015	3635	7	4	5.8	0.3	0.000609	4	0.280436	31	-1.2	1.1	2.4
B-3.1[d]	an e os	160	107	0.69	0.04	1.304	0.012	0.3384	0.0010	3656	5	0	5.6	0.3	0.000587	5	0.280413	29	-1.4	1.0	2.3
B-4.1	an m os	190	89	0.48	0.02	1.500	0.012	0.3009	0.0008	3475	4	6	6.6	0.3	0.000591	4	0.280432	34	-5.0	1.2	2.4
B-5.1[d]	p f m os	327	148	0.47	0.19	1.337	0.010	0.3343	0.0008	3637	4	1	5.6	0.3	0.000890	6	0.280441	26	-1.6	0.9	2.3
B-6.1	an e os	175	92	0.54	0.03	1.391	0.012	0.3254	0.0009	3595	4	3	6.2	0.3	0.000626	24	0.280434	35	-2.2	1.2	2.4
B-7.1	an m os	125	59	0.49	0.13	1.436	0.013	0.3084	0.0011	3513	6	3	6.2	0.3	0.000424	7	0.280425	33	-4.0	1.2	2.4
B-8.1	p e os	144	87	0.62	0.03	1.412	0.012	0.3216	0.0010	3578	5	4	6.4	0.3	0.000702	11	0.280443	28	-2.5	1.0	2.3
Weighted Mean[e] ± 95% confidence limits or Mean[f] ± 1σ										3635[f]	14		5.8[f]	0.6					-1.1 [e]		0.8
n										9 of 13			7 of 11						8 of 12		
MSWD																			0.2		
VM97/01 Granodioritic Ikkattoq gneiss (64°07.30'N 51°34.70'W)																					
1.1[d,g]	p e os	258	105	0.40	0.10	1.729	0.050	0.1998	0.0010	2825	9	4									
2.1[d,g]	p m os	410	192	0.47	0.21	1.854	0.052	0.1976	0.0013	2807	11	-1	3.8	0.5	0.000992	82	0.281017	32	-0.5	1.2	2.4
3.1[d,g]	p e os	431	127	0.29	0.10	1.737	0.044	0.1997	0.0009	2824	7	4	4.7	0.5	0.000893	47	0.281000	43	-0.5	1.5	2.6
4.1[d,g]	p e os	424	181	0.43	0.45	1.644	0.045	0.1981	0.0027	2811	23	9									
5.1[d,g]	p e os	437	156	0.35	0.11	1.718	0.049	0.1999	0.0010	2826	8	5	3.8	0.5	0.001671	34	0.280968	136	-3.1	4.8	5.3
5.2[d,g]	p e os	521	187	0.36	0.19	2.065	0.049	0.1970	0.0008	2801	7	-9	3.1	0.5							
6.1[d,g]	p f e os	368	174	0.47	0.09	1.790	0.064	0.1993	0.0018	2820	15	2									
7.1[d,g]	p e os	437	189	0.43	0.04	1.771	0.050	0.2000	0.0010	2826	8	2									

Sample Spot	Grain	U (ppm)	Th (ppm)	Th/U	Comm. ^{206}Pb%	^{238}U/^{206}Pb	1σ err	^{207}Pb/^{206}Pb	1σ err	^{207}Pb/^{206}Pb Age (Ma)	1σ err	Disc. (%)	$\delta^{18}O_{VSMOW}$ (‰)[a]	1σ err	^{176}Lu/^{177}Hf	2σ err[b]	^{176}Hf/^{177}Hf Meas.	2σ err[b]	ε_{Hf} Init.[c]	2σ err	Abs. err
8.1[d,g]	p e os	345	150	0.43	0.25	1.837	0.059	0.2006	0.0012	2831	10	-1									
9.1[d,g]	p e os	497	254	0.51	0.06	1.816	0.050	0.2000	0.0011	2827	9	0									
10.1[d,g]	p m os	507	212	0.42	0.12	1.699	0.041	0.2015	0.0012	2838	9	5	4.3	0.5							
Weighted Mean[e] ± 95% confidence limits or Mean[f] ± 1σ										2821[e]	8		4.0[e]	0.8					-0.7 [e]		1.6
n										11 of 11			5 of 5						3 of 3		
MSWD										1.7			1.3						0.5		
195392 Migmatite (64°16.33'N 51°04.00'W)																					
1.1[d]	p c os	248	119	0.48	0.00	1.388	0.041	0.3459	0.0016	3689	7	5	5.4	0.5	0.000436	8	0.280437	33	0.6	1.2	2.4
4.1[d]	p c os	42	39	0.93	0.08	1.348	0.046	0.3305	0.0042	3619	20	1									
6.1	p c os	53	53	1.00	0.00	1.591	0.051	0.3046	0.0034	3494	17	9	4.6	0.5	0.000440	21	0.280477	38	-2.6	1.4	2.5
10.1[d]	p c os	134	109	0.81	0.00	1.409	0.043	0.3274	0.0020	3605	10	4									
15.2[d]	p c os	94	37	0.39	0.33	1.447	0.043	0.3254	0.0017	3596	8	6									
16.1	p c os	183	46	0.25	0.14	1.321	0.041	0.3552	0.0042	3729	18	3	4.5	0.5							
B-1.1[d]	p c os	239	116	0.50	0.05	1.361	0.023	0.3401	0.0009	3663	4	3	4.4	0.4	0.0007704	88	0.280475	28	0.5	1.0	2.3
B-1.2[d]	p m os	1316	494	0.39	0.00	1.262	0.019	0.3447	0.0003	3684	1	-2	4.7	0.4	0.0008431	17	0.280416	23	-1.3	0.8	2.3
B-4.1[d]	p m os	166	260	1.62	0.27	1.410	0.033	0.3366	0.0009	3647	4	6	5.7	0.4	0.0028683	88	0.280575	46	-1.6	1.7	2.7
B-6.2[d]	p c os	1026	37	0.04	0.15	1.459	0.021	0.3271	0.0008	3603	4	7	4.2	0.4	0.0006074	15	0.280432	21	-2.0	0.7	2.2
B-8.2[d]	p c os	1244	86	0.07	0.00	1.321	0.021	0.3324	0.0006	3628	3	0	5.3	0.4	0.0007310	14	0.280371	23	-3.9	0.8	2.3
B-8.4[d]	p c os	904	90	0.10	0.06	1.358	0.020	0.3306	0.0003	3620	2	2	5.4	0.4	0.0007966	8	0.280417	19	-2.7	0.7	2.2
B-10.1[d]	an m h	1462	50	0.04	0.03	1.305	0.021	0.3351	0.0003	3640	1	-1	5.1	0.4							
B-11.1[d]	an c h	1476	56	0.04	0.00	1.365	0.020	0.3254	0.0009	3595	4	1	5.0	0.4	0.0012015	27	0.280424	18	-4.0	0.7	2.2
B-12.1[d]	p m os	254	28	0.11	0.10	1.495	0.026	0.3168	0.0007	3555	3	8	4.3	0.4	0.0004185	3	0.280416	23	-3.3	0.8	2.2
Weighted Mean[e] ± 95% confidence limits or Mean[f] ± 1σ										3627[f]	38		5.0[e]	0.4					-2.0 [f]		1.7
n										13 of 15			10 of 12						9 of 10		
MSWD													1.9								
7.1[d]	p c os	43	32	0.75	0.12	1.811	0.060	0.2355	0.0051	3090	35	8	3.5	0.5	0.000304	7	0.280434	56	-13.3	2.0	2.9
8.1[d]	p c os	396	31	0.08	0.29	1.866	0.055	0.2226	0.0012	2999	9	8									
9.1[d]	p c os	124	51	0.41	1.15	1.946	0.059	0.2202	0.0028	2982	21	9	4.1	0.5	0.000310	26	0.280421	30	-16.3	1.1	2.4
11.1[d]	p c os	1291	296	0.23	0.01	1.798	0.052	0.2325	0.0006	3069	4	7									
13.1[d]	p c os	103	40	0.38	0.42	1.797	0.059	0.2253	0.0021	3019	15	6	3.4	0.5	0.000684	22	0.280488	28	-13.8	1.0	2.3

Sample Spot	Grain	U (ppm)	Th (ppm)	Th/U	Comm. ^{206}Pb%	^{238}U/ ^{206}Pb	1σ err	^{207}Pb/ ^{206}Pb	1σ err	^{207}Pb/^{206}Pb Age (Ma)	1σ err	Disc. (%)	δ^{18}O $_{VSMOW}$ (‰)[a]	1σ err	^{176}Lu/^{177}Hf	2σ err[b]	^{176}Hf/^{177}Hf Meas.	2σ err[b]	ε_{Hf} Init.[c]	2σ err	Abs. err
15.1	p c os	64	25	0.39	0.58	1.727	0.055	0.2548	0.0048	3215	30	8									
Weighted Mean[e] ± 95% confidence limits or Mean[f] ± 1σ										3032[f]	46		3.7[e]	0.5					-14.6 [e]		4.0
n										5 of 6			3 of 3						3 of 3		
MSWD													0.7						1.7		
B-2.2[d]	an c os	824	72	0.09	0.11	1.953	0.029	0.1878	0.0003	2723	3	2	3.5	0.4							
B-3.1	p e os	214	27	0.13	0.13	1.972	0.031	0.1808	0.0006	2660	6	1	4.5	0.4							
B-6.1[d]	p m os	309	20	0.07	0.50	2.034	0.031	0.1877	0.0009	2722	8	6	3.5	0.4	0.0005730	14	0.280521	22	-19.3	0.8	2.2
B-8.1[d]	p m os	357	24	0.07	0.86	1.918	0.029	0.1896	0.0012	2739	10	1	4.8	0.4	0.0005417	6	0.280504	23	-19.5	0.8	2.2
B-8.3[d]	p e os	250	18	0.07	1.36	1.910	0.029	0.1891	0.0019	2735	17	1	4.1	0.4	0.0006016	8	0.280489	20	-20.2	0.7	2.2
B-9.1[d]	p m os	205	20	0.10	0.25	1.918	0.029	0.1875	0.0007	2721	6	1	3.9	0.4	0.0006371	19	0.280514	21	-19.7	0.7	2.2
B-9.2[d]	p c os	570	53	0.10	0.04	1.973	0.030	0.1886	0.0003	2730	3	3	3.9	0.4	0.0006884	15	0.280551	22	-18.3	0.8	2.2
Weighted Mean[e] ± 95% confidence limits or Mean[f] ± 1σ										2726[e]	5		4.0[e]	0.5					-19.4 [e]		1.0
n										6 of 7			6 of 7						5 of 5		
MSWD										1.2			1.6						0.4		
2.2[d]	p e h os	796	35	0.04	0.04	2.155	0.054	0.1707	0.0008	2564	8	4									
3.1[d]	p m os	180	67	0.37	0.19	2.087	0.062	0.1684	0.0017	2541	16	1									
5.1[d]	p m os	61	32	0.51	0.07	2.196	0.069	0.1688	0.0031	2546	31	5	4.4	0.5	0.000608	29	0.280786	39	-14.0	1.4	2.5
5.2[d]	p m os	98	70	0.72	0.28	2.097	0.064	0.1704	0.0027	2561	26	2									
12.1[d]	p e h os	104	54	0.53	0.47	1.989	0.060	0.1714	0.0017	2572	17	-2	4.5	0.5	0.000372	9	0.280526	35	-22.2	1.3	2.4
17.1[d]	p e h os	42	43	1.03	1.34	2.071	0.074	0.1704	0.0036	2561	35	1	5.1	0.5	0.000354	15	0.280510	48	-23.0	1.7	2.7
18.1[d]	p e h os	151	61	0.41	0.39	2.140	0.063	0.1702	0.0013	2559	13	3									
B-5.2[d]	an e h	1258	56	0.05	0.01	2.008	0.033	0.1715	0.0002	2572	2	-1	4.8	0.4	0.0005246	26	0.280651	18	-18.0	0.6	2.2
Weighted Mean[e] ± 95% confidence limits or Mean[f] ± 1σ										2570[e]	4		4.7[e]	0.4					-22.6 [e]		1.8
n										8 of 8			4 of 4						2 of 4		
MSWD										0.9			0.5						0.2		
1	Qtz												8.7	0.1							
2	Qtz												9.2	0.1							
195376 Qôrqut granite complex granite (64°16.50'N 51°00.00'W)																					
3.1[d]	p m os	1930	1703	0.91	0.11	2.125	0.031	0.1716	0.0003	2573	3	3	4.8	0.4	0.0006328	8	0.280712	22	-16.0	0.8	2.2
4.1	p m os	344	192	0.58	0.24	1.717	0.040	0.2327	0.0010	3071	7	4	4.6	0.4	0.0005037	28	0.280847	30	0.5	1.1	2.3
5.1[d]	p m os	3274	4684	1.48	0.01	2.019	0.034	0.1719	0.0010	2576	10	-1	3.7	0.4	0.0008013	21	0.280740	26	-15.3	0.9	2.3

Sample Spot	Grain	U (ppm)	Th (ppm)	Th/U	Comm. ^{206}Pb%	^{238}U/^{206}Pb	1σ err	^{207}Pb/^{206}Pb	1σ err	^{207}Pb/^{206}Pb Age (Ma)	1σ err	Disc. (%)	$\delta^{18}O_{VSMOW}$ (‰)[a]	1σ err	^{176}Lu/^{177}Hf	2σ err[b]	^{176}Hf/^{177}Hf Meas.	2σ err[b]	ε_{Hf} Init.[c]	2σ err	Abs. err
5.2[d]	p c rx	1117	1201	1.11	-0.01	1.997	0.065	0.1701	0.0017	2559	17	-2	4.9	0.4	0.0009886	30	0.280756	33	-15.4	1.2	2.4
6.1[d]	p m os	1493	1674	1.16	0.10	2.060	0.046	0.1699	0.0009	2556	9	0	3.5	0.4	0.0005367	6	0.280824	23	-12.3	0.8	2.3
8.1	p m os	83	8	0.10	0.09	1.472	0.024	0.3268	0.0040	3602	19	8									
9.1	p m os	804	86	0.11	0.00	1.649	0.024	0.2348	0.0008	3085	5	1	3.7	0.4	0.0009404	46	0.280867	38	0.7	1.4	2.5
Weighted Mean[e] ± 95% confidence limits or Mean[f] ± 1σ										2571[e]	10		4.2[f]	0.7					-14.7 [f]		1.7
n										4 of 7			4 of 6						4 of 6		
MSWD										1.3											
1	Qtz												8.2	0.1							
2	Qtz												8.9	0.1							

[a] = $[^{18}O/^{16}O_{sample} / (^{18}O/^{16}O_{reference\ measured} / {}^{18}O/^{16}O_{reference\ true}) - VSMOW] \times 1000/VSMOW$

[b] = $\times 10^{-6}$

[c] = $(^{176}Hf/^{177}Hf_{initial} / {}^{176}Hf/^{177}Hf_{CHUR} - 1) \times 10000$

CHUR: ^{176}Hf/^{177}Hf = 0.282785±11, ^{176}Lu/^{177}Hf = 0.0336±1 (Bouvier et al. 2008)

$\lambda^{176}Lu = 1.867 \pm 8 \times 10^{-11} y^{-1}$ (Scherer et al. 2001; Söderlund et al. 2004)

[d] = Analysis used for weighted mean or mean calculations

[e] = Weighted mean ± 95% confidence limits

[f] = Mean ± 1σ

[g] = U-Pb age determined by Nutman and Friend (2007)

Grain descriptions

Habit: p prismatic, an anhedral, f fragment

Analysis site: c core, m middle, e edge

Zonation: os oscillatory, h homogeneous, t turbid, rx recrystallised

Fig. 1

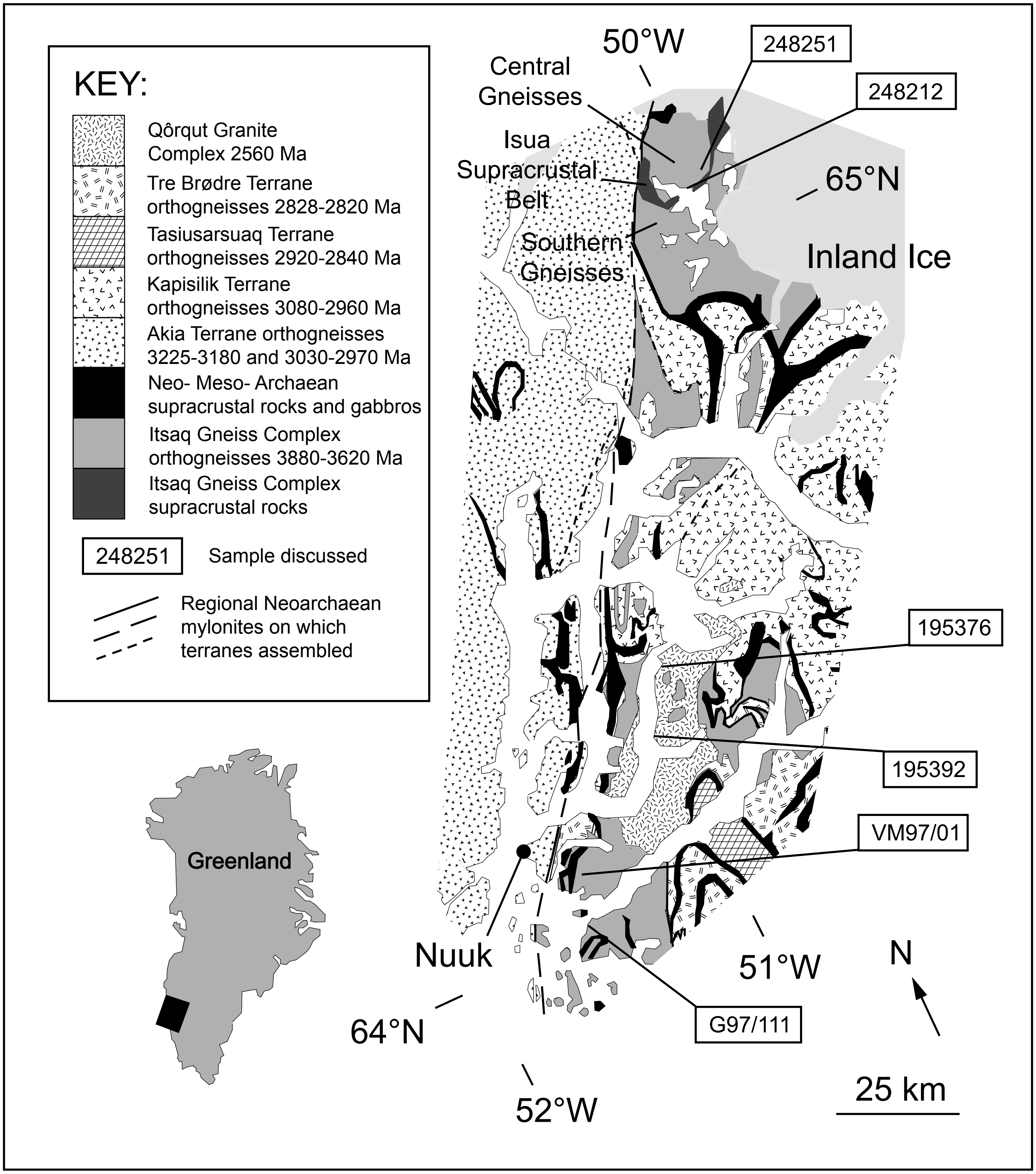
KEY:
Qôrqut Granite Complex 2560 Ma
Tre Brødre Terrane orthogneisses 2828-2820 Ma
Tasiusarsuaq Terrane orthogneisses 2920-2840 Ma
Kapisilik Terrane orthogneisses 3080-2960 Ma
Akia Terrane orthogneisses 3225-3180 and 3030-2970 Ma
Neo- Meso- Archaean supracrustal rocks and gabbros
Itsaq Gneiss Complex orthogneisses 3880-3620 Ma
Itsaq Gneiss Complex supracrustal rocks
248251
Sample discussed
Regional Neoarchaean mylonites on which terranes assembled
Greenland
50°W
248251
248212
Central Gneisses
Isua Supracrustal Belt
65°N
Southern Gneisses
Inland Ice
195376
195392
VM97/01
Nuuk
51°W
N
64°N
G97/111
25 km
52°W

Fig. 2

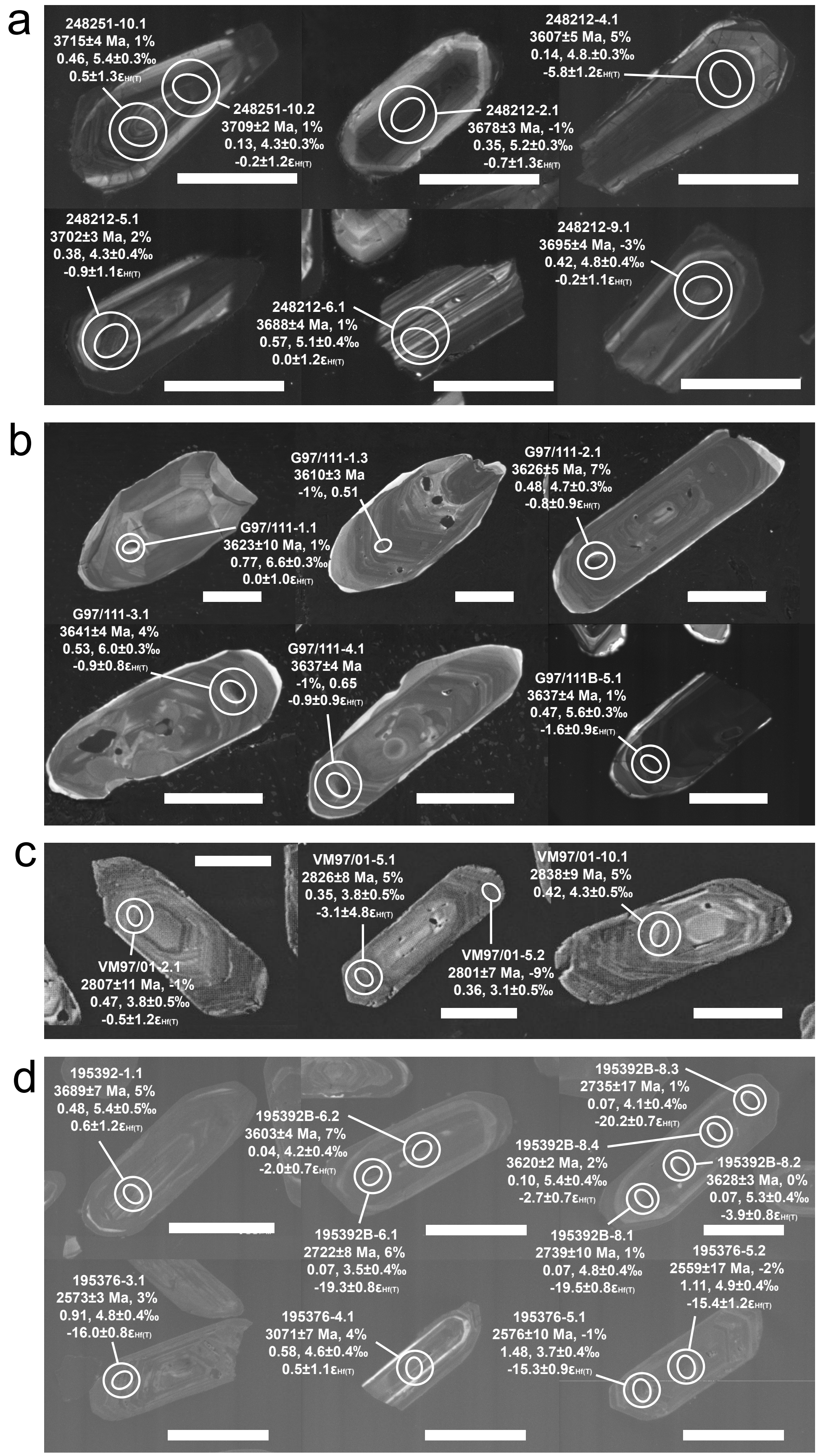
a
248251-10.1
3715±4 Ma, 1%
0.46, 5.4±0.3‰
0.5±1.3εHf(T)
248251-10.2
3709±2 Ma, 1%
0.13, 4.3±0.3‰
-0.2±1.2εHf(T)
248212-2.1
3678±3 Ma, -1%
0.35, 5.2±0.3‰
-0.7±1.3εHf(T)
248212-4.1
3607±5 Ma, 5%
0.14, 4.8.±0.3‰
-5.8±1.2εHf(T)
248212-5.1
3702±3 Ma, 2%
0.38, 4.3±0.4‰
-0.9±1.1εHf(T)
248212-6.1
3688±4 Ma, 1%
0.57, 5.1±0.4‰
0.0±1.2εHf(T)
248212-9.1
3695±4 Ma, -3%
0.42, 4.8±0.4‰
-0.2±1.1εHf(T)
b
G97/111-1.1
3623±10 Ma, 1%
0.77, 6.6±0.3‰
0.0±1.0εHf(T)
G97/111-1.3
3610±3 Ma
-1%, 0.51
G97/111-2.1
3626±5 Ma, 7%
0.48, 4.7±0.3‰
-0.8±0.9εHf(T)
G97/111-3.1
3641±4 Ma, 4%
0.53, 6.0±0.3‰
-0.9±0.8εHf(T)
G97/111-4.1
3637±4 Ma
-1%, 0.65
-0.9±0.9εHf(T)
G97/111B-5.1
3637±4 Ma, 1%
0.47, 5.6±0.3‰
-1.6±0.9εHf(T)
c
VM97/01-2.1
2807±11 Ma, -1%
0.47, 3.8±0.5‰
-0.5±1.2εHf(T)
VM97/01-5.1
2826±8 Ma, 5%
0.35, 3.8±0.5‰
-3.1±4.8εHf(T)
VM97/01-5.2
2801±7 Ma, -9%
0.36, 3.1±0.5‰
VM97/01-10.1
2838±9 Ma, 5%
0.42, 4.3±0.5‰
d
195392-1.1
3689±7 Ma, 5%
0.48, 5.4±0.5‰
0.6±1.2εHf(T)
195392B-6.2
3603±4 Ma, 7%
0.04, 4.2±0.4‰
-2.0±0.7εHf(T)
195392B-6.1
2722±8 Ma, 6%
0.07, 3.5±0.4‰
-19.3±0.8εHf(T)
195392B-8.3
2735±17 Ma, 1%
0.07, 4.1±0.4‰
-20.2±0.7εHf(T)
195392B-8.4
3620±2 Ma, 2%
0.10, 5.4±0.4‰
-2.7±0.7εHf(T)
195392B-8.2
3628±3 Ma, 0%
0.07, 5.3±0.4‰
-3.9±0.8εHf(T)
195392B-8.1
2739±10 Ma, 1%
0.07, 4.8±0.4‰
-19.5±0.8εHf(T)
195376-3.1
2573±3 Ma, 3%
0.91, 4.8±0.4‰
-16.0±0.8εHf(T)
195376-4.1
3071±7 Ma, 4%
0.58, 4.6±0.4‰
0.5±1.1εHf(T)
195376-5.1
2576±10 Ma, -1%
1.48, 3.7±0.4‰
-15.3±0.9εHf(T)
195376-5.2
2559±17 Ma, -2%
1.11, 4.9±0.4‰
-15.4±1.2εHf(T)

Fig. 3

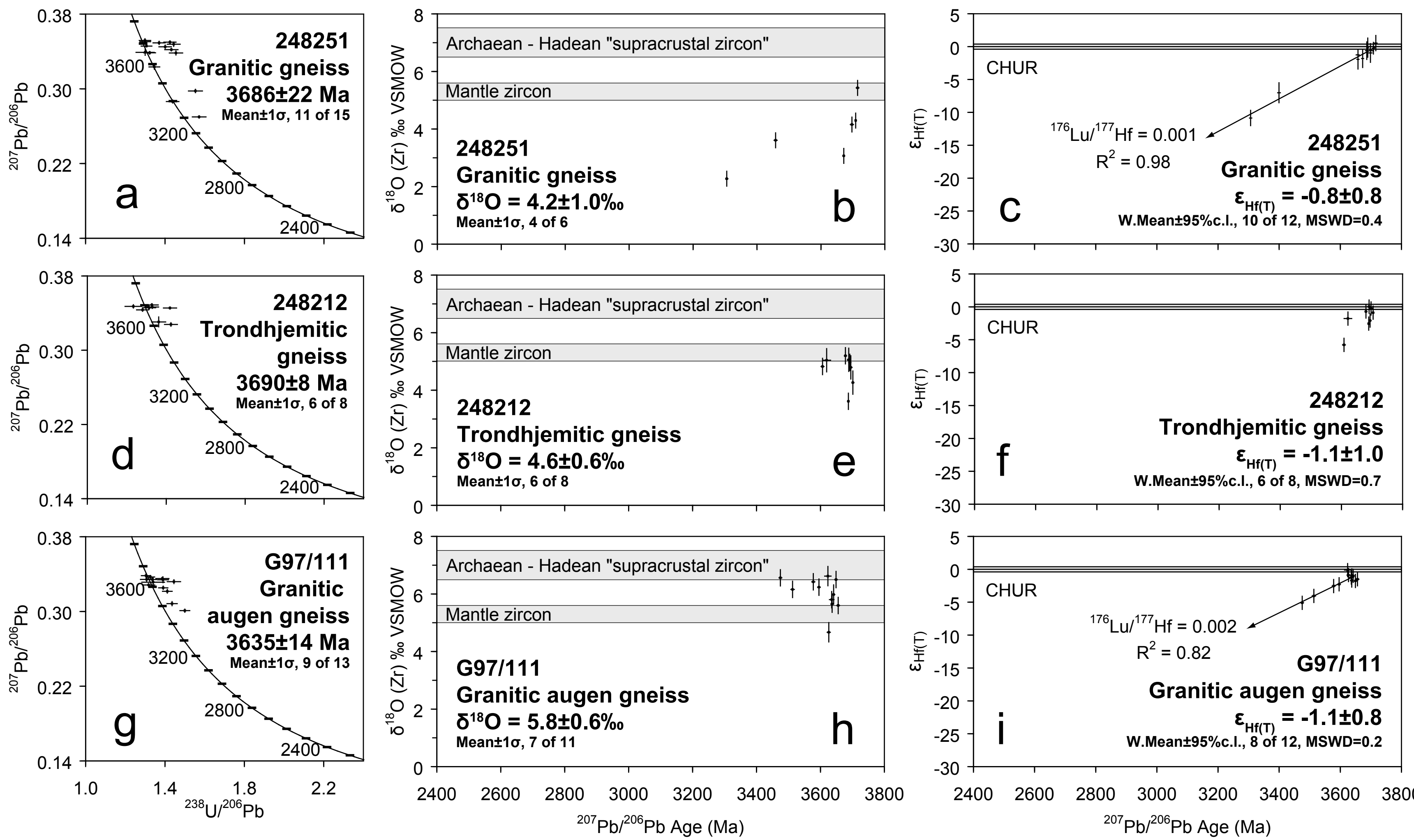

248251
Granitic gneiss
3686±22 Ma
Mean±1σ, 11 of 15
a
248251
Granitic gneiss
δ18O = 4.2±1.0‰
Mean±1σ, 4 of 6
b
Archaean - Hadean "supracrustal zircon"
Mantle zircon
CHUR
176Lu/177Hf = 0.001
R2 = 0.98
248251
Granitic gneiss
εHf(T) = -0.8±0.8
W.Mean±95%c.l., 10 of 12, MSWD=0.4
c
248212
Trondhjemitic gneiss
3690±8 Ma
Mean±1σ, 6 of 8
d
248212
Trondhjemitic gneiss
δ18O = 4.6±0.6‰
Mean±1σ, 6 of 8
e
248212
Trondhjemitic gneiss
εHf(T) = -1.1±1.0
W.Mean±95%c.l., 6 of 8, MSWD=0.7
f
G97/111
Granitic augen gneiss
3635±14 Ma
Mean±1σ, 9 of 13
g
G97/111
Granitic augen gneiss
δ18O = 5.8±0.6‰
Mean±1σ, 7 of 11
h
176Lu/177Hf = 0.002
R2 = 0.82
G97/111
Granitic augen gneiss
εHf(T) = -1.1±0.8
W.Mean±95%c.l., 8 of 12, MSWD=0.2
i
207Pb/206Pb
238U/206Pb
δ18O (Zr) ‰ VSMOW
εHf(T)
207Pb/206Pb Age (Ma)

Fig. 3 (cont.)

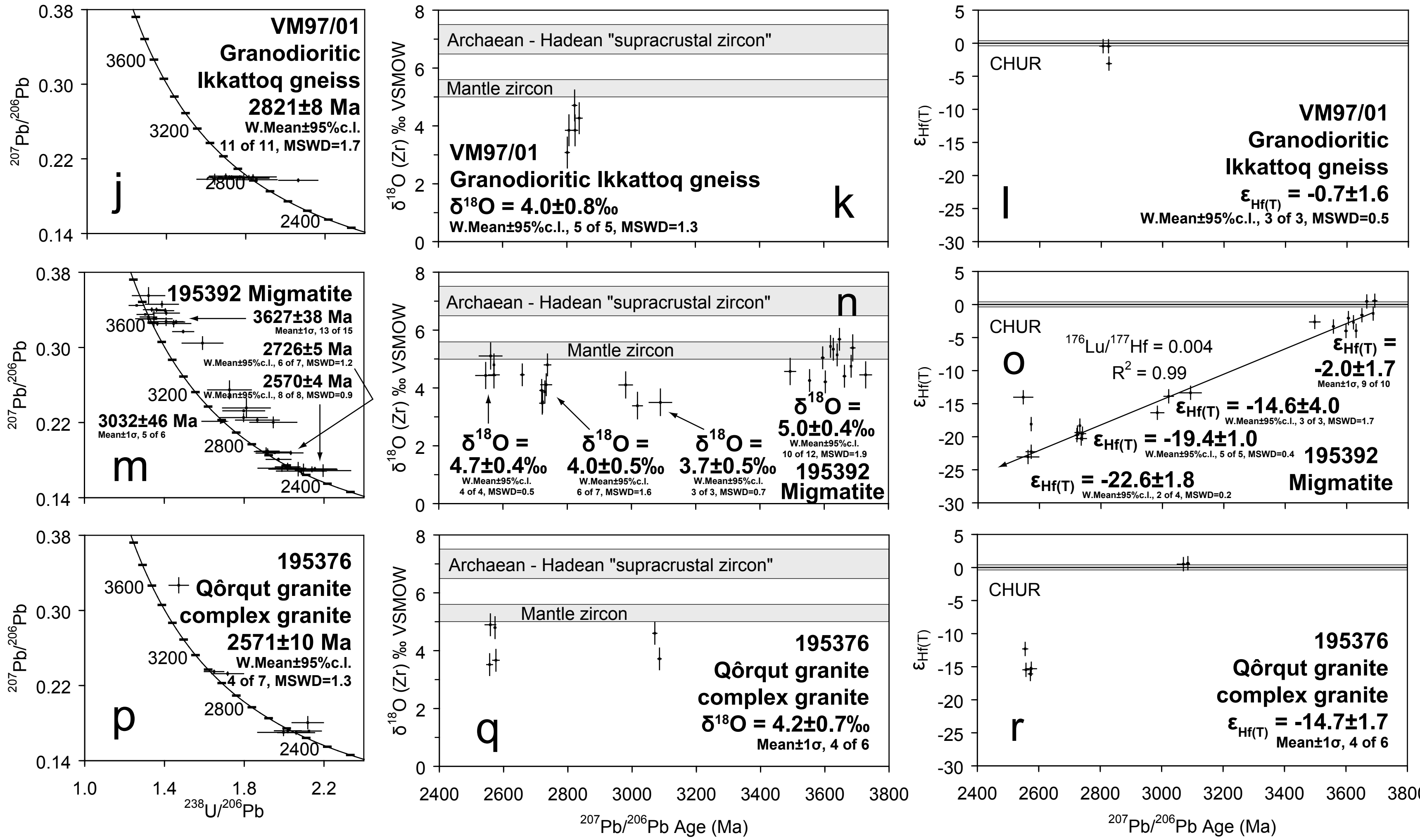

VM97/01
Granodioritic
Ikkattoq gneiss
2821±8 Ma
W.Mean±95%c.l.
11 of 11, MSWD=1.7
j
k
l
VM97/01
Granodioritic Ikkattoq gneiss
δ18O = 4.0±0.8‰
W.Mean±95%c.l., 5 of 5, MSWD=1.3
VM97/01
Granodioritic
Ikkattoq gneiss
εHf(T) = -0.7±1.6
W.Mean±95%c.l., 3 of 3, MSWD=0.5
Archaean - Hadean "supracrustal zircon"
Mantle zircon
CHUR
195392 Migmatite
3627±38 Ma
Mean±1σ, 13 of 15
2726±5 Ma
W.Mean±95%c.l., 6 of 7, MSWD=1.2
2570±4 Ma
W.Mean±95%c.l., 8 of 8, MSWD=0.9
3032±46 Ma
Mean±1σ, 5 of 6
m
n
δ18O = 4.7±0.4‰
W.Mean±95%c.l. 4 of 4, MSWD=0.5
δ18O = 4.0±0.5‰
W.Mean±95%c.l. 6 of 7, MSWD=1.6
δ18O = 3.7±0.5‰
W.Mean±95%c.l. 3 of 3, MSWD=0.7
δ18O = 5.0±0.4‰
W.Mean±95%c.l. 10 of 12, MSWD=1.9
195392
Migmatite
o
176Lu/177Hf = 0.004
R2 = 0.99
εHf(T) = -2.0±1.7
Mean±1σ, 9 of 10
εHf(T) = -14.6±4.0
W.Mean±95%c.l., 3 of 3, MSWD=1.7
εHf(T) = -19.4±1.0
W.Mean±95%c.l., 5 of 5, MSWD=0.4
εHf(T) = -22.6±1.8
W.Mean±95%c.l., 2 of 4, MSWD=0.2
195392
Migmatite
195376
Qôrqut granite
complex granite
2571±10 Ma
W.Mean±95%c.l.
4 of 7, MSWD=1.3
p
q
r
195376
Qôrqut granite
complex granite
δ18O = 4.2±0.7‰
Mean±1σ, 4 of 6
195376
Qôrqut granite
complex granite
εHf(T) = -14.7±1.7
Mean±1σ, 4 of 6
207Pb/206Pb
238U/206Pb
δ18O (Zr) ‰ VSMOW
εHf(T)
207Pb/206Pb Age (Ma)

Fig. 4

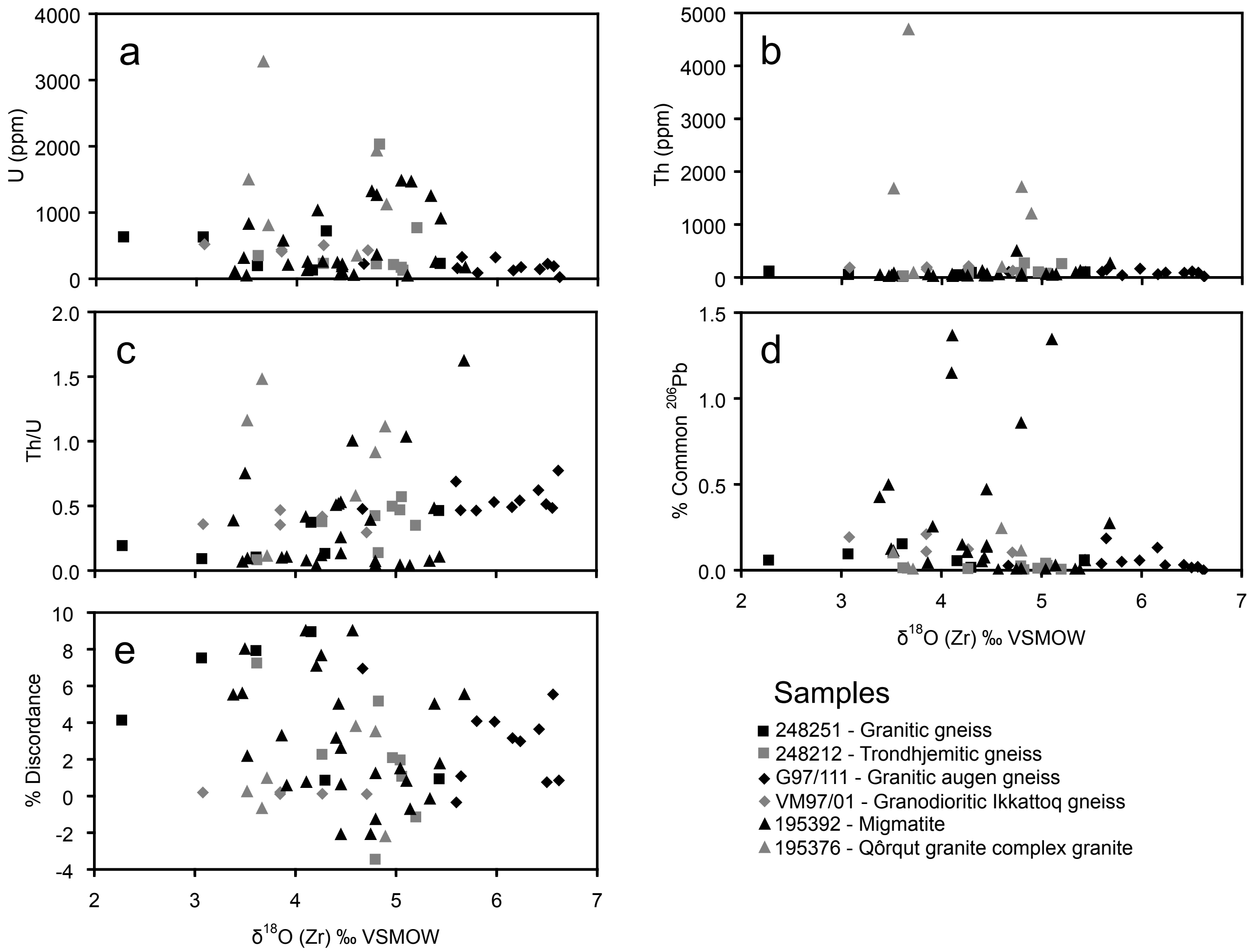

a
b
c
d
e
U (ppm)
Th (ppm)
Th/U
% Common ^{206}Pb
% Discordance
δ^{18}O (Zr) ‰ VSMOW
δ^{18}O (Zr) ‰ VSMOW
Samples
248251 - Granitic gneiss
248212 - Trondhjemitic gneiss
G97/111 - Granitic augen gneiss
VM97/01 - Granodioritic Ikkattoq gneiss
195392 - Migmatite
195376 - Qôrqut granite complex granite

Fig. 5

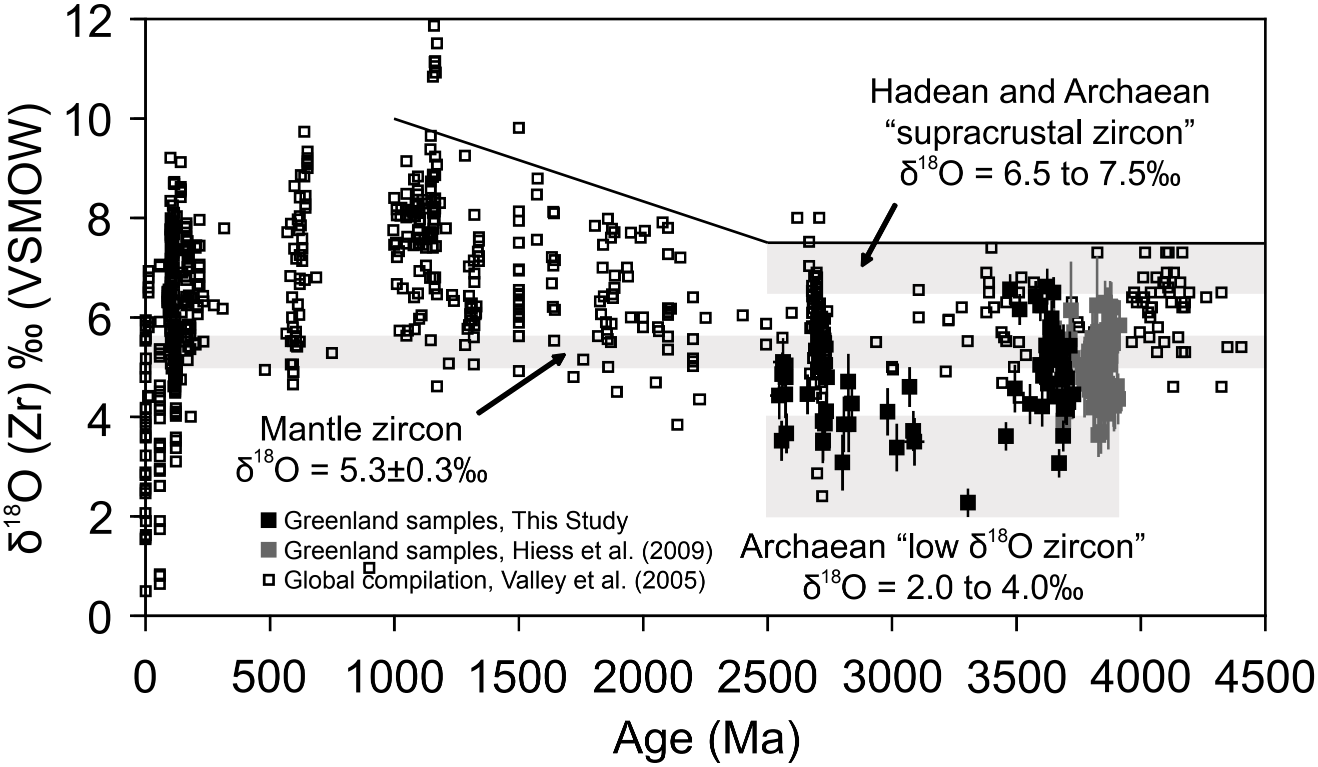

Hadean and Archaean
"supracrustal zircon"
δ18O = 6.5 to 7.5‰
Mantle zircon
δ18O = 5.3±0.3‰
Greenland samples, This Study
Greenland samples, Hiess et al. (2009)
Global compilation, Valley et al. (2005)
Archaean "low δ18O zircon"
δ18O = 2.0 to 4.0‰
δ18O (Zr) ‰ (VSMOW)
Age (Ma)
0
2
4
6
8
10
12
0
500
1000
1500
2000
2500
3000
3500
4000
4500

Fig. 5

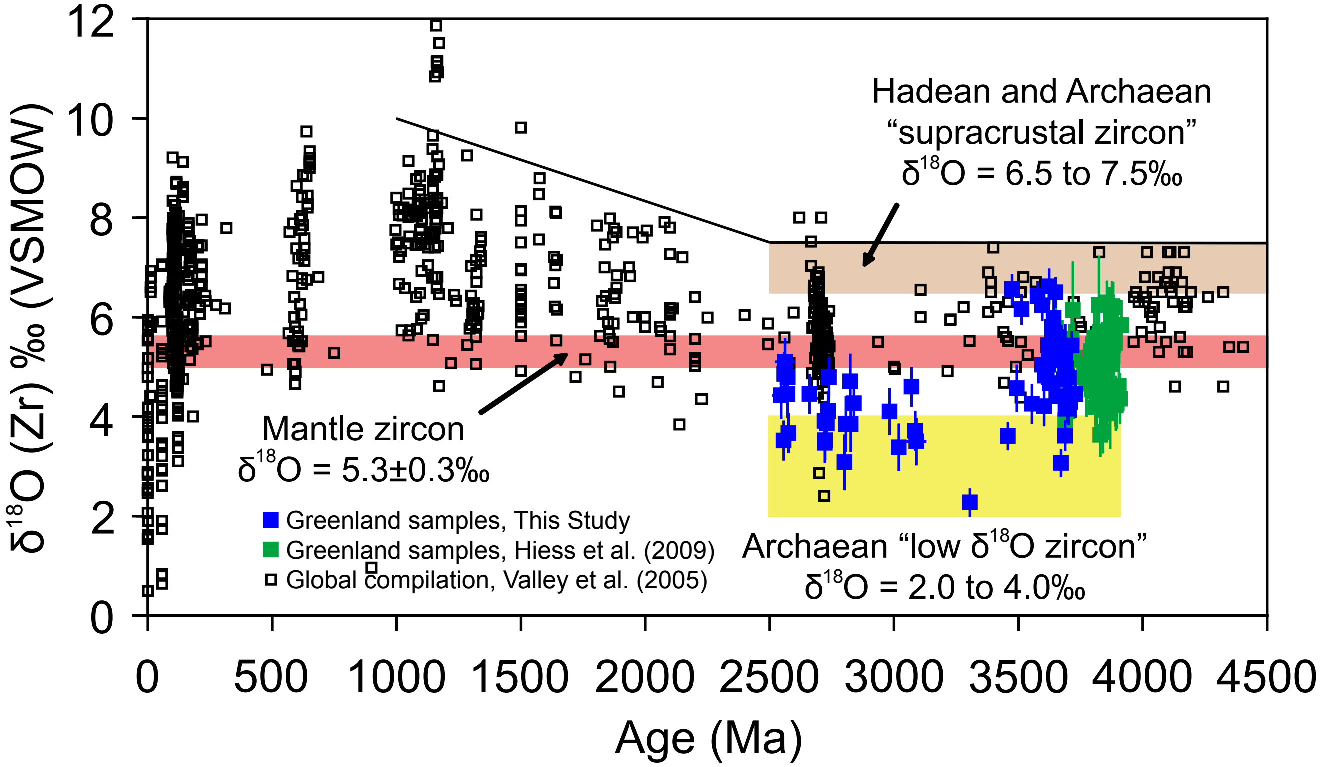

Hadean and Archaean
“supracrustal zircon”
δ18O = 6.5 to 7.5‰
Mantle zircon
δ18O = 5.3±0.3‰
Greenland samples, This Study
Greenland samples, Hiess et al. (2009)
Global compilation, Valley et al. (2005)
Archaean “low δ18O zircon”
δ18O = 2.0 to 4.0‰
δ18O (Zr) ‰ (VSMOW)
Age (Ma)
0
2
4
6
8
10
12
0
500
1000
1500
2000
2500
3000
3500
4000
4500

Fig. 6

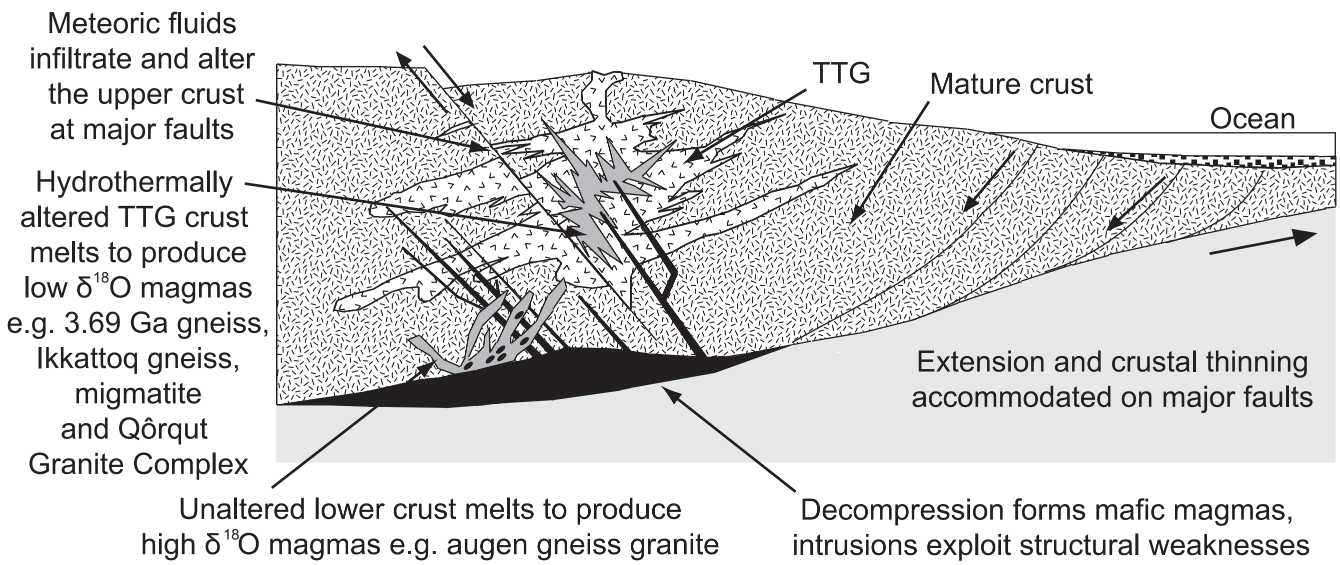
Meteoric fluids infiltrate and alter the upper crust at major faults
Hydrothermally altered TTG crust melts to produce low δ18O magmas e.g. 3.69 Ga gneiss, Ikkattoq gneiss, migmatite and Qôrqut Granite Complex
TTG
Mature crust
Ocean
Extension and crustal thinning accommodated on major faults
Unaltered lower crust melts to produce high δ18O magmas e.g. augen gneiss granite
Decompression forms mafic magmas, intrusions exploit structural weaknesses

Fig. 7

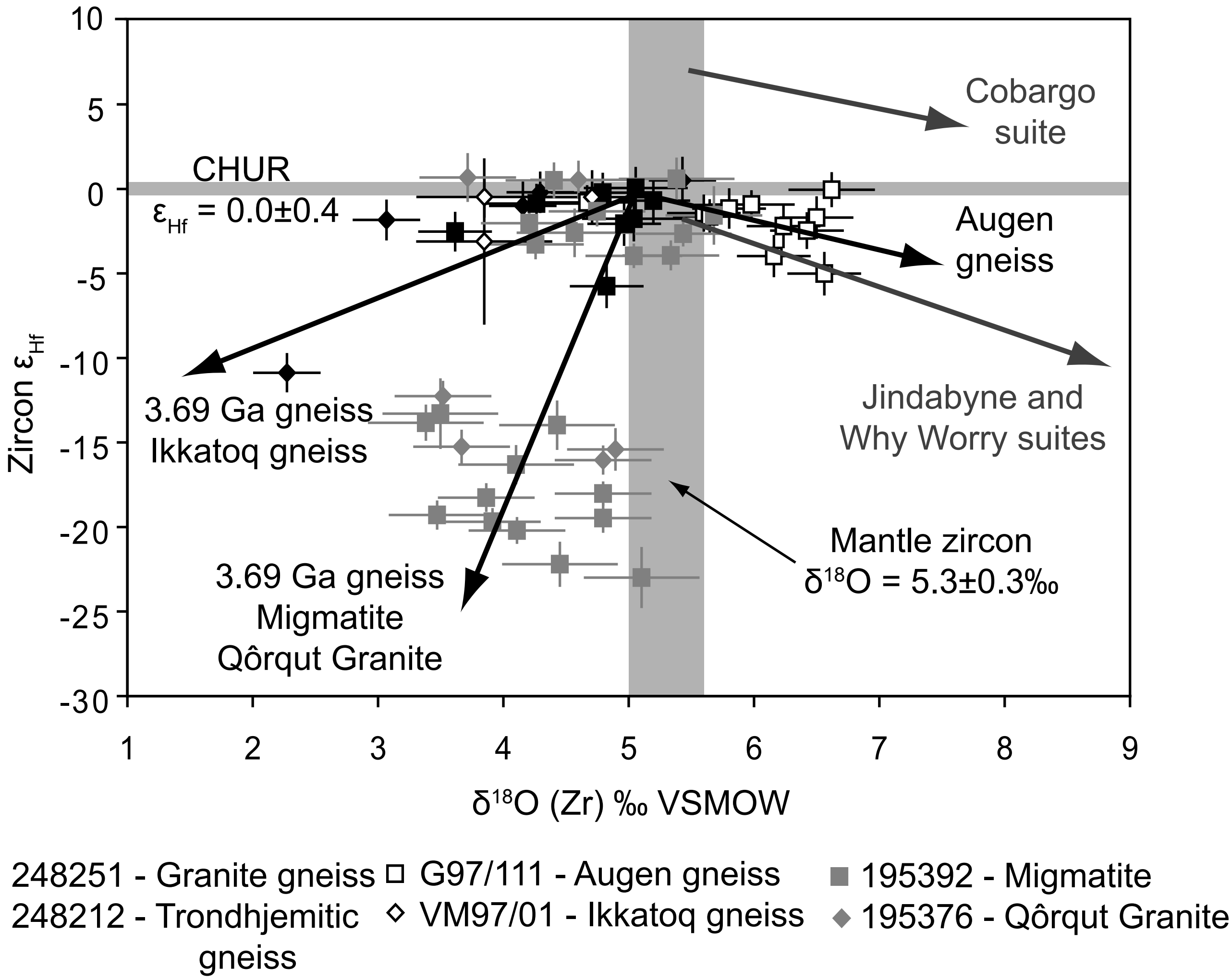
Cobargo
suite
CHUR
εHf = 0.0±0.4
Augen
gneiss
Jindabyne and
Why Worry suites
3.69 Ga gneiss
Ikkatoq gneiss
Mantle zircon
δ18O = 5.3±0.3‰
3.69 Ga gneiss
Migmatite
Qôrqut Granite
Zircon εHf
δ18O (Zr) ‰ VSMOW
10
5
0
-5
-10
-15
-20
-25
-30
1
2
3
4
5
6
7
8
9
■ 248251 - Granite gneiss
□ G97/111 - Augen gneiss
■ 195392 - Migmatite
◆ 248212 - Trondhjemitic gneiss
◇ VM97/01 - Ikkatoq gneiss
◆ 195376 - Qôrqut Granite

Archaean fluid-assisted crustal cannibalism recorded by low $\delta^{18}O$ and negative $\varepsilon_{Hf(T)}$ isotopic signatures of West Greenland granite zircon

Contributions to Mineralogy and Petrology

Joe Hiess[a,b]*, Vickie C. Bennett[a], Allen P. Nutman[a,c] and Ian S. Williams[a]

[a]Research School of Earth Sciences, Australian National University, Canberra, ACT 0200, Australia
[b]Division of Earth and Environmental Sciences, Korea Basic Science Institute, 804-1 Yangcheong-ri, Ochang, Cheongwon-gun, Chungbuk 363-883, South Korea
[c]School of Earth and Environmental Sciences, University of Wollongong, Wollongong, NSW 2522, Australia
*Corresponding author: jies@bgs.ac.uk

Online Resource 1
Analytical methods and the statistical treatment of data

1.1. Analytical methods

Sample preparation, data acquisition and reduction protocols for U-Pb, $^{18}O/^{16}O$ and $^{176}Hf/^{177}Hf$ isotopic analysis generally follow those previously described in detail by Hiess et al. (2009) and are summarized as follows.

1.2. Grain mounting and imaging

All zircon grains analysed here were taken from mineral separates extracted from rock samples collected for previous studies (see section 2 of main text). Crystals were isolated from hand samples by clean crushing, heavy liquid and magnetic separation techniques. Approximately 100 grains from each sample were transferred onto double sided adhesive tape with a fine-tipped needle under a binocular microscope and aligned with their c-axis horizontal. Zircon unknowns were mounted close to SL13, FC1, AS3 or Temora-2 reference material zircon that was dispersed over the mount surface. New generation SHRIMP megamounts were constructed to minimize geometric fractionation during O isotopic analysis (Ickert et al. 2008). All grains were cast in epoxy and polished with a rotary polisher and 1μm diamond paste to expose crystal mid-sections. Prior to each U-Pb or O analytical session, polished analytical surfaces were sequentially cleaned in an ultrasonic bath with petroleum spirit, ethanol, diluted laboratory detergent, 1M HCl (1 × quartz distilled), and deionized (18 mega Ω) H_2O before being dried in a 60°C oven. A 100-120Å Au or Al conductive layer was then evaporated onto the analytical surface and electronically checked for uniform and adequate conductivity before loading into the instrument. A 100Å Au coat was used for all U-Pb analyses, and a 120Å Al coat was used for subsequent O analyses.

Prior to U-Pb analysis, the zircon was imaged with reflected light, transmitted light and SEM cathodoluminesence (CL) spectroscopy. This allowed identification of grain cracks, mineral inclusions and 2-dimensional growth and recrystallisation textures to guide spot placement onto least-disturbed, oscillatory zoned, igneous growth domains. Following U-Pb analysis, the zircons were again imaged with reflected light to record the precise location of the ~2 µm deep age determination sputtered pits to assist future beam-positioning. Mounts were then lightly re-polished, removing ~5 µm of zircon to expose a second ‘fresh’ surface for O isotopic analysis, free of topography from earlier pits, or extraneous O implanted by the O^-_2 primary beam during the earlier U-Pb work (Benninghoven et al. 1987). Prior to O analysis this second analytical surface was imaged with CL to check for continuity of the zircon oscillatory growth zoning between the first and second surfaces. For Hf isotopic analysis by MC-ICPMS, the laser, which penetrates ~50 µm into the zircon, was subsequently centered directly over the pit formed during O analysis and within the same oscillatory growth domain. This method most reliably correlated the zircon O and Hf isotopic composition with a crystallisation age, given the limiting tradeoff between spatial resolution and analytical precision.

1.3. U-Pb geochronology with SHRIMP RG

Zircon U-Pb ages were measured using the SHRIMP RG ion microprobe at the Research School of Earth Sciences (RSES), the Australian National University. The methods employed here are in standard use and described in detail by Stern (1998) and Williams (1998) and are summarized as follows. A 2-4 nA mass filtered O_2^- primary beam was focused to a ~30 µm (long axis) elliptical spot and the beam rastered for 120 s to clean the mount surface prior to data acquisition. The magnet was stepped through peaks of $^{90}Zr_2{}^{16}O$, ^{204}Pb, ^{206}Pb, ^{207}Pb, ^{208}Pb, ^{238}U, $^{232}Th^{16}O$ and $^{238}U^{16}O$. FC1 zircon reference material was analysed once every 3 unknowns. Data were reduced using the Excel^{TM} macro SQUID (Ludwig 2001). Zircon reference materials SL13 (Claoué-Long et al. 1995; U = 238 ppm) and FC1 or AS3 (Paces and Miller 1993; $^{206}Pb/^{238}U$ age = 1099.0±0.5 Ma) were used for U abundance and $^{206}Pb/^{238}U$ calibrations respectively. Decay constants and the atomic $^{238}U/^{235}U$ ratio of 137.88 recommended by the IUGS Subcommission on Geochronology (Steiger and Jäger 1977) were used to calculate ages. Corrections for common Pb were based on small amounts of measured ^{204}Pb with isotopic compositions corresponding to a Pb growth model age of 3700 Ma (Stacey and Kramers 1975). Analytical uncertainties for individual spots are reported as 1σ within-spot errors. From the 6 samples dated, a total of 90 spots yielded U-Pb ages that were >90% concordant (see Table 1). These areas on each grain were selected for further O and Hf isotopic analysis.

To calculate the igneous age for each sample population as a single value, analyses were culled to selectively remove outliers. Outliers were statistically and/or geologically identified as younger U-Pb ages that were products of local recrystallisation or Pb-loss. The population of un-rejected analyses from each sample was then pooled to produce crystallisation ages with the Excel^{TM} macro Isoplot (Ludwig 2003) in either of two ways. 1) In samples VM97/01, 195392 (2726±5 Ma and 2570±4 Ma populations) and 195376, weighted mean ages were calculated as the mean square of weighted deviates (MSWD’s) for these sample populations was <2.0, (1.7, 1.2, 0.9 and 1.3 respectively). Weighted mean 95% confidence limit (c.l.) uncertainties for each respective sample were calculated from the inverse square of the assigned within-spot errors. 2) In samples 248251, 248212, G97/111, 195392 (3627±38 Ma and 3032±46 Ma populations) where weighted mean MSWD’s were >2.0, mean ages were instead calculated for each sample. Mean 1σ uncertainties were calculated from one standard deviation of the population age. Weighted mean or mean $^{207}Pb/^{206}Pb$ ages from this study typically have larger errors, owing to fewer pooled analyses, but lie in agreement with previous age determinations on these samples, except for samples 248251 and 248212 (see discussion in main text and Online Resource 3.1).

1.4. Oxygen isotopic analysis with SHRIMP II multi-collector

Zircon oxygen isotopic compositions were determined using the SHRIMP II multi-collector ion microprobe at the RSES over 7 analytical sessions. A session for O isotopic analysis is defined as an uninterrupted period of data collection, with the same standard calibration. Sessions are separated by cold restarts, mount changes, interruptions to operation, or a major retuning of the instrument's primary or secondary beam. Instrumental conditions (Ickert et al. 2008) were typically set with a 3.5 nA, 15 keV Cs^+ primary beam focused to an elliptical 30 µm (long axis) spot, sampling ~2 ng of mineral per analysis. Surface charge was neutralized by a 45° incident, broadly focused, moderate energy (1.1 keV) e^- beam, delivering ~1 µA of electrons from a Kimball Physics ELG-5 electron gun at a working distance of 20 mm. The electron gun is mounted off the extraction lens housing and floated at primary column potential. The 10 kV secondary extraction yields ~320 pA of secondary current, or ~4.0×10^6 cps of ^{18}O and ~2.0×10^9 cps of ^{16}O on zircon. Isotopic ratios were produced by simultaneous measurement of $^{18}O^-$ and $^{16}O^-$ ions by dual Faraday cups with 10^{11} Ω and 10^{10} Ω resistors respectively. Background counts of ~3.5×10^3 cps on ^{18}O and ~1.2×10^4 cps on ^{16}O were measured and subtracted during setup configuration. A 150 µm source slit and 300 µm collector slits limit beam truncation to <5%, providing a mass resolution of ~2,500 at 1% peak height. This is sufficient to separate potential isobaric interferences on $^{18}O^-$ from $^{17}OH^-$, $^{16}OD^-$ and $^{16}OH_2^-$. A 180 s pre-sputter and secondary auto-tuning in z and y directions (horizontal and vertical along the beam line for extracted secondary ions) preceded ratio measurements. Data acquisition consisted of 1 set of 10 scans, each with 10 s integration times, leading to total count times of ~100 s and complete analyses within approximately 5 minutes. Within this time period within-spot precision, based on counting statistics for both samples and reference materials reached near theoretical limits of ±0.3‰ (1σ). Operating conditions were held constant during a single given session.

Each reference materials and unknowns measured $^{18}O/^{16}O$ ratios, drift, within-spot and spot-to-spot precisions are summarized in Online Resource 2a and 2b. Over the 7 analytical sessions, 62 sample analyses were calibrated against 80, time integrated, bracketing analyses of reference materials FC1 or AS3 zircon ($\delta^{18}O$ = 5.34±0.03‰, $^{18}O/^{16}O$ = 0.0020159, Trail et al. 2007) or Temora-2 zircon ($\delta^{18}O$ = 8.20±0.01‰, $^{18}O/^{16}O$ = 0.0020216, Valley 2003; Black et al. 2004). All $^{18}O/^{16}O$ ratios are presented as $\delta^{18}O$ notation, expressed as deviations from Vienna standard mean ocean water (VSMOW, $^{18}O/^{16}O$ = 0.0020052, Baertschi 1976) in parts per thousand. Instrumental drift in all sessions was <0.06‰ per analysis and corrected for using a linear fit. Electron-induced secondary ion emission (EISIE; Ickert et al. 2008) was monitored before and after analysis, and found to provide a systematic and insignificantly minor contribution to the total secondary signal (typically <10^6 cps of ^{16}O at analysis end). Spot-to-spot reproducibility of nominally homogeneous reference materials for a single session ranged from ±0.5‰ to ±0.3‰ (1σ; Online Resource 2c). Spot-to-spot precision was always worse than within-spot precision and was subsequently considered to be the best measure of precision for any given analysis.

Oxygen isotopic compositions for each sample correspond to grains with age determinations. Weighted mean or mean compositions were calculated from the same zircon spots that were used for to provide pooled $^{207}Pb/^{206}Pb$ ages. For samples VM97/01 and all 195392 populations weighted mean calculations were made as MSWD's were all <2.0 (1.3, 1.9, 0.7, 1.6 and 0.5 respectively). Weighted mean 95% confidence limit uncertainties were calculated from the inverse square of the assigned error from each analysis. For samples 248251, 248212, G97/111 and 195376 where weighted mean MSWD's were >2.0, mean ages were calculated with 1σ uncertainties from one standard deviation of the pooled population. Oxygen isotopic compositions of quartz separated from whole rock of samples 195392 and 195376 were analysed by GNS Stable Isotope Laboratory, Lower Hutt, New Zealand.

1.5. Zircon hafnium abundances with LA-ICPMS

As the amount of oxygen isotope fractionation during ion-microprobe analysis can be matrix dependent (e.g. Peck et al. 2001), we determined HfO_2 concentrations for three standard zircon reference materials and two selected samples to assess matrix variability. Following the acquisition of $^{18}O/^{16}O$ data on SHRIMP II, HfO_2 concentrations were measured using the RSES Aligent 7500 ICPMS equipped with a Lamda Physik LPX 1201 UV ArF eximer laser and Ar–He flushed sample cell (Eggins et al. 1998). The laser was operated at 22 kV with 120 mJ energy per pulse at 4 Hz. Each acquisition consisted of a 20 s background followed by a 150 s collection period. Blocks of 10 unknowns were bracketed by analyses of NIST 612 glass reference material. Raw counts were converted to concentrations using "LABRAT 0.93" written for Lab VIEW by A. Kallio. Corrections for mass bias in the samples were made using NIST 612. Zircon HfO_2 abundances were normalized to stoichiometric (32.77 wt.%) SiO_2. Mean HfO_2 concentrations for FC1 (1.2±0.2 wt.%, 95% c.l., n=18), Temora-2 (1.0±0.1 wt.%, 95% c.l., n=9) and 91500 (0.6±0.1 wt.%, 95% c.l., n=5) are all in agreement with published values for these reference materials of 1.20±0.11 wt.% (Black et al. 2004), 0.98±0.01 wt.% (Black et al. 2004) and 0.695 wt.% (Wiedenbeck et al. 2004) respectively. Samples G97/111 (1.2±0.1 wt.%, 95% c.l., n=5) and 248251 (1.7±0.1 wt.%, 95% c.l., n=6) contain similar HfO_2 abundances to reference materials (FC1 and Temora-2) demonstrating that corrections for variations in instrumental mass fractionation (IMF) resulting from large variations in Hf content (Eiler et al. 1997) were not necessary. A more comprehensive test of the sensitivity of oxygen isotopic IMF to matrix effects in SHRIMP II was presented by Ickert et al. (2008).

1.6. Hafnium isotopic analysis with LA-MC-ICPMS

Zircon hafnium isotopic compositions were determined over 4 analytical sessions using the RSES ThermoFinnigan Neptune multi-collector ICPMS coupled to a ArF λ=193 nm eximer 'HelEx' laser ablation system following methods described by Harrison et al. (2005). The laser was focused to a 47 μm diameter circular spot firing at 5 Hz with an energy density at the sample surface of ~10 J/cm^2. ^{171}Yb, ^{173}Yb, ^{174}Hf, ^{175}Lu, ^{176}Hf, ^{177}Hf, ^{178}Hf, ^{179}Hf and ^{181}Ta isotopes were simultaneously measured in static-collection mode on 9 Faraday cups with 10^{11} Ω resistors. A large zircon crystal from the Monastery kimberlite was used to tune the mass spectrometer to optimum sensitivity. Analysis of a gas blank and a suite of secondary reference zircons (Monastery, Mud Tank, 91500, Temora-2 and FC1; Woodhead and Hergt 2005) was systematically performed after every 10-12 samples. Data was acquired in 1 s integrations over 100 s, but time slices were later cropped to periods maintaining steady $^{176}Hf/^{177}Hf$ signals during data reduction on a custom Excel^{TM} spreadsheets written by S. Eggins. For sessions 1 to 3, amplifier gains were calibrated at the start of each session. The Excel^{TM} spreadsheet used for session 4 incorporated a dynamic amplifier correction within run. Total Hf signal intensity typically fell from 5 to 2V during a single analysis.

The measured ^{178}Hf/^{177}Hf, ^{174}Hf/^{177}Hf, ^{176}Lu/^{177}Hf and ^{176}Hf/^{177}Hf ratios with 2σ uncertainties for each of the 211 reference material and 63 sample analyses and are presented in Online Resource 2d and 2e. No corrections were applied to the data to normalize the measured ^{176}Hf/^{177}Hf ratios to published solution values. Mass bias was corrected using an exponential law (Russell et al. 1978; Chu et al. 2002; Woodhead et al. 2004) and a compositions for ^{179}Hf/^{177}Hf of 0.732500 (Patchett et al. 1981). As a quality check of this procedure ^{178}Hf/^{177}Hf ratios for all zircon reference materials and samples are reported (n=274). A mean value of 1.467239±101 (2σ) lies within uncertainty of values published by Thirlwall and Anczkiewicz (2004).

Yb and Lu mass bias factors were assumed to be identical and normalized using an exponential correction to a ^{173}Yb/^{171}Yb ratio of 1.123456 (Thirlwall and Anczkiewicz 2004). The intensity of the ^{176}Hf peak was accurately determined by removing isobaric interferences from ^{176}Lu and ^{176}Yb. Interference-free ^{175}Lu and ^{173}Yb were measured and the interference peaks subtracted according to reported ^{176}Lu/^{175}Lu and ^{176}Yb/^{173}Yb isotopic abundances of Thirlwall and Anczkiewicz (2004) in sessions 1 to 3 and Chu et al. (2002) in session 4. Owing to the substantial ^{174}Yb interference at mass 174, ^{174}Hf/^{177}Hf ratios are also reported to demonstrate the effectiveness of the Yb interference correction procedure. An average ratio of 0.008653±86 (2σ, n=274) is in agreement with values published by Thirlwall and Anczkiewicz (2004).

Zircon ^{176}Lu/^{177}Hf ratios should be accurately determined by LA-MC-ICPMS to enable corrections for in-growth of radiogenic ^{176}Hf. Average measured ^{176}Lu/^{177}Hf ratios within reference zircon (Monastery, 0.000010; Mud Tank, 0.000036; 91500, 0.000357; Temora-2, 0.001088; FC1, 0.001060) are in good agreement with the solution values reported by Woodhead and Hergt (2005) of 0.000009, 0.000042, 0.000311, 0.001090 and 0.001262 respectively. The range of ^{176}Lu/^{177}Hf measured in the reference zircons brackets the mean measured ^{176}Lu/^{177}Hf ratios from samples 248251 (0.001017), 248212 (0.000955), G97/111 (0.000629), VM97/01 (0.001185), 195392 (0.000696) and 195376 (0.000734).

The mean ^{176}Hf/^{177}Hf ratios for the 5 reference zircons (Monastery: 0.282726±43; Mud Tank: 0.282499±44; 91500: 0.282304±74; Temora-2: 0.282675±69; FC1: 0.282156±71, 2σ) deviate from published solution values of Woodhead and Hergt (2005) by only -0.4, -0.3, -0.1, -0.4 and -1.0 ε_{Hf} units respectively (Online Resource 2d). The mean of all ^{176}Hf/^{177}Hf analyses for each reference zircon lies within 2σ uncertainty of their respective solution value. No correlation exists between ^{176}Hf/^{177}Hf and ^{178}Hf/^{177}Hf, ^{174}Hf/^{177}Hf or ^{176}Lu/^{177}Hf ratios for any zircon reference materials, including high Lu/Hf Temora-2 and FC1 (Online Resource 2f). This indicates that calculations for mass bias and Yb interference corrections were accurately applied. The -1.0 epsilon unit discrepancy between measured and published ^{176}Hf/^{177}Hf ratios in FC1 reference material may in part relate to the variability in ^{176}Hf/^{177}Hf solution analyses reported by Woodhead and Hergt (2005). That is, there is likely real variation in the Hf isotopic composition of this reference zircon population.

For the unknown zircons, initial $^{176}Hf/^{177}Hf$ ratios for each spot were calculated using their individual SHRIMP measured $^{207}Pb/^{206}Pb$ ages, present day CHUR compositions of $^{176}Hf/^{177}Hf$ = 0.282785±11, $^{176}Lu/^{177}Hf$ = 0.0336±1 (Bouvier et al. 2008), and a $\lambda^{176}Lu$ decay constant of $1.867 \pm 8 \times 10^{-11} y^{-1}$ (Scherer et al. 2001; Söderlund et al. 2004).

For zircons from each rock, weighted mean or mean initial Hf isotopic compositions were also calculated and correspond with their igneous crystallisation age and oxygen isotopic composition, in that all were measured from the same zircon domains. Again only analyses that were used for earlier weighted mean or mean age determinations were included. For samples 248251, 248212, G97/111, VM97/01, 195392 (3032±46, 2726±5 and 2570±4 Ma) populations, weighted mean calculations were made as MSWD's were all <2.0 (0.4, 0.7, 0.2, 0.5, 1.7, 0.4 and 0.2 respectively). Weighted mean 95% confidence limit uncertainties were calculated from the inverse square of the assigned absolute error from each analysis. For the other 195392 (3627±38 Ma) population and sample 195376 where weighted mean MSWD's were both 2.2, mean ages were calculated with 1σ uncertainties from one standard deviation of the pooled population. Within-spot uncertainties for each analysis are typically ±0.8 to ±1.7 ε_{Hf} units at the 2σ level. Several sources of uncorrelated error may exist within these LA-MC-ICPMS analyses that do not account for the external scatter seen in some reference zircons (e.g. 91500, Temora-2 and FC1). Therefore, a conservative approach is taken to estimate the absolute uncertainty of each spot that is used to calculate weighted mean ε_{Hf} compositions. Within-spot errors for individual analyses are summed in quadrature with an estimate of external reproducibility from the zircon reference materials. This is taken to be ±2.1 ε_{Hf} units, based on the long-term average external reproducibility of all 5 reference materials, over all four session (Monastery = ±1.5 ε_{Hf}, Mud Tank = ±1.6 ε_{Hf}, 91500 = ±2.6 ε_{Hf}, Temora-2 = ±2.4 ε_{Hf}, FC1 = 2.4 ε_{Hf}). Within-spot errors are quoted in the text, and figures, while the inverse square of assigned absolute errors are used to calculate weighted mean (± 95% c.l.) compositions.

References

Baertschi P (1976) Absolute ^{18}O content of Standard Mean Ocean Water. Earth Planet Sci Lett 31:341-344

Benninghoven A, Rüdenauer FG, Werner HW (1987) Secondary Ion Mass Spectrometry: Basic Concepts, Instrumental Aspects, Applications and Trends, vol. John Wiley, Hoboken, N. J., p 1227

Black LP, Kamo SL, Allen CM, Davis DW, Aleinikoff JN, Valley JW, Mundil R, Campbell IH, Korsch RJ, Williams IS, Foudoulis C (2004) Improved $^{206}Pb/^{238}U$ microprobe geochronology by the monitoring of a trace-element-related matrix effect; SHRIMP, ID-TIMS, ELA-ICP-MS and oxygen isotope documentation for a series of zircon standards. Chem Geol 205:115-140

Bouvier A, Vervoort JD, Patchett J (2008) The Lu-Hf and Sm-Nd isotopic composition of CHUR: Constraints from unequilibrated chondrites and implications for the bulk composition of the terrestrial planets. Earth Planet Sci Lett 273:48-57

Chu NC, Taylor RN, Chavagnac V, Nesbitt RW, Boella RM, Milton JA, German CR, Bayon G, Burton K (2002) Hf isotope ratio analysis using multi-collector inductively coupled plasma mass spectrometry: an evaluation of isobaric interference corrections. J Analy Atom Spectrom 17:1567-1574

Claoué-Long JC, Compston W, Roberts J, Fanning CM (1995) Two Carboniferous ages: a comparison of SHRIMP zircon dating with conventional zircon ages and $^{40}Ar/^{39}Ar$ analysis. In: Berggren WA, Kent DV, Aubry MP, Hardenbol J (eds) Geochronology, Time Scales and Global Stratigraphic Correlation. SEPM Special Publication vol 54. pp 3-21

Eggins SM, Kinsley LPJ, Shelley JMG (1998) Deposition and element fractionation processes during atmospheric pressure laser sampling for analysis by ICP-MS. App Surf Sci 127-129:278-286

Eiler JM, Graham C, Valley JW (1997) SIMS analysis of oxygen isotopes: matrix effects in complex minerals and glasses. Chem Geol 138:221-244

Harrison TM, Blichert-Toft J, Müller W, Albarede F, Holden P, Mojzsis SJ (2005) Heterogeneous Hadean Hafnium: Evidence of Continental Crust at 4.4 to 4.5 Ga. Science 310:1947-1950

Hiess J, Bennett VC, Nutman AP, Williams IS (2009) In situ U–Pb, O and Hf isotopic compositions of zircon and olivine from Eoarchaean rocks, West Greenland: New insights to making old crust. Geochim Cosmochim Acta 73:4489-4516

Ickert RB, Hiess J, Williams IS, Holden P, Ireland TR, Lanc P, Schram N, Foster JJ, Clement SW (2008) Determining high precision, in situ, oxygen isotope ratios with a SHRIMP II: Analyses of MPI-DING silicate-glass reference materials and zircon from contrasting granites. Chem Geol 257:114-128

Ludwig KR (2001) Squid 1.02 User's Manual, Berkley Geochronology Centre, Special Publication No. 2, Rev. June 20, 19p.

Ludwig KR (2003) Isoplot 3.00 User's Manual: A Geochronological Toolkit for Microsoft Excel, Berkeley Geochronological Center, Special Publication No. 4, Rev. May 30, 70p.

Paces JB, Miller JD (1993) Precise U-Pb age of Duluth Complex and related mafic intrusions, northeastern Minnesota: Geochronological insights to physical, petrogenetic, paleomagnetic, and tectonomagnetic processes associated with the 1.1 Ga midcontinent rift system. J Geophys Res 98(B8):13997–14013

Patchett PJ, Kouvo O, Hedge CE, Tatsumoto M (1981) Evolution of continental crust and mantle heterogeneity:evidence from Hf isotopes. Contrib Mineral Petrol 78:279-297

Peck WH, Valley JW, Wilde SA, Graham CM (2001) Oxygen isotope ratios and rare earth elements in 3.3 to 4.4 Ga zircons: Ion microprobe evidence for high $\delta^{18}O$ continental crust and oceans in the Early Archean. Geochim Cosmochim Acta 65:4215-4229

Russell WA, Papanastassiou DA, Tombrello TA (1978) Ca isotope fractionation on the Earth and other solar system materials. Geochim Cosmochim Acta 42:1075-1090

Scherer E, Munker C, Mezger K (2001) Calibration of the Lutetium-Hafnium Clock. Science 293:683-687

Söderlund U, Patchett PJ, Vervoort JD, Isachsen CE (2004) The ^{176}Lu decay constant determined by Lu-Hf and U-Pb isotope systematics of Precambrian mafic intrusions. Earth Planet Sci Lett 219:311-324

Stacey JS, Kramers JD (1975) Approximation of terrestrial lead isotope evolution by a two-stage model. Earth Planet Sci Lett 26:207-221

Steiger RH, Jäger E (1977) Subcommission on geochronology: convention on the use of decay constants in geo- and cosmochronology. Earth Planet Sci Lett 36:359-362

Stern RA (1998) High-resolution SIMS determination of radiogenic trace-isotope ratios in minerals. In: Cabri LJ, Vaughan DJ (eds) Modern Approaches to Ore and Environmental Mineralogy. Mineralogical Association of Canada Short Course Series, vol 27. pp 241–268

Thirlwall MF, Anczkiewicza R (2004) Multidynamic isotope ratio analysis using MC–ICP–MS and the causes of secular drift in Hf, Nd and Pb isotope ratios. Int J Mass Soec 235:59-81

Trail D, Mojzsis SJ, Harrison TM, Schmitt AK, Watson EB, Young ED (2007) Constraints on Hadean zircon protoliths from oxygen isotopes, Ti-thermometry, and rare earth elements. Geochem Geophy Geosys 8, Q06014:doi:10.1029/2006GC001449

Valley JW (2003) Oxygen isotopes in zircon. In: Hanchar JM, Hoskin PWO (eds) Zircon. Reviews in Mineralogy and Geochemistry, vol 53. pp 343-385

Wiedenbeck M, Hanchar JM, Peck WH, Sylvester P, Valley J, Whitehouse M, Kronz A, Morishita Y, Nasdala L, Fiebig J, Franchi I, Girard JP, Greenwood RC, Hinton R, Kita N, Mason PRD, Norman M, Ogasawara M, Piccoli PM, Rhede D, Satoh H, Schulz-Dobrick B, Skår Ø, Spicuzza MJ, Terada K, Tindle A, Togashi S, Vennemann T, Xie Q, Zheng Y-F (2004) Further characterization of the zircon 91500 crystal. Geostand Geoanaly Res 28:9-39

Williams IS (1998) U-Th-Pb geochronology by ion microprobe. Rev Econ Geol 7:1-35

Woodhead J, Hergt J (2005) A Preliminary Appraisal of Seven Natural Zircon Reference Materials for *In Situ* Hf Isotope Determination. Geostand Geoanaly Res 29:183-195

Woodhead J, Hergt J, Shelley M, Eggins S, Kemp R (2004) Zircon Hf-isotope analysis with an excimer laser, depth profiling, ablation of complex geometries, and concomitant age estimation. Chem Geol 209:121-135

Online Resource 2a
Zircon reference materials δ^{18}O

Reference Spot	Session	$^{18}O/^{16}O$ Meas.[a]	Drift ‰ / analysis	WS err 1σ (‰)	δ$^{18}O_{VSMOW}$ (‰)	STS err 1σ (‰)
TEMD-9.1	1	0.0021534		0.1	8.4	0.3
TEMD-1.2	1	0.0021519		0.1	7.6	0.3
TEMD-3.3	1	0.0021531		0.2	8.2	0.3
TEMD-5.2	1	0.0021536		0.1	8.4	0.3
TEMD-7.2	1	0.0021535		0.4	8.4	0.3
Mean	**n=5**	**0.0021531**	**0.06**	**0.2**	**8.2**	**0.3**
FC1-1.1	2	0.0021706		0.1	5.4	0.3
FC1-2.1	2	0.0021709		0.2	5.5	0.3
FC1-3.1	2	0.0021714		0.3	5.8	0.3
FC1-4.1	2	0.0021698		0.2	5.0	0.3
FC1-5.1	2	0.0021704		0.2	5.3	0.3
FC1-6.1	2	0.0021701		0.3	5.2	0.3
FC1-7.1	2	0.0021700		0.2	5.1	0.3
Mean	**n=7**	**0.0021705**	**-0.01**	**0.2**	**5.3**	**0.3**
FC1-2.1	3	0.0021622		0.3	5.8	0.3
FC1-3.1	3	0.0021614		0.1	5.4	0.3
FC1-4.1	3	0.0021610		0.2	5.2	0.3
FC1-5.1	3	0.0021607		0.2	5.1	0.3
FC1-6.1	3	0.0021616		0.4	5.5	0.3
FC1-7.1	3	0.0021620		0.3	5.7	0.3
FC1-8.1	3	0.0021618		0.2	5.6	0.3
FC1-9.1	3	0.0021604		0.2	4.9	0.3
FC1-10.1	3	0.0021610		0.3	5.2	0.3
FC1-11.1	3	0.0021607		0.2	5.1	0.3
Mean	**n=10**	**0.0021613**	**-0.01**	**0.2**	**5.3**	**0.3**
FC1-14.1	4	0.0021574		0.2	5.6	0.4
FC1-15.1	4	0.0021575		0.3	5.6	0.4
FC1-16.1	4	0.0021576		0.3	5.7	0.4
FC1-17.1	4	0.0021581		0.2	5.9	0.4
FC1-18.1	4	0.0021556		0.4	4.7	0.4
FC1-19.1	4	0.0021571		0.2	5.4	0.4
FC1-20.1	4	0.0021562		0.2	5.0	0.4
FC1-20.2	4	0.0021567		0.3	5.2	0.4
FC1-21.1	4	0.0021558		0.4	4.8	0.4
Mean	**n=9**	**0.0021569**	**-0.03**	**0.3**	**5.3**	**0.4**
AS3-1.1	5	0.0021638		0.4	6.2	0.5
AS3-1.2	5	0.0021608		0.3	4.8	0.5
AS3-2.1	5	0.0021619		0.2	5.3	0.5
AS3-2.2	5	0.0021628		0.3	5.7	0.5
AS3-3.1	5	0.0021618		0.3	5.3	0.5
AS3-4.1	5	0.0021629		0.3	5.8	0.5
AS3-5.1	5	0.0021629		0.3	5.8	0.5
AS3-6.1	5	0.0021618		0.3	5.3	0.5
AS3-7.1	5	0.0021604		0.3	4.6	0.5
AS3.8.1	5	0.0021605		0.2	4.7	0.5

Mean	**n=10**	**0.0021620**	**-0.05**	**0.3**	**5.3**	**0.5**
FC1-1.1	6	0.0021588		0.4	5.3	0.5
FC1-2.1	6	0.0021579		0.2	4.9	0.5
FC1-4.1	6	0.0021576		0.3	4.7	0.5
FC1-5.1	6	0.0021589		0.4	5.3	0.5
FC1-6.1	6	0.0021602		0.2	5.9	0.5
FC1-7.1	6	0.0021600		0.4	5.8	0.5
FC1-8.1	6	0.0021579		0.3	4.9	0.5
FC1-9.1	6	0.0021590		0.2	5.4	0.5
FC1-10.1	6	0.0021580		0.1	4.9	0.5
FC1-11.1	6	0.0021589		0.3	5.3	0.5
FC1-12.1	6	0.0021608		0.3	6.2	0.5
FC1-13.1	6	0.0021585		0.4	5.1	0.5
FC1-14.1	6	0.0021592		0.3	5.5	0.5
Mean	**n=13**	**0.0021589**	**0.02**	**0.3**	**5.3**	**0.5**
FC1-1.1	7	0.0020483		0.4	5.6	0.4
FC1-2.1	7	0.0020482		0.6	5.6	0.4
FC1-3.1	7	0.0020485		0.6	5.7	0.4
FC1-1.1	7	0.0020483		0.4	5.6	0.4
FC1-2.1	7	0.0020482		0.6	5.6	0.4
FC1-3.1	7	0.0020485		0.6	5.7	0.4
FC1-4.1	7	0.0020488		0.4	5.9	0.4
FC1-5.1	7	0.0020464		0.7	4.7	0.4
FC1-6.1	7	0.0020484		0.6	5.7	0.4
FC1-7.1	7	0.0020476		0.7	5.3	0.4
FC1-8.1	7	0.0020485		0.3	5.7	0.4
FC1-9.1	7	0.0020484		0.6	5.7	0.4
FC1-11.1	7	0.0020469		0.3	5.0	0.4
FC1-12.1	7	0.0020487		0.4	5.8	0.4
FC1-13.1	7	0.0020483		0.6	5.6	0.4
FC1-14.1	7	0.0020474		0.5	5.2	0.4
FC1-15.1	7	0.0020477		0.7	5.3	0.4
FC1-16.1	7	0.0020470		0.5	5.0	0.4
FC1-17.1	7	0.0020478		0.5	5.4	0.4
FC1-18.1	7	0.0020472		0.6	5.1	0.4
FC1-19.1	7	0.0020478		0.3	5.4	0.4
FC1-20.1	7	0.0020465		0.6	4.8	0.4
FC1-21.1	7	0.0020420		0.5	5.0	0.4
FC1-22.1	7	0.0020462		0.7	4.6	0.4
FC1-23.1	7	0.0020475		0.4	5.2	0.4
FC1-24.1	7	0.0020475		0.5	5.2	0.4
Mean	**n=26**	**0.0020477**	**-0.01**	**0.5**	**5.3**	**0.4**

[a] = Measured $^{18}O/^{16}O$ corrected for background

Online Resource 2b
Zircon unknowns δ^{18}O

Reference Spot	Session	$^{18}O/^{16}O$ Meas.[a]	WS err 1σ (‰)	δ^{18}O $_{VSMOW}$ (‰)	STS err 1σ (‰)
248251-3.1	2	0.0021659	0.2	3.1	0.3
248251-4.1	2	0.0021683	0.3	4.2	0.3
248251-10.1	2	0.0021709	0.1	5.4	0.3
248251-10.2	2	0.0021685	0.4	4.3	0.3
248251-11.1	2	0.0021675	0.2	3.6	0.3
248251-12.1	2	0.0021647	0.3	2.3	0.3
248212-1.1	3	0.0021598	0.2	5.0	0.3
248212-2.1	3	0.0021605	0.2	5.2	0.3
248212-3.1	3	0.0021572	0.2	3.6	0.3
248212-4.1	3	0.0021597	0.3	4.8	0.3
248212-5.1	4	0.0021551	0.2	4.3	0.4
248212-6.1	4	0.0021568	0.2	5.1	0.4
248212-7.1	4	0.0021568	0.3	5.0	0.4
248212-9.1	4	0.0021564	0.2	4.8	0.4
G97/111-1.1	1	0.0021491	0.4	6.6	0.3
G97/111-2.1	1	0.0021458	0.4	4.7	0.3
G97/111-3.1	1	0.0021488	0.3	6.0	0.3
G97/111B-1.1	3	0.0021635	0.3	6.5	0.3
G97/111B-2.1	3	0.0021623	0.3	5.8	0.3
G97/111B-3.1	3	0.0021623	0.3	5.6	0.3
G97/111B-4.1	3	0.0021645	0.3	6.6	0.3
G97/111B-5.1	3	0.0021626	0.3	5.6	0.3
G97/111B-6.1	3	0.0021638	0.3	6.2	0.3
G97/111B-7.1	3	0.0021631	0.2	6.2	0.3
G97/111B-8.1	3	0.0021632	0.2	6.4	0.3
VM97/01-2.1	5	0.0021591	0.3	3.8	0.5
VM97/01-3.1	5	0.0021610	0.3	4.7	0.5
VM97/01-5.1	5	0.0021579	0.3	3.8	0.5
VM97/01-5.2	5	0.0021556	0.4	3.1	0.5
VM97/01-10.1	5	0.0021606	0.3	4.3	0.5
195392-1.1	6	0.0021598	0.3	5.4	0.5
195392-5.1	6	0.0021576	0.3	4.4	0.5
195392-6.1	6	0.0021568	0.3	4.6	0.5
195392-7.1	6	0.0021557	0.4	3.5	0.5
195392-9.1	6	0.0021558	0.2	4.1	0.5
195392-12.1	6	0.0021559	0.2	4.5	0.5
195392-13.1	6	0.0021559	0.3	3.4	0.5
195392-16.1	6	0.0021566	0.2	4.5	0.5
195392-17.1	6	0.0021572	0.3	5.1	0.5
195392B-1.1	7	0.0020465	0.4	4.4	0.4
195392B-1.2	7	0.0020472	0.4	4.7	0.4
195392B-2.2	7	0.0020450	0.4	3.5	0.4
195392B-3.1	7	0.0020458	0.4	4.5	0.4
195392B-4.1	7	0.0020477	0.3	5.7	0.4
195392B-5.2	7	0.0020474	0.4	4.8	0.4

195392B-6.1	7	0.0020446	0.5	3.5	0.4
195392B-6.2	7	0.0020461	0.7	4.2	0.4
195392B-8.1	7	0.0020468	0.7	4.8	0.4
195392B-8.2	7	0.0020477	0.6	5.3	0.4
195392B-8.3	7	0.0020447	0.5	4.1	0.4
195392B-8.4	7	0.0020476	0.3	5.4	0.4
195392B-9.1	7	0.0020453	0.5	3.9	0.4
195392B-9.2	7	0.0020450	0.4	3.9	0.4
195392B-10.1	7	0.0020472	0.1	5.1	0.4
195392B-11.1	7	0.0020469	0.6	5.0	0.4
195392B-12.1	7	0.0020462	0.6	4.3	0.4
195376-3.1	7	0.0020463	0.7	4.8	0.4
195392-4.1	7	0.0020462	0.2	4.6	0.4
195376-5.1	7	0.0020440	0.5	3.7	0.4
195376-5.2	7	0.0020462	0.3	4.9	0.4
195376-6.1	7	0.0020431	0.3	3.5	0.4
195376-9.1	7	0.0020442	0.4	3.7	0.4

[a] = Measured $^{18}O/^{16}O$ corrected for background

Online Resource 2c
Zircon reference materials $\delta^{18}O$ and ε_{Hf}

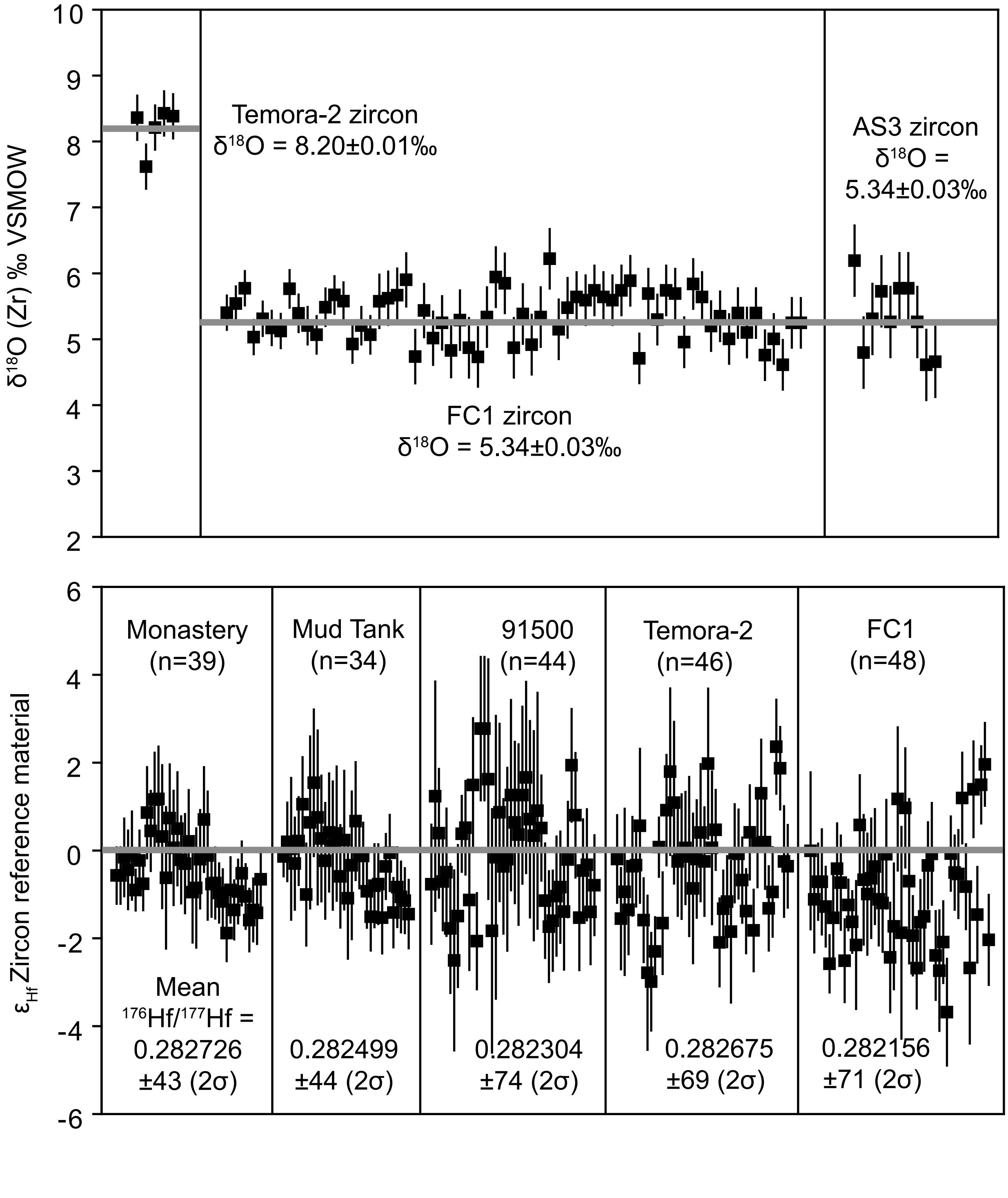

Online Resource 2d
Zircon reference materials ε_{Hf}

Reference Spot	Session	$^{178}Hf/^{177}Hf$	err[a] 2σ	$^{174}Hf/^{177}Hf$	err[a] 2σ	$^{176}Lu/^{177}Hf$	err[a] 2σ	$^{176}Hf/^{177}Hf$ Meas.	err[a] 2σ	ε_{Hf} Ref.	err 2σ
Monastery											
MON-1	1	1.467255	56	0.008671	16	0.000016	0	0.282722	18	-0.6	0.6
MON-2	1	1.467224	50	0.008667	18	0.000016	0	0.282722	18	-0.6	0.6
MON-3	1	1.467275	54	0.008673	16	0.000016	0	0.282734	25	-0.2	0.9
MON-4	1	1.467227	57	0.008662	20	0.000019	0	0.282725	25	-0.4	0.9
MON-5	1	1.467290	60	0.008674	20	0.000009	0	0.282735	28	-0.1	1.0
MON-7	1	1.467274	36	0.008653	8	0.000012	0	0.282713	13	-0.9	0.5
MON-8	1	1.467261	41	0.008652	12	0.000029	0	0.282732	19	-0.2	0.7
MON-9	1	1.467260	48	0.008646	11	0.000015	0	0.282717	17	-0.8	0.6
MON-10	1	1.467274	62	0.008618	21	0.000010	0	0.282762	29	0.9	1.0
MON-11	1	1.467246	58	0.008640	20	0.000010	0	0.282751	26	0.4	0.9
MON-1	2	1.467257	65	0.008667	25	0.000010	0	0.282771	30	1.2	1.1
MON-2	2	1.467233	64	0.008657	28	0.000010	0	0.282771	34	1.2	1.2
MON-2B	2	1.467247	91	0.008659	34	0.000020	1	0.282747	46	0.3	1.6
MON-3	2	1.467274	85	0.008601	41	0.000008	1	0.282720	46	-0.6	1.6
MON-4	2	1.467240	67	0.008673	29	0.000013	0	0.282759	35	0.7	1.2
MON-5	2	1.467317	75	0.008677	30	0.000009	0	0.282740	37	0.1	1.3
MON-6	2	1.467301	78	0.008648	31	0.000011	0	0.282752	36	0.5	1.3
MON-7	3	1.467215	56	0.008659	19	0.000014	0	0.282732	28	-0.2	1.0
MON-8	3	1.467267	63	0.008666	23	0.000014	0	0.282730	32	-0.3	1.1
MON-9	3	1.467263	63	0.008651	26	0.000011	0	0.282744	33	0.2	1.2
MON-10	3	1.467256	66	0.008656	28	0.000010	0	0.282711	32	-1.0	1.1
MON-12	3	1.467243	77	0.008630	26	0.000013	0	0.282714	38	-0.9	1.4
MON-13	3	1.467252	68	0.008698	31	0.000011	0	0.282732	32	-0.2	1.1
MON-14	3	1.467273	72	0.008625	30	0.000016	0	0.282758	34	0.7	1.2
MON-15	3	1.467351	127	0.008696	32	0.000014	0	0.282735	41	-0.1	1.5
MON-1	4	1.467263	51	0.008663	16	0.000004	0	0.282716	21	-0.8	0.7
MON-2	4	1.467254	59	0.008661	17	0.000004	0	0.282717	23	-0.7	0.8
MON-3	4	1.467260	48	0.008665	20	0.000004	0	0.282711	19	-1.0	0.7
MON-4	4	1.467208	57	0.008657	18	0.000004	0	0.282705	21	-1.2	0.7
MON-5	4	1.467213	50	0.008661	20	0.000004	0	0.282685	18	-1.9	0.6
MON-6	4	1.467267	66	0.008647	20	0.000005	0	0.282713	21	-0.9	0.7
MON-7	4	1.467281	57	0.008651	20	0.000004	0	0.282700	19	-1.4	0.7
MON-8	4	1.467302	58	0.008676	20	0.000005	0	0.282712	20	-0.9	0.7
MON-9	4	1.467198	59	0.008667	20	0.000004	0	0.282723	21	-0.5	0.7
MON-10	4	1.467205	54	0.008669	24	0.000004	0	0.282708	21	-1.0	0.7
MON-11	4	1.467266	60	0.008629	24	0.000005	0	0.282693	20	-1.6	0.7
MON-12	4	1.467229	57	0.008647	20	0.000004	0	0.282700	20	-1.4	0.7
MON-13	4	1.467253	46	0.008646	19	0.000004	0	0.282698	20	-1.4	0.7
MON-14	4	1.467248	55	0.008680	20	0.000004	0	0.282719	19	-0.7	0.7
Mean[b]	**n=39**	**1.467257**	**62**	**0.008657**	**39**	**0.000010**	**11**	**0.282726**	**43**	**-0.4**	**1.5**
WH (2005) Soln[c]						**0.000009**		**0.282738**	**8**		
WH (2005) LA[d]								**0.282739**	**26**		
Mud Tank											
MT-1	1	1.467272	38	0.008670	8	0.000050	0	0.282503	13	-0.1	0.4
MT-2	1	1.467219	51	0.008681	22	0.000048	0	0.282513	25	0.2	0.9
MT-3	1	1.467258	85	0.008677	42	0.000047	1	0.282508	46	0.0	1.6
MT-4	1	1.467288	62	0.008669	25	0.000047	0	0.282499	30	-0.3	1.0

MT-5	1	1.467317	73	0.008678	20	0.000050	0	0.282513	28	0.2	1.0
MT-6	1	1.467257	50	0.008696	21	0.000049	0	0.282537	30	1.0	1.1
MT-1	2	1.467228	80	0.008652	28	0.000059	0	0.282479	33	-1.0	1.2
MT-2B	2	1.467186	96	0.008670	50	0.000052	1	0.282525	55	0.6	2.0
MT-3	2	1.467290	101	0.008619	52	0.000067	0	0.282551	47	1.5	1.7
MT-3B	2	1.467281	75	0.008628	33	0.000053	1	0.282528	56	0.8	2.0
MT-6	2	1.467288	77	0.008688	39	0.000050	1	0.282515	40	0.3	1.4
MT-7	3	1.467201	68	0.008644	24	0.000052	0	0.282500	37	-0.2	1.3
MT-8	3	1.467254	80	0.008668	34	0.000050	1	0.282519	38	0.4	1.3
MT-9	3	1.467345	103	0.008644	32	0.000050	1	0.282510	41	0.1	1.5
MT-10	3	1.467313	83	0.008681	34	0.000047	1	0.282518	43	0.4	1.5
MT-11	3	1.467212	67	0.008638	28	0.000050	0	0.282490	33	-0.6	1.2
MT-12	3	1.467228	85	0.008667	31	0.000052	1	0.282514	45	0.2	1.6
MT-13	3	1.467254	78	0.008702	36	0.000052	1	0.282476	39	-1.1	1.4
MT-14	3	1.467232	68	0.008603	38	0.000052	1	0.282497	47	-0.3	1.7
MT-15	3	1.467300	87	0.008649	33	0.000049	1	0.282526	38	0.7	1.3
MT-1	4	1.467237	47	0.008668	21	0.000015	0	0.282504	21	-0.1	0.7
MT-2	4	1.467219	62	0.008681	24	0.000012	0	0.282503	21	-0.1	0.8
MT-3	4	1.467226	57	0.008666	21	0.000012	0	0.282481	23	-0.9	0.8
MT-4	4	1.467200	63	0.008643	26	0.000012	0	0.282464	22	-1.5	0.8
MT-5	4	1.467190	58	0.008673	23	0.000012	0	0.282484	27	-0.8	0.9
MT-6	4	1.467209	69	0.008672	26	0.000012	0	0.282485	26	-0.8	0.9
MT-7	4	1.467232	67	0.008631	27	0.000032	0	0.282464	23	-1.5	0.8
MT-8	4	1.467248	62	0.008676	24	0.000012	0	0.282497	21	-0.4	0.7
MT-9	4	1.467239	57	0.008664	22	0.000011	0	0.282505	24	-0.1	0.9
MT-10	4	1.467220	61	0.008664	22	0.000012	0	0.282467	22	-1.4	0.8
MT-11	4	1.467307	61	0.008633	25	0.000012	0	0.282483	26	-0.8	0.9
MT-12	4	1.467259	54	0.008661	24	0.000011	0	0.282477	23	-1.1	0.8
MT-13	4	1.467294	61	0.008643	25	0.000012	0	0.282475	21	-1.1	0.7
MT-14	4	1.467238	71	0.008680	26	0.000022	0	0.282466	22	-1.4	0.8
Mean[b]	**n=34**	**1.467251**	**80**	**0.008661**	**45**	**0.000036**	**39**	**0.282499**	**44**	**-0.3**	**1.6**
WH (2005) Soln[c]						**0.000042**		**0.282507**	**6**		
WH (2005) LA[d]								**0.282506**	**26**		
91500											
91500-1	1	1.467282	66	0.008663	30	0.000326	1	0.282284	38	-0.8	1.4
91500-2	1	1.467219	134	0.008651	87	0.000316	1	0.282341	74	1.2	2.6
91500-2A	1	1.467222	75	0.008637	35	0.000332	1	0.282317	41	0.4	1.5
91500-3	1	1.467269	89	0.008660	39	0.000317	1	0.282286	31	-0.7	1.1
91500-4	1	1.467248	107	0.008699	36	0.000322	1	0.282292	41	-0.5	1.4
91500-5	1	1.467251	69	0.008687	43	0.000317	1	0.282256	41	-1.8	1.5
91500-6	1	1.467219	91	0.008676	45	0.000335	1	0.282235	58	-2.5	2.0
91500-7	1	1.467249	72	0.008675	36	0.000337	1	0.282264	46	-1.5	1.6
91500-8	1	1.467240	59	0.008693	22	0.000330	1	0.282317	24	0.4	0.9
91500-9	1	1.467267	74	0.008730	25	0.000322	1	0.282321	30	0.5	1.1
91500-10	1	1.467253	84	0.008604	44	0.000308	1	0.282274	45	-1.1	1.6
91500-11	1	1.467187	82	0.008623	37	0.000332	1	0.282348	43	1.5	1.5
91500-12	1	1.467329	153	0.008604	79	0.001180	97	0.282248	31	-2.1	1.1
91500-1	2	1.467249	99	0.008722	51	0.000362	1	0.282384	46	2.8	1.6
91500-1B	2	1.467173	105	0.008644	76	0.000362	1	0.282384	46	2.8	1.6
91500-2	2	1.467206	107	0.008730	61	0.000360	1	0.282352	77	1.6	2.7
91500-4	2	1.467299	103	0.008677	53	0.000338	1	0.282254	78	-1.8	2.8
91500-5	2	1.467251	179	0.008806	102	0.000331	4	0.282302	91	-0.2	3.2
91500-6	2	1.467295	98	0.008671	47	0.000338	1	0.282330	57	0.9	2.0
91500-7	3	1.467272	60	0.008613	34	0.000391	1	0.282296	43	-0.4	1.5
91500-8	3	1.467281	88	0.008674	45	0.000332	1	0.282300	59	-0.2	2.1

91500-9	3	1.467273	107	0.008613	45	0.000320	1	0.282342	61	1.3	2.2
91500-10	3	1.467321	110	0.008655	53	0.000338	1	0.282324	52	0.6	1.8
91500-10B	3	1.467302	101	0.008617	49	0.000316	1	0.282316	58	0.4	2.1
91500-11	3	1.467239	127	0.008683	42	0.000332	3	0.282342	57	1.3	2.0
91500-12	3	1.467178	87	0.008628	46	0.000338	1	0.282353	61	1.7	2.2
91500-13	3	1.467233	112	0.008714	55	0.000317	1	0.282326	63	0.7	2.2
91500-14	3	1.467249	106	0.008620	59	0.000333	1	0.282315	67	0.3	2.4
91500-15	3	1.467301	103	0.008678	53	0.000328	1	0.282332	76	0.9	2.7
91500-1	4	1.467223	81	0.008693	40	0.000337	1	0.282320	34	0.5	1.2
91500-2	4	1.467237	89	0.008693	44	0.000391	1	0.282274	37	-1.1	1.3
91500-3	4	1.467177	86	0.008684	36	0.000355	1	0.282257	36	-1.7	1.3
91500-4	4	1.467236	84	0.008668	41	0.000347	1	0.282261	32	-1.6	1.1
91500-5	4	1.467256	97	0.008686	40	0.000336	1	0.282277	38	-1.0	1.4
91500-6	4	1.467258	87	0.008625	36	0.000348	1	0.282282	36	-0.8	1.3
91500-7	4	1.467175	87	0.008639	55	0.000326	3	0.282267	37	-1.4	1.3
91500-8	4	1.467332	79	0.008674	44	0.000334	2	0.282300	37	-0.2	1.3
91500-9	4	1.467241	77	0.008718	48	0.000324	1	0.282361	36	1.9	1.3
91500-10	4	1.467268	85	0.008697	51	0.000388	1	0.282329	40	0.8	1.4
91500-12	4	1.467205	80	0.008647	46	0.000348	1	0.282263	34	-1.5	1.2
91500-13	4	1.467276	81	0.008677	47	0.000325	1	0.282293	33	-0.5	1.2
91500-13B	4	1.467257	73	0.008638	48	0.000349	1	0.282297	36	-0.3	1.3
91500-14	4	1.467252	88	0.008664	42	0.000359	2	0.282267	34	-1.4	1.2
91500-14B	4	1.467239	78	0.008678	44	0.000348	2	0.282284	32	-0.8	1.1
Mean[b]	**n=44**	**1.467250**	**79**	**0.008669**	**80**	**0.000357**	**257**	**0.282304**	**74**	**-0.1**	**2.6**
WH (2005) Soln[c]						**0.000311**		**0.282306**	**8**		
WH (2005) LA[d]								**0.282296**	**28**		
Temora-2											
TEM-1	1	1.467226	75	0.008727	33	0.000729	55	0.282681	28	-0.2	1.0
TEM-2	1	1.467244	59	0.008676	22	0.001491	10	0.282642	33	-1.6	1.2
TEM-3	1	1.467280	59	0.008673	22	0.001597	185	0.282659	53	-0.9	1.9
TEM-4	1	1.467219	67	0.008669	30	0.001330	13	0.282648	29	-1.4	1.0
TEM-7_1	1	1.467216	58	0.008659	28	0.000946	5	0.282676	32	-0.4	1.1
TEM-6_2	1	1.467280	57	0.008636	118	0.001620	41	0.282677	27	-0.3	0.9
TEM-8_1	1	1.467229	91	0.008733	56	0.001097	7	0.282702	50	0.6	1.8
TEM-5	1	1.467229	61	0.008584	32	0.000667	2	0.282641	27	-1.6	1.0
TEM-6	1	1.467257	71	0.008666	27	0.001631	191	0.282607	50	-2.8	1.8
TEM-7	1	1.467242	54	0.008635	19	0.000807	48	0.282602	31	-3.0	1.1
TEM-8	1	1.467206	92	0.008622	40	0.000876	9	0.282621	22	-2.3	0.8
TEM-9	1	1.467256	53	0.008658	20	0.000813	27	0.282688	19	0.1	0.7
TEM-10	1	1.467228	78	0.008589	32	0.000992	24	0.282639	33	-1.7	1.2
TEM-11	1	1.467218	65	0.008678	27	0.000880	11	0.282712	36	0.9	1.3
TEM-1	2	1.467211	86	0.008667	59	0.001310	53	0.282737	54	1.8	1.9
TEM-2	2	1.467216	101	0.008653	43	0.000638	9	0.282717	52	1.1	1.8
TEM-4	2	1.467244	84	0.008649	33	0.000674	18	0.282679	35	-0.3	1.2
TEM-7	3	1.467261	70	0.008605	34	0.001120	21	0.282682	40	-0.1	1.4
TEM-8	3	1.467275	70	0.008579	38	0.000620	24	0.282688	36	0.1	1.3
TEM-9	3	1.467308	83	0.008620	49	0.001118	19	0.282682	51	-0.1	1.8
TEM-10	3	1.467299	80	0.008640	35	0.000571	7	0.282662	48	-0.9	1.7
TEM-11	3	1.467240	65	0.008674	34	0.001092	8	0.282680	38	-0.2	1.3
TEM-12	3	1.467210	82	0.008663	45	0.001024	5	0.282698	44	0.4	1.6
TEM-13	3	1.467195	84	0.008599	40	0.000674	18	0.282679	35	-0.3	1.2
TEM-14	3	1.467197	88	0.008597	53	0.001388	28	0.282742	48	2.0	1.7
TEM-15	3	1.467322	73	0.008708	48	0.001370	14	0.282688	49	0.1	1.7
TEM-1	4	1.467299	61	0.008703	33	0.000927	48	0.282699	26	0.5	0.9
TEM-1B	4	1.467194	73	0.008611	47	0.001166	7	0.282627	28	-2.1	1.0

TEM-2	4	1.467222	51	0.008678	27	0.000726	41	0.282649	24	-1.3	0.9
TEM-3	4	1.467212	74	0.008652	39	0.000489	8	0.282653	29	-1.2	1.0
TEM-4	4	1.467194	79	0.008652	43	0.001243	21	0.282634	46	-1.8	1.6
TEM-4B	4	1.467169	86	0.008699	35	0.000545	8	0.282684	32	-0.1	1.1
TEM-5	4	1.467242	67	0.008696	34	0.000992	14	0.282684	29	-0.1	1.0
TEM-6	4	1.467221	72	0.008684	36	0.000986	15	0.282667	27	-0.7	1.0
TEM-7	4	1.467267	59	0.008628	29	0.001333	20	0.282647	27	-1.4	1.0
TEM-8B	4	1.467259	62	0.008692	30	0.000927	4	0.282698	30	0.4	1.1
TEM-8C	4	1.467313	65	0.008640	27	0.000573	3	0.282635	26	-1.8	0.9
TEM-8D	4	1.467311	65	0.008693	34	0.001534	34	0.282691	28	0.2	1.0
TEM-9	4	1.467218	73	0.008683	41	0.002349	12	0.282723	35	1.3	1.2
TEM-10B	4	1.467155	70	0.008694	35	0.001383	34	0.282691	30	0.2	1.1
TEM-11	4	1.467298	74	0.008622	31	0.001101	16	0.282649	27	-1.3	1.0
TEM-12	4	1.467210	89	0.008626	45	0.001301	13	0.282659	29	-0.9	1.0
TEM-13	4	1.467284	69	0.008757	39	0.001436	20	0.282753	30	2.4	1.1
TEM-13B	4	1.467213	62	0.008763	33	0.001223	28	0.282739	27	1.9	0.9
TEM-14	4	1.467262	71	0.008700	36	0.001529	17	0.282679	36	-0.3	1.3
TEM-14B	4	1.467230	72	0.008679	34	0.001208	12	0.282676	27	-0.4	0.9
Mean[b]	**n=46**	**1.467241**	**79**	**0.008661**	**86**	**0.001088**	**753**	**0.282675**	**69**	**-0.4**	**2.4**
WH (2005) Soln[c]						**0.001090**		**0.282686**	**8**		
WH (2005) LA[d]								**0.282680**	**22**		
FC1											
FC1-1	1	1.467243	85	0.008715	51	0.001861	29	0.282184	50	0.0	1.8
FC1-2	1	1.467271	56	0.008685	35	0.000765	1	0.282153	34	-1.1	1.2
FC1-3	1	1.467282	71	0.008687	28	0.000833	2	0.282164	24	-0.7	0.9
FC1-4	1	1.467252	50	0.008644	26	0.001150	4	0.282164	34	-0.7	1.2
FC1-0_2	1	1.467299	55	0.008697	19	0.002035	4	0.282148	26	-1.3	0.9
FC1-2_2	1	1.467248	71	0.008660	29	0.000951	2	0.282111	18	-2.6	0.7
FC1-4_2	1	1.467205	57	0.008689	25	0.000844	20	0.282141	31	-1.5	1.1
FC1-5	1	1.467250	54	0.008734	28	0.001052	3	0.282172	29	-0.4	1.0
FC1-6	1	1.467285	58	0.008655	25	0.000983	12	0.282163	30	-0.7	1.1
FC1-7	1	1.467265	61	0.008615	33	0.001285	25	0.282113	27	-2.5	0.9
FC1-8	1	1.467299	44	0.008642	17	0.000700	1	0.282149	16	-1.2	0.6
FC1-9	1	1.467273	49	0.008647	20	0.000716	21	0.282138	20	-1.6	0.7
FC1-10	1	1.467261	71	0.008623	39	0.000719	2	0.282123	41	-2.2	1.5
FC1-1	2	1.467270	74	0.008804	51	0.000616	4	0.282200	32	0.6	1.1
FC1-2	2	1.467198	73	0.008613	33	0.001286	21	0.282165	42	-0.7	1.5
FC1-4	2	1.467308	88	0.008686	50	0.000798	6	0.282156	39	-1.0	1.4
FC1-5	2	1.467254	70	0.008600	34	0.001098	1	0.282166	38	-0.6	1.4
FC1-6	2	1.467322	84	0.008626	36	0.000917	1	0.282174	37	-0.4	1.3
FC1-7	3	1.467333	86	0.008486	34	0.002059	3	0.282153	30	-1.1	1.0
FC1-8	3	1.467272	60	0.008613	34	0.000683	5	0.282150	31	-1.2	1.1
FC1-9	3	1.467231	68	0.008618	27	0.000656	20	0.282182	35	-0.1	1.2
FC1-10	3	1.467327	70	0.008576	34	0.000450	9	0.282115	35	-2.4	1.2
FC1-11	3	1.467259	81	0.008596	31	0.000998	9	0.282135	40	-1.7	1.4
FC1-12	3	1.467194	63	0.008636	32	0.001093	6	0.282217	46	1.2	1.6
FC1-13	3	1.467107	81	0.008693	40	0.002163	231	0.282131	68	-1.9	2.4
FC1-14	3	1.467273	80	0.008680	95	0.000854	25	0.282211	38	1.0	1.4
FC1-15B	3	1.467200	78	0.008586	36	0.000594	4	0.282164	53	-0.7	1.9
FC1-1	4	1.467215	72	0.008601	36	0.000990	6	0.282129	25	-1.9	0.9
FC1-2	4	1.467229	60	0.008659	30	0.000918	8	0.282108	26	-2.7	0.9
FC1-3	4	1.467195	76	0.008657	27	0.000945	4	0.282138	27	-1.6	1.0
FC1-4B	4	1.467198	117	0.008611	45	0.001344	8	0.282142	35	-1.5	1.2
FC1-4C	4	1.467193	92	0.008701	27	0.000642	9	0.282174	28	-0.3	1.0
FC1-4D	4	1.467167	79	0.008699	26	0.001421	20	0.282182	33	-0.1	1.2

FC1-5	4	1.467216	104	0.008659	62	0.001175	19	0.282117	28	-2.4	1.0
FC1-6	4	1.467181	121	0.008706	31	0.000737	14	0.282107	39	-2.7	1.4
FC1-6B	4	1.467276	58	0.008646	40	0.001292	5	0.282125	26	-2.1	0.9
FC1-7	4	1.467163	86	0.008605	58	0.001115	26	0.282080	34	-3.7	1.2
FC1-8	4	1.467245	79	0.008728	27	0.001110	9	0.282182	24	-0.1	0.8
FC1-8B	4	1.467234	57	0.008683	26	0.001148	2	0.282170	24	-0.5	0.8
FC1-8C	4	1.467246	90	0.008672	26	0.001167	7	0.282169	28	-0.5	1.0
FC1-8D	4	1.467260	70	0.008742	37	0.001086	22	0.282218	29	1.2	1.0
FC1-9	4	1.467201	64	0.008692	29	0.001354	2	0.282161	27	-0.8	1.0
FC1-10	4	1.467097	124	0.008718	71	0.001109	28	0.282109	49	-2.7	1.7
FC1-11	4	1.467283	67	0.008661	31	0.001174	2	0.282223	31	1.4	1.1
FC1-12	4	1.467212	61	0.008669	34	0.001011	3	0.282143	31	-1.5	1.1
FC1-13	4	1.467267	64	0.008706	31	0.001397	33	0.282226	25	1.5	0.9
FC1-13B	4	1.467292	71	0.008778	35	0.000947	17	0.282239	27	2.0	0.9
FC1-14	4	1.467277	71	0.008638	35	0.000642	8	0.282127	29	-2.0	1.0
Mean[b]	**n=48**	**1.467242**	**102**	**0.008661**	**111**	**0.001060**	**757**	**0.282156**	**71**	**-1.0**	**2.5**
WH (2005) Soln[c]						**0.001262**		**0.282184**	**16**		
WH (2005) LA[d]								**0.282172**	**42**		

[a] = $\times 10^{-6}$

[b] = Reference material isotopic ratio or ε_{Hf} mean ± 2σ

[c] = Woodhead and Hergt (2005) solution analysis isotopic ratio mean ± 2σ

[d] = Woodhead and Hergt (2005) laser ablation analysis isotopic ratio mean ± 2σ

Online Resource 2e

Zircon unknowns ε_{Hf}

Sample Spot	Session	$^{178}Hf/^{177}Hf$	err[a] 2σ	$^{174}Hf/^{177}Hf$	err[a] 2σ	$^{176}Lu/^{177}Hf$	err[a] 2σ	$^{176}Hf/^{177}Hf$ Meas.	err[a] 2σ	ε_{Hf} Meas.	$^{176}Hf/^{177}Hf$ Initial	err[a] 2σ	CHUR Initial	ε_{Hf} Initial	err 2σ	err abs.
248251-3.1	3	1.467247	61	0.008607	17	0.000950	25	0.280417	32	-83.7	0.280350	32	0.280401	-1.8	1.1	2.4
248251-4.1	3	1.467146	70	0.008636	24	0.001008	45	0.280428	39	-83.4	0.280356	39	0.280384	-1.0	1.4	2.5
248251-8.2	3	1.467178	77	0.008590	19	0.000537	14	0.280412	40	-83.9	0.280374	40	0.280392	-0.7	1.4	2.5
248251-10.1	3	1.467155	58	0.008608	23	0.001151	17	0.280469	37	-81.9	0.280386	37	0.280372	0.5	1.3	2.5
248251-10.2	3	1.467135	76	0.008631	25	0.001160	94	0.280454	32	-82.4	0.280370	32	0.280376	-0.2	1.2	2.4
248251-12.1	3	1.467121	70	0.008549	16	0.001350	26	0.280427	31	-83.4	0.280341	31	0.280646	-10.9	1.1	2.4
248251-13.1	3	1.467207	82	0.008594	24	0.000792	27	0.280417	33	-83.7	0.280361	33	0.280380	-0.7	1.2	2.4
248251-14.1	3	1.467268	97	0.008608	34	0.000850	31	0.280430	49	-83.3	0.280369	49	0.280377	-0.3	1.7	2.7
248251-18.1	3	1.467216	62	0.008571	16	0.000827	8	0.280414	25	-83.8	0.280356	25	0.280411	-2.0	0.9	2.3
248251-20.1	3	1.467152	70	0.008555	23	0.000884	50	0.280445	41	-82.8	0.280387	41	0.280584	-7.0	1.5	2.6
248251-22.1	3	1.467115	77	0.008585	24	0.001217	31	0.280471	43	-81.8	0.280384	43	0.280390	-0.2	1.5	2.6
248251-23.1	3	1.467152	63	0.008648	34	0.001471	137	0.280479	41	-81.5	0.280375	41	0.280412	-1.3	1.5	2.6
248212-1.1	3	1.467183	64	0.008598	20	0.001108	30	0.280408	34	-84.0	0.280329	34	0.280387	-2.1	1.2	2.4
248212-2.1	3	1.467227	63	0.008630	22	0.001014	16	0.280449	35	-82.6	0.280377	35	0.280396	-0.7	1.3	2.4
248212-3.1	3	1.467238	79	0.008645	15	0.000659	3	0.280366	31	-85.5	0.280319	31	0.280390	-2.5	1.1	2.4
248212-4.1	3	1.467218	69	0.008510	21	0.001022	97	0.280354	34	-86.0	0.280283	34	0.280445	-5.8	1.2	2.4
248212-5.1	3	1.467197	71	0.008626	24	0.001040	20	0.280431	31	-83.2	0.280357	31	0.280381	-0.9	1.1	2.4
248212-6.1	3	1.467205	70	0.008645	21	0.000609	17	0.280434	33	-83.1	0.280391	33	0.280390	0.0	1.2	2.4
248212-7.1	3	1.467245	73	0.008650	21	0.001171	58	0.280469	36	-81.9	0.280387	36	0.280436	-1.8	1.3	2.5
248212-9.1	3	1.467189	68	0.008630	20	0.001018	28	0.280452	31	-82.5	0.280379	31	0.280385	-0.2	1.1	2.4
G97/111-1.1	1	1.467239	59	0.008668	13	0.000602	5	0.280474	27	-81.7	0.280432	27	0.280433	0.0	1.0	2.3
G97/111-2.1	1	1.467189	76	0.008630	14	0.000663	28	0.280456	27	-82.4	0.280409	27	0.280432	-0.8	0.9	2.3
G97/111-3.1	1	1.467204	71	0.008629	14	0.000494	11	0.280430	22	-83.3	0.280395	22	0.280421	-0.9	0.8	2.2
G97/111-4.1	1	1.467164	67	0.008607	14	0.000642	4	0.280445	25	-82.7	0.280400	25	0.280424	-0.9	0.9	2.3
G97/111B-1.1	3	1.467194	73	0.008645	17	0.000712	24	0.280419	33	-83.7	0.280369	33	0.280416	-1.7	1.2	2.4
G97/111B-2.1	2	1.467194	71	0.008644	20	0.000609	4	0.280436	31	-83.1	0.280393	31	0.280425	-1.2	1.1	2.4
G97/111B-3.1	3	1.467252	62	0.008642	15	0.000587	5	0.280413	29	-83.9	0.280372	29	0.280412	-1.4	1.0	2.3
G97/111B-4.1	2	1.467244	68	0.008581	17	0.000591	4	0.280432	34	-83.2	0.280392	34	0.280533	-5.0	1.2	2.4
G97/111B-5.1	3	1.467232	63	0.008619	15	0.000890	6	0.280441	26	-82.9	0.280379	26	0.280424	-1.6	0.9	2.3
G97/111B-6.1	2	1.467246	68	0.008612	19	0.000626	24	0.280434	35	-83.1	0.280390	35	0.280452	-2.2	1.2	2.4

G97/111B-7.1	2	1.467184	76	0.008610	20	0.000424	7	0.280425	33	-83.5	0.280396	33	0.280507	-4.0	1.2	2.4
G97/111B-8.1	3	1.467246	59	0.008653	16	0.000702	11	0.280443	28	-82.8	0.280395	28	0.280464	-2.5	1.0	2.3
VM97/01-2.1	3	1.467117	144	0.008623	41	0.000992	82	0.281017	32	-62.5	0.280964	32	0.280977	-0.5	1.2	2.4
VM97/01-3.1	3	1.467329	99	0.008526	52	0.000893	47	0.281000	43	-63.1	0.280952	43	0.280966	-0.5	1.5	2.6
VM97/01-5.1	3	1.467330	136	0.008565	205	0.001671	34	0.280968	136	-64.3	0.280877	136	0.280965	-3.1	4.8	5.3
195392-1.1	3	1.467047	153	0.008624	21	0.000436	8	0.280437	33	-83.0	0.280406	33	0.280389	0.6	1.2	2.4
195392-5.1	3	1.466978	189	0.008548	46	0.000608	29	0.280786	39	-70.7	0.280756	39	0.281149	-14.0	1.4	2.5
195392-6.1	3	1.467373	163	0.008639	47	0.000440	21	0.280477	38	-81.6	0.280447	38	0.280520	-2.6	1.4	2.5
195392-7.1	3	1.467344	196	0.008712	51	0.000304	7	0.280434	56	-83.1	0.280416	56	0.280790	-13.3	2.0	2.9
195392-9.1	3	1.467233	114	0.008623	28	0.000310	26	0.280421	30	-83.6	0.280403	30	0.280861	-16.3	1.1	2.4
195392-12.1	3	1.467209	64	0.008652	13	0.000372	9	0.280526	35	-79.9	0.280508	35	0.281132	-22.2	1.3	2.4
195392-13.1	3	1.467194	64	0.008599	17	0.000684	22	0.280488	28	-81.2	0.280448	28	0.280837	-13.8	1.0	2.3
195392-17.1	3	1.467072	125	0.008664	20	0.000354	15	0.280510	48	-80.4	0.280493	48	0.281139	-23.0	1.7	2.7
195392B-1.1	4	1.467250	133	0.008610	36	0.000770	88	0.280475	28	-81.7	0.280421	28	0.280407	0.5	1.0	2.3
195392B-1.2	4	1.467143	144	0.008611	31	0.000843	17	0.280416	23	-83.8	0.280356	23	0.280393	-1.3	0.8	2.3
195392B-4.1	4	1.467249	174	0.008600	87	0.002868	88	0.280575	46	-78.1	0.280373	46	0.280417	-1.6	1.7	2.7
195392B-5.2	4	1.467243	83	0.008661	21	0.000525	26	0.280651	18	-75.5	0.280625	18	0.281132	-18.0	0.6	2.2
195392B-6.1	4	1.467243	109	0.008623	19	0.000573	14	0.280521	22	-80.1	0.280491	22	0.281033	-19.3	0.8	2.2
195392B-6.2	4	1.467215	120	0.008624	26	0.000607	15	0.280432	21	-83.2	0.280390	21	0.280447	-2.0	0.7	2.2
195392B-8.1	4	1.467245	132	0.008587	23	0.000542	6	0.280504	23	-80.7	0.280475	23	0.281022	-19.5	0.8	2.2
195392B-8.2	4	1.467237	106	0.008621	28	0.000731	14	0.280371	23	-85.4	0.280320	23	0.280430	-3.9	0.8	2.3
195392B-8.3	4	1.467253	111	0.008625	20	0.000602	8	0.280489	20	-81.2	0.280457	20	0.281025	-20.2	0.7	2.2
195392B-8.4	4	1.467230	117	0.008626	23	0.000797	8	0.280417	19	-83.7	0.280361	19	0.280436	-2.7	0.7	2.2
195392B-9.1	4	1.467237	99	0.008678	25	0.000637	19	0.280514	21	-80.3	0.280481	21	0.281034	-19.7	0.7	2.2
195392B-9.2	4	1.467232	111	0.008691	27	0.000688	15	0.280551	22	-79.0	0.280515	22	0.281028	-18.3	0.8	2.2
195392B-11.1	4	1.467201	85	0.008564	21	0.001201	27	0.280424	18	-83.5	0.280341	18	0.280452	-4.0	0.7	2.2
195392B-12.1	4	1.467267	114	0.008617	22	0.000418	3	0.280416	23	-83.8	0.280387	23	0.280480	-3.3	0.8	2.2
195376-3.1	4	1.467227	129	0.008655	27	0.000633	8	0.280712	22	-73.3	0.280680	22	0.281131	-16.0	0.8	2.2
195376-4.1	4	1.467228	164	0.008674	33	0.000504	28	0.280847	30	-68.5	0.280818	30	0.280802	0.5	1.1	2.3
195376-5.1	4	1.467266	127	0.008656	39	0.000801	21	0.280740	26	-72.3	0.280701	26	0.281130	-15.3	0.9	2.3
195376-5.2	4	1.467224	171	0.008648	47	0.000989	30	0.280756	33	-71.8	0.280708	33	0.281141	-15.4	1.2	2.4
195376-6.1	4	1.467146	171	0.008629	40	0.000537	6	0.280824	23	-69.3	0.280798	23	0.281142	-12.3	0.8	2.3
195376-9.1	4	1.467209	189	0.008678	42	0.000940	46	0.280867	38	-67.8	0.280812	38	0.280793	0.7	1.4	2.5

[a] = $\times 10^{-6}$

Online Resource 2f
Zircon reference materials ε_{Hf}

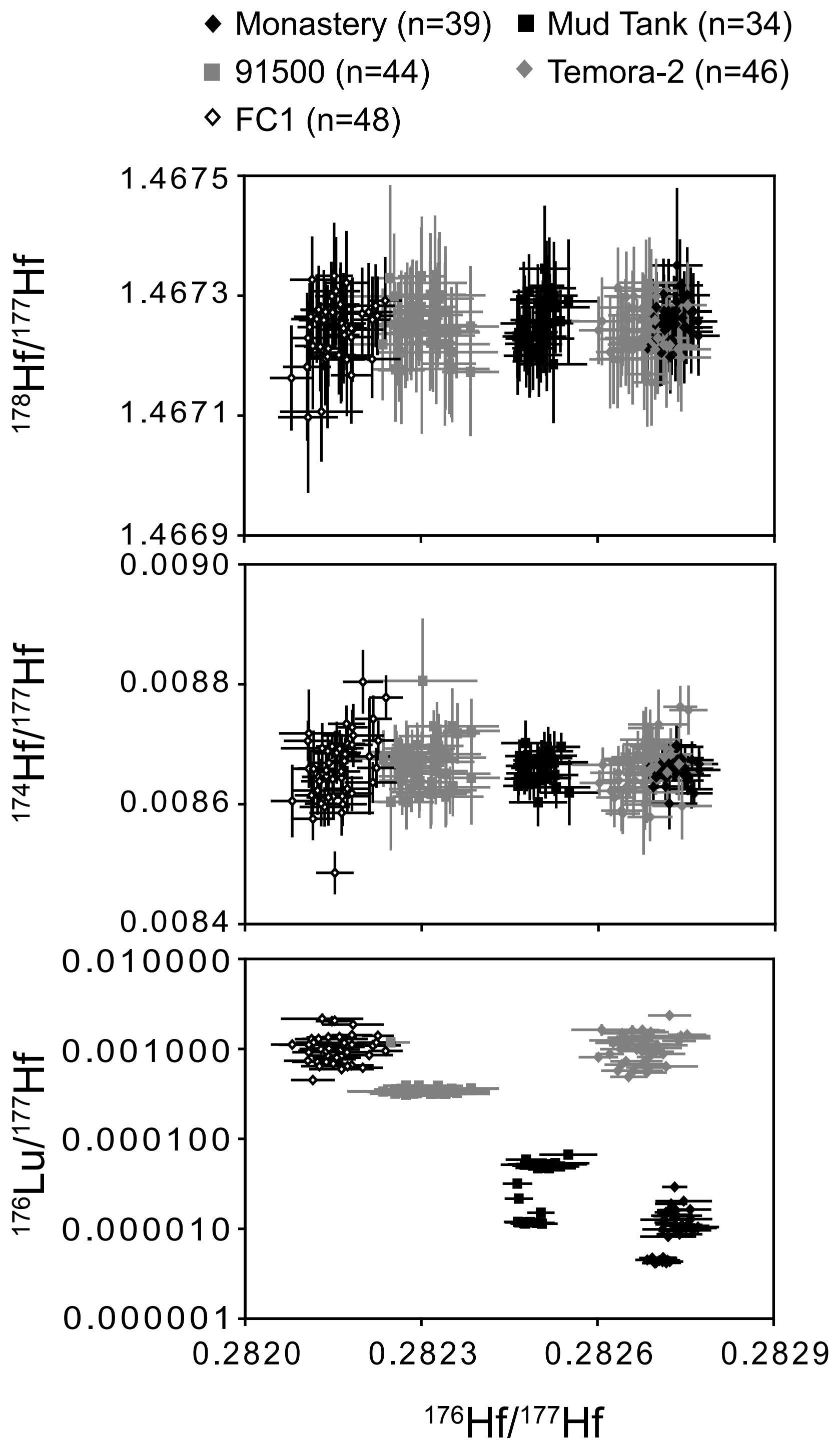

Online Resource 3
Zircon characteristics and main geochemical results

3.1. ~3690 Ma granitic gneiss 248251 and trondhjemite 248212

Zircon from samples 248251 and 248212 are typically prismatic and 100 - 200 microns in length (Fig. 2a). Most display fine scaled oscillatory zonation, while some grains contain inherited cores and/or dark overgrowths. Earlier bulk U-Pb zircon geochronology on samples 248251 and 248212 by Baadsgaard (1983) gave slightly discordant $^{207}Pb/^{206}Pb$ ages up to ~3650 Ma. Our SHRIMP U-Pb concordant analyses suggest they formed slightly earlier at ~3690 Ma. Based on this new data, samples 248251 and 248212 are therefore not ~3650 Ma white gneisses. Regardless, their evolved compositions, however, are anomalous to the generally tonalitic, 3690 Ma suite represented by sample 248228 of Hiess et al. (2009). Based on their compositional characteristics, samples 248251 and 248212 are regarded as early evolved phases, which are likely to involve cannibalization of older crustal components, such as the 3720-3710 Ma tonalite suite.

For sample 248251, 15 U-Pb analyses on 13 grains provided $^{207}Pb/^{206}Pb$ ages ranging from 3715±4 Ma to 3305±4 Ma, with a mean of 3686±22 Ma (1σ; Fig. 3a; Table 1). Th/U ratios were low to moderate, ranging from 0.00 to 0.46. $\delta^{18}O$ from 6 analyses ranged from 5.4±0.3‰ at 3715 Ma to 2.3±0.3‰ at 3305 Ma (Fig. 3b). The mean $\delta^{18}O$ for the 4 analyses within the oldest population is 4.2±1.0‰ (1σ). $\delta^{18}O$ measurements were made on grains with U concentrations ranging from 132 to 722 ppm (Fig. 4a), and with Th/U ratios ranging from 0.09 to 0.46 (Fig. 4c). No correlation exists between $\delta^{18}O$ and U, Th, Th/U, % common ^{206}Pb, and % discordance (Fig. 4). Initial ε_{Hf} from 12 analyses range from 0.5±1.3 to -10.9±1.1 defining a $\varepsilon_{Hf(T)}$ – $^{207}Pb/^{206}Pb$ array equivalent to a $^{176}Lu/^{177}Hf$ ratio of 0.001 (Fig. 3c). This array intersects the chondritic reference line at ~3724 Ma. The weighted mean $\varepsilon_{Hf(T)}$ for the 10 analyses within the oldest population is -0.8±0.8 (95% c.l.). Within the oldest population, analysis 10.1 was made within a core domain recording the oldest age at 3715±4 Ma, a mantle-like $\delta^{18}O$ composition of 5.4±0.3‰ and near-chondritic $\varepsilon_{Hf(T)}$ of 0.5±1.3 (Fig. 2a). On the same grain, away from the core analysis spot 10.2 records a slightly younger age of 3709±2 Ma, a slightly lower $\delta^{18}O$ composition of 4.3±0.3‰ and slightly lower $\varepsilon_{Hf(T)}$ of -0.2±1.2. These Hf and zircon inheritance results are noteworthy, as they are indication that the sample's evolved composition might have been brought about by cannibilisation of ~3720 Ma tonalities in the vicinity.

For trondhjemitic sample 248212, 8 SHRIMP U-Pb analyses provided $^{207}Pb/^{206}Pb$ ages ranging from 3702±3 Ma (248212-5.1, Fig. 2a), to 3607±5 Ma, (248212-4.1, Fig. 2a), with a mean of 3690±8 Ma (1σ) for 6 spots >3675 Ma (Fig. 3d). Uranium concentrations typically ranged from 128 to 350 with one analysis (3607±5 Ma) at 2032 ppm. Th/U ratios were low to moderate, ranging from 0.08 to 0.57. $\delta^{18}O$ from 8 analyses ranged from 5.2±0.3‰ within grain core of 248212-2.1 (Fig. 2a), down to 3.6±0.3‰ (Fig. 3e). The mean $\delta^{18}O$ for the 6 analyses within the oldest population was 4.6±0.6‰ (1σ). No correlation exists between $\delta^{18}O$ and U, Th, Th/U, % common ^{206}Pb, and % discordance (Fig. 4). Initial ε_{Hf} from 8 analyses range from 0.0±1.2 (248212-6.1, Fig. 2a) to -5.8±1.2 (248212-4.1, Fig. 2a, 3f) with a weighted mean $\varepsilon_{Hf(T)}$ of -1.1±1.0 (95% c.l.) for the 6 analyses within the oldest population. Anhedral grains 248212-6.1, 7.1 and 9.1 (Fig. 2a) record ages and compositions consistent with those of prismatic habit.

3.2. ~3640 Ma augen gneiss granite G97/111

Zircon from A-type augen gneiss G97/111 are prismatic or anhedral and 150 – 300 microns in length (Fig. 2b). Most display fine scaled oscillatory zonation and all lack inherited cores. Grain edges are occasionally corroded and often replaced by thin, light overgrowth rims. Thirteen U-Pb analyses provided $^{207}Pb/^{206}Pb$ ages ranging from 3656±5 Ma to 3475±4 Ma, with a mean of 3635±14 Ma (1σ) for 9 spots >3600 Ma (Fig. 3g). Uranium concentrations ranged from 24 ppm in light tone G97/111-1.1 (Fig. 2b), to 327 ppm in dark tone G97/111B-5.1 (Fig. 2b). Th/U ratios were moderate, ranging from 0.46 to 0.77. $\delta^{18}O$ from 11 analyses typically range from 6.6±0.3‰ (G97/111-1.1, Fig. 2b) to 5.6±0.3‰ (G97/111B-5.1, Fig. 2b) with one outlier at 4.7±0.3‰ (oscillatory zoned G97/111-2.1, Fig. 2b, 3h). The mean $\delta^{18}O$ for the 7 analyses within the oldest population (including the outlier) is 5.8±0.6‰ (1σ). No correlation exists between $\delta^{18}O$ and U, Th, Th/U, % common ^{206}Pb, and % discordance (Fig. 4). Initial ε_{Hf} from 12 analyses range from 0.0±1.0 to -5.0±1.2 defining a $\varepsilon_{Hf(T)}$ – $^{207}Pb/^{206}Pb$ array equivalent to a $^{176}Lu/^{177}Hf$ ratio of 0.002 (Fig. 3i). This array projects to an intersection with the chondritic reference line at ~3681 Ma. The weighted mean $\varepsilon_{Hf(T)}$ for the 8 analyses within the oldest population is -1.1±0.8 (95% c.l.).

3.3. ~2820 Ma granodioritic Ikkattoq gneiss VM97/01

Zircons from sample VM97/01 are prismatic and ~200 - 250 µm in length, with fine scaled oscillatory zonation and recrystallised grain centers (Fig. 2c). Eleven U-Pb analyses provided $^{207}Pb/^{206}Pb$ ages ranging from 2838±9 Ma (VM97/01-10.1, Fig. 2c) to 2801±7 Ma (VM97/01-5.2, Fig. 2c), with a weighted mean of 2821±8 Ma (95% c.l., Fig. 3j). Uranium concentrations ranged from 258 to 521 ppm. Th/U ratios were moderate, ranging from 0.29 to 0.51. $\delta^{18}O$ from 5 analyses ranged from 4.7±0.5‰ to 3.1±0.5‰ with a weighted mean of 4.0±0.8‰ (95% c.l., Fig. 3k). Again no correlation exists between $\delta^{18}O$ and U, Th, Th/U, % common ^{206}Pb, and % discordance (Fig. 4). Initial ε_{Hf} from three analyses range from -0.5±1.2 (VM97/01-2.1, Fig. 2c) to -3.1±4.8 (VM97/01-10.1, Fig. 2c) with a weighted mean $\varepsilon_{Hf(T)}$ of -0.7±1.6 (95% c.l., Fig. 3l).

3.4. Neoarchaean migmatite 195392 and Qôrqut granite complex granite 195376

Zircon from samples 195392 and 195376 are prismatic and 100 - 200 µm in length (Fig. 2d). Grains are typically dark in CL and display faintly defined, oscillatory zonation. For sample 195392, migmatite sample spatially associated with the QGC, zircons can be divided into four separate populations.

The oldest Eoarchaean population consists of 15 U-Pb analyses, 11 within definite structural grain cores and 4 on grain middle regions. $^{207}Pb/^{206}Pb$ ages ranged from 3729±18 Ma to 3494±17 Ma, with a mean of 3627±38 Ma (1σ) for 13 spots >3500 Ma and <3700 Ma (Fig. 3m). U concentrations were variable, ranging from 42 to 1476 ppm. Th/U ratios were variable, ranging from 0.04 to 1.62. $\delta^{18}O$ from 12 analyses range from 5.7±0.4‰ (195392B-4.1) to 4.2±0.4‰ (195392B-6.2, Fig. 2d, 3n). The weighted mean $\delta^{18}O$ for the 10 analyses within the coherent age population is 5.0±0.4‰ (95% c.l.). Initial ε_{Hf} range from 0.6±1.2 at 3689±7 Ma in inherited core 195392-1.1, Fig. 2d) to -4.0±0.7 at 3595±4 Ma (Fig. 3o).

A ~3032 Ma Mesoarchaean population is given by six U-Pb analyses which provided $^{207}Pb/^{206}Pb$ ages ranging from 3215±30 Ma to 2982±21 Ma, with a mean of 3032±46 Ma (1σ) for 5 spots <3100 Ma (Fig. 3m). U concentrations ranged from 43 to 1291 ppm. Th/U ratios, ranged from 0.08 to 0.75. $\delta^{18}O$ from 3 analyses ranged from 4.1±0.5‰ to 3.4±0.5‰ with a weighted mean of 3.7±0.5‰. (95% c.l., Fig. 3n). The $\delta^{18}O$ measurements were made on grains with U concentrations ranging from 43 to 124 ppm (Fig. 4a), and with Th/U ratios ranging from 0.38 to 0.75 (Fig. 4c). Initial ε_{Hf} from 3 analyses range from -13.3±2.0 to -16.3±1.1 with a weighted mean of -14.6±4.0 (95% c.l., Fig. 3o).

A ~2726 Ma Neoarchaean population is given by seven U-Pb analyses which provided $^{207}Pb/^{206}Pb$ ages ranging from 2739±10 Ma to 2660±6 Ma, with a weighted mean of 2726±5 Ma (95% c.l.) for 6 spots >2700 Ma (Fig. 3m). U concentrations ranged from 205 to 824 ppm and Th/U ratios ranged from 0.07 to 0.13. $\delta^{18}O$ from 7 analyses ranged from 4.8±0.4‰ (195392B-8.1, Fig. 2d) to 3.5±0.4‰ (195392B-6.1, Fig. 2d, Fig. 3n). The weighted mean $\delta^{18}O$ for the 6 analyses within the oldest population is 4.0±0.5‰ (95% c.l.). Initial ε_{Hf} from 5 analyses range from -18.3±0.8 to -20.2±0.7 with a weighted mean of -19.4±1.0 (95% c.l., Fig. 3o).

A youngest ~2570 Ma Neoarchaean population is given by eight U-Pb analyses, 3 on grain mid regions and 4 on grain edges. With an age of ~2570 Ma, this migmatite component is coincident, or marginally older than the QGC with an emplacement age of 2565-2560 Ma from all SHRIMP U-Pb zircon geochronology (Nutman et al. 2007; In review). $^{207}Pb/^{206}Pb$ ages ranged from 2572±17 Ma to 2541±16 Ma, with a weighted mean of 2570±4 Ma (95% c.l., Fig. 3m). U concentrations ranged from 42 to 1258 ppm and Th/U ratios ranged from 0.04 to 1.03. $\delta^{18}O$ from 4 analyses ranged from 5.1±0.5‰ to 4.4±0.5‰ with a weighted mean of 4.7±0.4‰ (95% c.l., Fig. 3n). No correlation exists between $\delta^{18}O$ and U, Th, Th/U, % common ^{206}Pb, and % discordance for any of the 195392 populations (Fig. 4). Initial ε_{Hf} from 4 analyses range from -14.0±1.4 to -23.0±1.7 with a weighted mean from the two lowest analyses of -22.6±1.8 (95% c.l., Fig. 3o).

Excluding two $\varepsilon_{Hf(T)}$ analysis of -14.0±1.4 (2546±31 Ma) and -18.0±0.6 (2572±2 Ma), the plot of $\varepsilon_{Hf(T)}$ – $^{207}Pb/^{206}Pb$ for 195392 populations defines an array equivalent to a $^{176}Lu/^{177}Hf$ ratio of 0.004 (Fig. 3o). This array projects to an intersection with the chondritic reference line at ~3735 Ma (Fig. 3o). One clearly defined oscillatory zoned core 195392-1.1 (Fig. 2d) with a $^{207}Pb/^{206}Pb$ age of 3689±7 Ma records a primitive $\delta^{18}O$ composition of 5.4±0.5‰ and near-chondritic $\varepsilon_{Hf(T)}$ of 0.6±1.2. Of the grains that were analysed for oxygen isotopes on multiple spots, grain 195392B-6 records an Eoarchaean core and Neoarchaean mid region (Fig. 2d). Both $\delta^{18}O$ compositions are lower than mantle zircon and show an apparent decrease from grain core to mid region. Grain 195392B-8 records two core analyses on Eoarchaean domains, one mid grain and one grain edge analysis, both made on Neoarchaean domains (Fig. 2d). Eoarchaean core analyses record $\delta^{18}O$ compositions that lie within the range of mantle zircon, Neoarchaean analyses record $\delta^{18}O$ compositions that are lower than mantle compositions. Duplicate quartz $\delta^{18}O$ (VSMOW) analyses from this sample recorded compositions of 8.7±0.1‰ and 9.2±0.1‰.

For QGC homogeneous granite sample 195376, seven U-Pb analyses recorded $^{207}Pb/^{206}Pb$ ages ranging from 3602±19 Ma to 2556±9 Ma. Four spots <2580 Ma provide a weighted mean age of 2571±10 Ma (95% c.l.), within error of the previous reported 2564±12 Ma based on more measurements (Nutman et al. 2007), while Mesoarchaean (3071±7 Ma, 3085±5 Ma) and

Eoarchaean (3602±19) analyses are associated with inherited components (Fig. 3p). U concentrations and Th/U ratios within the Neoarchaean analyses were high, ranging from 1117 to 3274 ppm and 0.91 to 1.48 respectively (e.g. 195376-3.1, 5.1 and 5.2, Fig. 2d). In contrast, Mesoarchaean (344 ppm and 0.58, 804 ppm and 0.11) and Eoarchaean (83 ppm and 0.10) analyses were significantly lower in U and Th/U (e.g. 195376-4.1, Fig. 2d). $\delta^{18}O$ from 6 analyses ranged from 4.9±0.4‰ to 3.5±0.4‰ (Fig. 3q). The mean $\delta^{18}O$ for the 4 analyses within the youngest population is 4.2±0.7‰ (1σ) but indistinguishable from analyses made on Mesoarchaean domains. Again no correlation exists between $\delta^{18}O$ and U, Th, Th/U, % common ^{206}Pb, and % discordance (Fig. 4). Initial ε_{Hf} from 4 analyses within the youngest (<2580 Ma) population range from -12.3±0.8 to -16.0±0.8 with a mean of -14.7±1.7 (1σ, Fig. 3r). Two Mesoarchaean analyses lie within error of CHUR at 0.7±1.4 (3085±5 Ma, 195376-9.1) and 0.5±1.1 (3071±7 Ma, 195376-4.1, Fig. 2d). Duplicate quartz $\delta^{18}O$ (VSMOW) analyses from this sample recorded compositions of 8.2±0.1‰ and 8.9±0.1‰.

References

Baadsgaard H (1983) U-Pb isotope systematics on minerals from the gneiss complex at Isukasia, West Greenland. Rapport Grønlands Geologiske Undersøgelse 112:35-42

Hiess J, Bennett VC, Nutman AP, Williams IS (2009) In situ U–Pb, O and Hf isotopic compositions of zircon and olivine from Eoarchaean rocks, West Greenland: New insights to making old crust. Geochim Cosmochim Acta 73:4489-4516

Nutman AP, Christiansen O, Friend CRL (2007) 2635 Ma amphibolite facies mineralisation near a terrane boundary (suture?) on Storø, Nuuk region, southern West Greenland. Precambrian Research 159:19-32

Nutman AP, Friend CRL, Hiess J (In Press) Setting of the ~2560 Ma Qôrqut Granite Complex in the Archean crustal evolution of southern West Greenland. American Journal of Science